

**SIGNAL DESIGN AND PROCESSING TECHNIQUES  
FOR WSR-88D AMBIGUITY RESOLUTION**

**PART - I**

**National Severe Storms Laboratory Report**  
prepared by: **M. Sachidananda**  
with contributions by: **D.S. Zrnic and R.J. Doviak**

**July 1997**

**NOAA, National Severe Storms Laboratory**  
**1313 Halley Circle, Norman, Oklahoma 73069**

# SIGNAL DESIGN AND PROCESSING TECHNIQUES FOR WSR-88D AMBIGUITY RESOLUTION

## Part-I

### Table of Contents

<b>List of symbols</b>	iii
<b>1. Introduction</b>	1
1.1. Range and velocity ambiguity	1
<b>2. Simulation study</b>	6
2.1. Weather radar signal simulation	6
2.2. The autocovariance algorithm	7
2.3. Procedure for evaluation of the algorithms	11
2.4. Programs	12
<b>3. Peak Sorting Method</b>	14
3.1. Introduction	14
3.2. Conceptual development	14
3.3. The peak sorting algorithm	20
3.4. Simulation study and results	21
3.5. Conclusions	24
<b>4. Random phase coding</b>	25
4.1. Introduction	25
4.2. Random phase coding and spectral parameter estimation	26
4.3. Choice of code	36
4.4. Some sample spectra and illustration of processing	39
4.5. The random phase algorithm	45
4.6. Simulation and results	47
4.7. Possible extension to 3rd and 4th trips	58
4.8. Conclusions	58
<b>5. Systematic phase coding</b>	59
5.1. Introduction	59
5.2. Systematic phase coding and spectrum modification	59

5.3. $\pi/4$ phase code	60
5.3.1. $\pi/4$ phase coding and spectral parameter estimation	60
5.3.2. The $\pi/4$ decoding algorithm	64
5.3.3. Simulation and results	65
5.4. $\pi/2$ phase coding	69
5.4.1. $\pi/2$ phase code and estimation of spectral moments	69
5.4.2. The algorithm development	71
5.4.3. The $\pi/2$ decoding algorithm	74
5.4.4. Simulation and results	80
5.5. Optimizing the systematic code	86
5.5.1. Conceptual development	86
5.5.2. The decoding algorithm for optimum systematic code	91
5.5.3. Simulation results and discussion	93
<b>6. Summary and conclusions.</b>	<b>96</b>
<b>7. References</b>	<b>100</b>

## LIST OF SYMBOLS:

$a_k, b_k, s_k, q_k$	-	$k^{\text{th}}$ spectral coefficient
$c$	-	speed of light
$C_{ab}(1)$	-	cross correlation of 1st and 2nd trip signals
$C_k$	-	complex modulation code [ $C_k = \exp(j\phi_k)$ ]
$e1, e2$	-	complex time series of 1st and 2nd trips
$E1$	-	complex time series with 1st trip coherent and 2nd trip coded
$E2$	-	complex time series with 2nd trip coherent and 1st trip coded
$E_i$	-	complex time series samples
$\text{err}( )$	-	error in the parameter in brackets
$f_d$	-	Doppler frequency
$f_a$	-	Nyquist frequency
$G_k$	-	spectral coefficients (fitted to the Gaussian shape)
$i, k, n, m$	-	used as indices
$j$	-	$(-1)^{1/2}$
$M$	-	number of samples
$n_w$	-	notch filter width normalized by $2v_a$
$nw$	-	notch filter width in terms of number of spectral coefficients
$N_k$	-	noise power in the $k^{\text{th}}$ coefficient
$p1, p2$	-	mean power of 1st and 2nd trips
$pm1, pm2$ etc.	-	mean powers estimated from long PRT data
$pw1, pw2$	-	recovered 1st and 2nd trip powers (peak sorting algorithm)
$P_k$	-	power of the $k^{\text{th}}$ spectral coefficient
$r, r_c$	-	range
$r_a$	-	unambiguous range
$R_a(1), R_b(1)$	-	autocorrelation of signals $a$ and $b$
$r(k)$	-	random number array of length $k$
$R(n)$	-	autocorrelation for $n$ PRT lag
$R_p$	-	residual power ratio ( the ratio of power before notch filtering to the power after notch filtering, for the stronger signal)
$R_o$	-	overlapped power to total power ratio
$S_k$	-	power of the $k^{\text{th}}$ spectral coefficient of the signal
$S1, S2$	-	spectrum of $E1$ and $E2$ [ $S1 = \text{DFT}(E1)$ ]
$T$	-	pulse repetition time
$v_r$	-	radial velocity
$v_a$	-	unambiguous velocity (short PRT)
$v_{al}$	-	unambiguous velocity (long PRT)
$v_m$	-	mean velocity
$v1, v2$	-	mean velocity of 1st and 2nd trips
$vm1, vm2$ , etc.	-	mean velocities from long PRT data

$vp1(i), vp2(i)$	-	estimated velocity aliases of the 1st and 2nd trips from long PRT data, $i=1,2,3$ & 4 (aliasing interval number)
$w1, w2$	-	spectrum width of 1st and 2nd trips
$z$	-	$\exp(j2\pi/M)$
$\hat{\phantom{z}}$	-	estimate
$\mathcal{P}$	-	probability
$\mathcal{E}$	-	expected value
$\tau$	-	range time
$\Psi_k$	-	switching phase sequence
$\Phi_k$	-	modulation phase sequence

#### ABBREVIATIONS:

SNR	-	Signal-to-Noise Ratio
PRT	-	Pulse Repetition Time
GCF	-	Ground Clutter Filter
DFT, IDFT	-	Discrete Fourier Transform, Inverse DFT
FFT	-	Fast Fourier Transform
S&S	-	Smoothing and Subtraction
$\pi/4$ code	-	{ 0 , $\pi/4$ , 0, $\pi/4$ , ... }
$\pi/2$ code	-	{ 0 , 0, $\pi/2$ , $\pi/2$ , ... }

# SIGNAL DESIGN AND PROCESSING TECHNIQUES FOR WSR-88D AMBIGUITY RESOLUTION

## PART - 1

### 1. INTRODUCTION

The Operational Support Facility (OSF) of the National Weather Service (NWS) has funded the National Severe Storms Laboratory (NSSL), the National Center for Atmospheric Research (NCAR), and the Forecast Systems Laboratory (FSL) to address the mitigation of range and velocity ambiguities in the WSR-88D system. This is the first part of the report on the ambiguity resolution in WSR-88D. It documents the work done at the NSSL in the first year of the project. Selected techniques that rely on spectral processing to sort out overlaid echoes are investigated, and the best candidate is selected for further scrutiny.

#### 1.1. Range and velocity ambiguity

The range to scatterers is found by measuring the time delay between a transmitted pulse and its echo. If a transmitted pulse is part of an equi-spaced pulse train, the measured range is ambiguous because the echo signal could be due to any one of the pulses transmitted earlier (Doviak and Zrníc 1993). Therefore, the measured range,  $r$ , for a delay time,  $\tau$ , is given by

$$\begin{aligned} r &= (n-1) cT/2 + c\tau/2 ; \quad 0 \leq \tau \leq T \\ &= (n-1) r_a + r_\tau , \end{aligned} \tag{1.1}$$

where  $T$  is the pulse repetition time,  $c$  is the speed of light,  $r_a$  is the unambiguous range, and  $n$  is an integer or the trip number. Range ambiguity resolution is the determination of the trip number,  $n$ . Equation (1.1) implies that the echo measured at delay time  $\tau$  could be due to any one of the pulses transmitted earlier, or in other words, the echo is due to scatterers located at any of the range cells corresponding to the time delay,  $[(n-1)T + \tau]$ . One simple method of determining the correct range is to choose  $T$  large enough to make  $r_a = cT/2$  encompass ranges beyond which radar beam is about 16 km above ground so that no storms are intercepted, and  $n=1$  can be assumed safely. However, this is not an acceptable solution because it severely curtails the velocity measurement capability of the radar.

The radial velocity of scatterers is obtained from the measurement of Doppler frequency,

$f_d$ . The radial velocity of the scatterer is related to the Doppler frequency by

$$v_r = - \lambda f_d / 2 , \quad (1.2)$$

where  $\lambda$  is the free-space wavelength. By convention, scatterers moving away from the radar have a positive velocity which produce negative Doppler shift. Because the echoes are discrete samples taken at intervals,  $T$ , the maximum Doppler frequency that can be unambiguously extracted from the sample sequence is given by

$$f_a = 1/(2T), \quad (1.3)$$

which is known as the Nyquist frequency. A fully coherent radar can recover Doppler frequencies within the interval  $\pm f_a$ . Any frequency outside this interval is seen by the processor as a measured Doppler frequency,  $f_{da}$ , within the aliasing interval such that

$$f_d - f_{da} = \pm 2 m f_a. \quad (1.4)$$

Here,  $f_{da}$  is the actual Doppler frequency. The integer,  $m$ , is the aliasing interval number. Therefore, the actual Doppler frequency is known only within an unknown integer,  $\pm m$ . Corresponding to the unambiguous frequency interval,  $\pm f_a$ , the unambiguous velocity interval is  $\pm v_a$ , where  $v_a = \lambda/4T$ . Since both  $v_a$  and  $r_a$  are functions of pulse repetition time,  $T$ , we can combine them to get

$$r_a v_a = c \lambda / 8. \quad (1.5)$$

Thus, if  $r_a$  is increased by increasing  $T$ ,  $v_a$  decreases correspondingly. This is a fundamental limitation of a pulsed Doppler radar transmitting uniformly spaced pulses. However, the problem is overcome if means are found to determine the trip number,  $n$ , and the aliasing interval number,  $\pm m$ .

Discussions so far assume that the scatterers are located at only one of the several ambiguous locations corresponding to the delay,  $[(n-1)T+\tau]$ , and are moving with a certain radial velocity. In a pulsed Doppler weather radar, the situation is somewhat more complicated because the scatterers are precipitation particles that can be distributed quasi-continuously over a large area ( $> 10^2 \text{ km}^2$ ), and the dynamic range of the echo strength can be as large as 80 dB. Therefore, the echo sample can consist of echoes from more than one ambiguous range cell. If this is the case, the signals are said to be overlaid. Typical radial velocities encountered in storms can span a  $\pm 50 \text{ m s}^{-1}$  interval (Doviak and Zrnicek 1993, p. 165, Fig. 7.4). The unambiguous range requirement for a 10 cm wavelength weather radar, such as WSR-88D, is about 460 km. Because of the curvature of the earth, the antenna beam would top most of the storms at about this range. If  $T$  is chosen to obtain  $r_a=460 \text{ km}$ , the unambiguous velocity interval is too small to effectively de-alias velocities using data processing techniques. On the other hand, if  $T$  is chosen small enough to give at least  $\pm 22 \text{ m s}^{-1}$  unambiguous velocity, the echo signals from different range cells, corresponding to different trip numbers,  $n$ , may be overlaid.

In this case, one needs to separate the signals and then estimate their spectral parameters. Therefore, in the case of weather radar, ambiguity resolution must also include signal separation, in addition to the determination of trip number  $n$  and aliasing interval number,  $m$ .

In general, it may not be necessary to determine both  $m$  and  $n$  because if there is a technique to determine the trip number,  $n$ , one can choose a  $T$  short enough to make  $v_a$  encompass all the expected values of velocities so that  $m$  can be safely taken to be zero. Similarly, if there is a technique to find the aliasing interval, then  $T$  could be increased to yield a larger  $r_a$ . But echoes from subsequent pulses become less correlated as  $T$  increases, and therefore, spectral moment estimates deteriorate (Doviak and Zrnich 1993). At a 10 cm wavelength and a spectrum width of weather signals of  $4 \text{ m s}^{-1}$  (the median in severe storms), the decorrelation time (lag at which the correlation is  $e^{-1/2}$ ) is about 2 ms, and the corresponding  $r_a = 300 \text{ km}$ . Therefore, overlaid echoes are inevitable, and some kind of pulse to pulse coding (in time, frequency, phase, amplitude, polarization, etc.) or some a-priori information about the echoes, must be used to sort them.

Several methods which seek to ameliorate the problem of range and velocity ambiguity have been reported in the literature. Notable among them are (a) staggered PRT scheme (Zrnich and Mahapatra 1985) which can be considered as time coding, (b) random phase coding (Zrnich and Mahapatra 1985), (c) systematic phase coding (Sachidananda and Zrnich 1986), and (d) polarization coding (Doviak and Sirmans 1973). A radar that alternately transmits horizontally and vertically polarized waves can increase the unambiguous range by a factor of 2 (Zahrai and Zrnich 1993).

All these methods fall under the category of signal design and processing. There are other techniques developed to obtain aliasing interval information based on the continuity of velocity fields and/or knowledge of environmental winds. These techniques are implemented after fields of velocity are collected and can be classified as data field processing techniques.

The WSR-88D transmits pulses at two PRTs on sequential azimuthal scans or adjacent radials. The long PRT mode is for estimating the reflectivities over a large range, and the short PRT is for velocities over a smaller unambiguous range interval. In this scheme, unambiguous reflectivity information obtained in the long PRT scan is used to assign appropriate trip numbers,  $n$ , to signals in the short PRT scan. But in the case of overlaid echoes, only the stronger one is recovered in the WSR-88D signal processor. Further spectral processing could often recover the weaker echo as well. For example, the signal in the short PRT scan can be analyzed to locate peaks in the spectral domain and assign appropriate ranges to the corresponding velocities using the reflectivity information available from the long PRT scan. Such techniques fall in the category of spectral peak sorting, or simply peak sorting.

This report deals with signal design and processing techniques and examines methods that utilize a uniform PRT sequence with a sufficient number of samples for meaningful Fourier analysis (typically 64). Specifically, the following three are studied: (a) peak sorting, (b) random phase coding, and (c) systematic discrete phase coding. An in-depth simulation study has been carried out to evaluate their potential for possible implementation on the WSR-88D radar.

Except for peak sorting, the other two methods fall under the category of pulse to pulse coding or modulation. The main idea behind coding is to imprint some signature on the return signals corresponding to different transmitted pulses. These signatures are used to decode or separate the signals belonging to different trips. The methods (b) and (c) are different to the

extent that the code sequence is chosen differently, and an appropriate decoding scheme is evolved based on the properties of the modulated spectrum.

The report is organized in the following manner. In section 2, weather signal simulation procedure is discussed, along with the methodology for evaluating the algorithms developed for range and velocity ambiguity resolution in the presence of overlaid echoes. Then, in the subsequent three sections, several algorithms are discussed including the simulation results on the performance of the algorithms. In simulating the weather signal time series and in comparison of the methods of ambiguity resolution, the following assumptions are made:

- a) **the ground clutter is absent**
- b) **the noise is absent**
- c) **the window effect is absent**
- d) **the spectra have a Gaussian shape**
- e) **only the 1st and 2nd trip signals are present in the time series.**

The decoding algorithms presented in this report are also developed with these assumptions. In practice, several of these effects, such as the window effect, the ground clutter, the noise, etc., are present and have to be accounted for in the algorithms. However, these are common to all, and would affect all the methods in some way or other in limiting their performance; hence they were neglected in evaluating the relative performance of the methods in order to identify the best one. These assumptions help bring out the basic capability of the methods which otherwise would be masked by some of these effects. The effect of the signal-to-noise ratio, the window effect, the ground clutter, and many more practical aspects of implementation of the algorithm on the WSR-88D are analyzed in Part 2 of this report where the selected method is scrutinized in much greater detail.

The WSR-88D in the present configuration can be operated in two different volume coverage patterns (vcp-11 and vcp-21), and in both, several preset PRT values are used which can be grouped as long PRT and short PRT. The long PRT is about 3 ms, and the short PRT is selected from a pre-defined set of values between 0.7 and 1 ms. The long PRT scan is called the surveillance scan (CS) and the short PRT scan is called the Doppler scan (CD). The volume coverage includes an azimuth scan of  $360^\circ$  at discrete elevation angles from  $0.5^\circ$  to  $19.5^\circ$  degrees. At the lowest two elevations ( $0.5^\circ$  and  $1.45^\circ$ ), two scans each (CS and CD) provide reflectivity to about 460 km and velocity to about 115 km, if there are no overlaid echoes. The number of samples available for spectral parameter estimation is about 16 to 17 samples in the long PRT scan and 44 to 66 samples in the short PRT scan, in the vcp-11 mode. In the vcp-21 mode, the number of samples is 28 for the CS scan and 75 to 111 for the CD scan.

In the scans at elevations  $2^\circ$  to  $6.5^\circ$ , the long and short PRT are used in alternate radials in each scan, called batch mode (B). The number of samples available for spectral parameter estimation is 6 to 10 with the long PRT, and 35 to 50 with the short PRT, in vcp-11. The corresponding numbers are 8 to 12 and 59 to 88 for vcp-21. Above  $6.5^\circ$  elevation, only the short PRT Doppler scan is used.

In the lower elevation scans ( $< 6.5^\circ$ ), the velocity recovery is hampered by overlaid echoes. The aim of this study is to evolve a solution to this problem. From the assumption (e) given above, it is obvious that the ambiguity resolution methods considered can, at best, extend

the range to only two trips. And if the unambiguous velocity is to be near  $35 \text{ m s}^{-1}$ , this extended range would be about 230 km. In the two lowest elevation scans, the unambiguous range requirement is about 460 km for the reflectivity; therefore, the long PRT scan must be retained. This leads us to the possibility of using the information from the long PRT scan data in ambiguity resolution algorithms applied to short PRT data. However, in the intermediate elevation scans ( $2^\circ$  to  $6.5^\circ$ ), the antenna beam tops a typical storm within the first two trips (about 230 km). Hence, there may be a possibility of replacing the batch scan with the Doppler scan, if the algorithm is able to extract all three spectral parameters of both the 1st and the 2nd trip echoes, with the required accuracy. Therefore, the methods of ambiguity resolution presented in this report are developed as stand-alone methods (not using long PRT data), whenever possible. But some methods are based on the availability of the long PRT data and cannot operate in a stand-alone mode. This is indicated in each algorithm.

## 2. SIMULATION STUDY.

### 2.1. Weather radar signal simulation.

In order to test the effectiveness of techniques for mitigating the range and Doppler ambiguities, it is desirable to make tests on overlaid radar signals. Comprehensive tests are necessary but are practical only on simulated radar signals because only with simulation can the actual individual signal parameters (i.e., the mean power, mean velocity, and spectrum width) be accurately known. The recovered parameters can be compared with the specified input parameters to determine the error in the estimates. However, the inferences drawn by this study can be meaningful only if the simulated weather spectra truly represent the radar signals from storms. Zrnic (1975) gives a procedure to simulate the weather signal on a digital computer using a random number generator available in most computers. The complex sample,  $E_i$ , in a time series can be expressed as a discrete Fourier series;

$$E_i = 1/M \sum_{k=0}^{M-1} P_k^{1/2} \exp(j\theta_k) \exp(j2\pi ki/M). \quad (2.1)$$

Here,  $P_k$  is the exponentially distributed instantaneous power of the signal plus noise in the  $k^{\text{th}}$  spectral coefficient. The signal part is frequency dependent, and the noise part is white;  $\theta_k$  is a uniformly distributed phase; and  $P_k$  and  $\theta_k$  are statistically independent. With  $S_k$  as the signal power and  $N_k$  as the noise power, in the  $k^{\text{th}}$  coefficient  $P_k$ , the probability density of  $P_k$  can be written as

$$\mathcal{P}\{P_k\} = 1/(S_k+N_k) \exp[-P_k/(S_k+N_k)]. \quad (2.2)$$

This is the basic equation used in the simulation of weather spectra. The steps include the generation of a Gaussian shaped  $S_k$  and adding a noise to get the desired signal-to-noise ratio (SNR). These coefficients are multiplied by the logarithm of a uniformly distributed random number (0 to 1) to get  $P_k$ . The phases,  $\theta_k$ , are generated from the same uniform number generator but are independent.

This procedure was followed to generate weather signal spectra, and the inverse discrete Fourier transform (IDFT) was used to obtain the time series. To simulate the window effect, a very long time series is generated, and a short part, of length  $M$ , is taken and multiplied with appropriate weights. The window effect is not very critical in the evaluation of algorithms because it increases the spectrum width by a small amount. Simulating the window effect takes more computer time because long time series need to be generated. Therefore, for initial evaluations, the window effect was not included. The velocity aliasing is simulated by generating a time series without aliasing and then selecting alternate samples to simulate one-time aliases. Multiple aliasing is simulated by dropping  $n$  samples after each selected sample.

The program developed for time series simulation, "TSR1.M", has mean power, velocity, spectrum width, and number of samples,  $M$ , as the inputs. The output is a time series of complex samples (i.e., in-phase samples,  $I$ , and quadrature samples,  $Q$ ) of length  $M$ . Three other

parameters, SNR, transmitter frequency, and PRT, are also included as inputs but are normally kept constant for most of the simulation. Although noise level is included in the time series simulation program, it is set to zero ( SNR = infinity ) in all the simulation studies presented in this report. Fig. 2.1 shows typical simulated in-phase and quadrature components of the time series and the spectrum. The parameters used for generating the signal are given in the figure.

The program, "TSR2.M", combines two time series, the 1st and the 2nd trip signals, into a single overlaid time series. The inputs to this program are the 1st and the 2nd trip parameters and the time series length,  $M$ . The program is made general so that any coding scheme can be implemented. The output time series has a coherent 1st trip, and the 2nd trip signal is coded. The options provided for the second trip coding are: (a) no coding, (b)  $\pi/4$  and  $\pi/2$  phase coding (Sachidananda and Zrnic 1986), (c) coding with a fixed predesigned random code, (d) phase code derived from  $\phi_k=(n\pi k^2/M)$  with  $n$  as input (Chu 1972), and (e) internally generated random phase code every time it is called. In case (d),  $M$  is the time series length, and  $n$  is chosen as nearly prime to  $M$  (i.e.,  $M$  is not divisible by  $n$ ). This gives a phase code sequence,  $\phi_k$ , which has cyclic autocorrelation zero for all lags except 0. If  $n$  is chosen such that  $M$  is an integer multiple of  $n$ , the code has a special property that its autocorrelation is non-zero and equal only for some discrete values of lags, and is zero for the rest. The  $\pi/4$  code (Sachidananda and Zrnic 1986) is one such code which can be derived from this expression (i.e.,  $n/M=1/2$ ). The outputs of the program (TSR2.M) are a time series and the code sequence (except for option "a") which is required for processing. Thus, two overlaid signals of known spectral parameters can be obtained from this program. A sample spectrum of overlaid signal is shown in Fig. 2.2, as obtained from the simulation program.

In order to see how good our simulated signal is, we selected a nearly Gaussian-looking weather data from WSR-88D and generated a time series using the simulation program with the same spectral parameters. The two spectra are compared in Fig. 2.3, which shows a fairly good match.

## 2.2. The autocovariance algorithm.

When the echo signal is from a single range cell (i.e., no overlaid signal), the mean velocity is commonly estimated using the phase of the autocorrelation,  $R(1)$ , for one PRT lag. The autocorrelation  $R(1)$  is estimated from the complex samples,  $E_i = I_i + jQ_i$ , using the formula,

$$\hat{R}(1) = (1/M) \sum_{i=0}^{M-1} E_i^* E_{i+1} , \quad (2.3)$$

and the mean velocity estimate is obtained from

$$\hat{v} = - (\lambda/4\pi T) \arg\{ \hat{R}(1) \} . \quad (2.4)$$

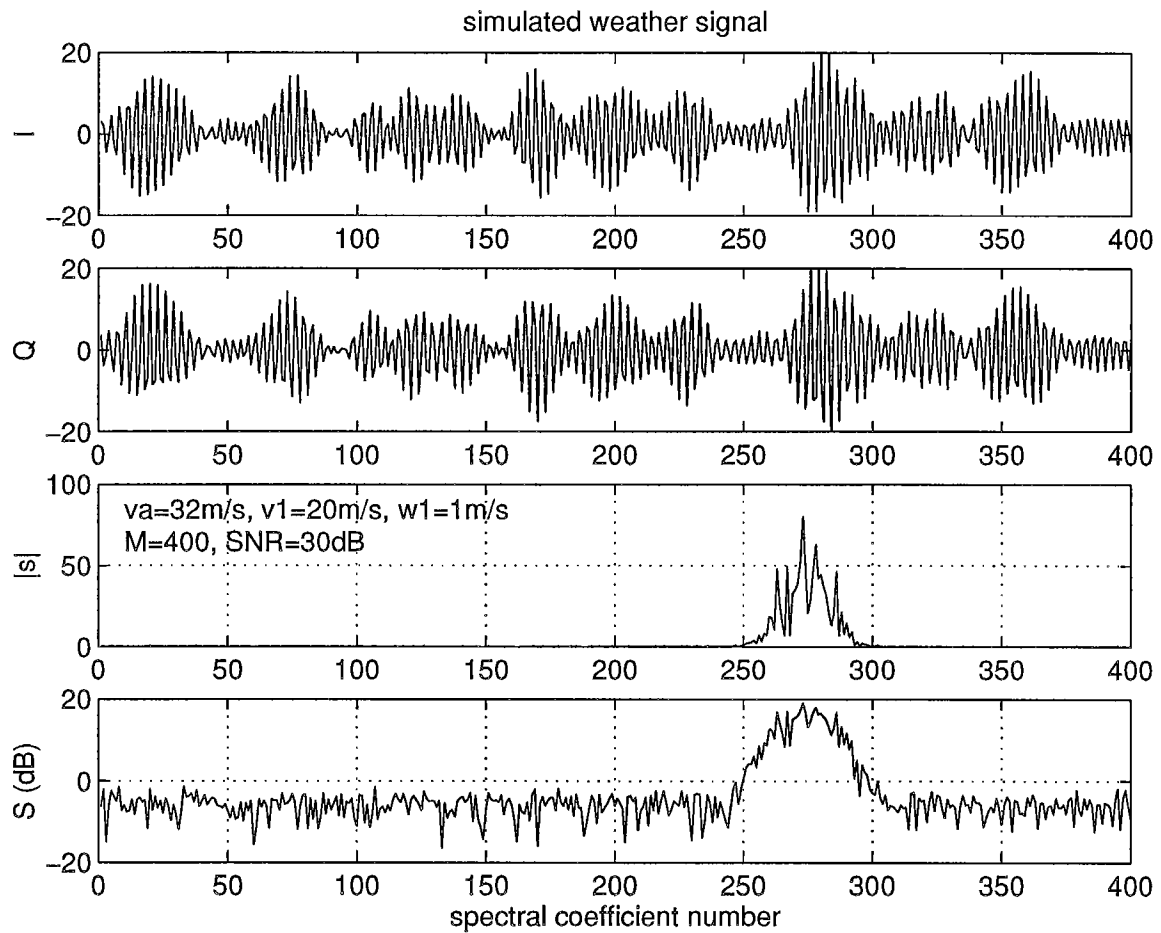


**Fig. 2.1.** A typical simulated weather signal; time series and frequency spectra. (a) the in-phase component,  $I$ , (b) the quadrature component,  $Q$ , (c) the magnitude spectrum,  $|s| = \sqrt{I^2 + Q^2}$ , (the square root of the power spectrum on linear scale), (d) the power spectrum (dB scale).

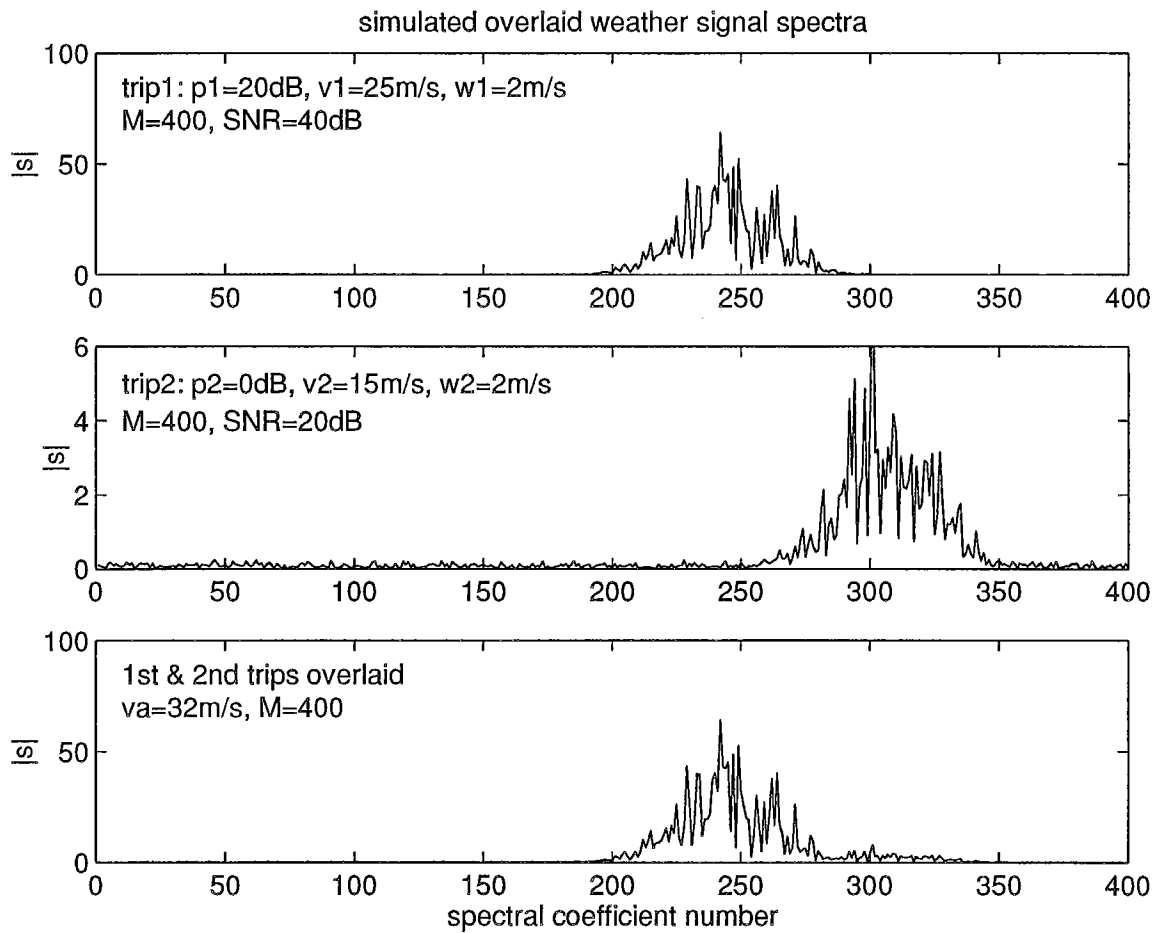


**Fig. 2.2.** A typical frequency spectra for simulated overlaid signals. (a) the 1st trip signal, (b) the 2nd trip signal, (c) the spectra of 1st and 2nd trip signals overlaid.

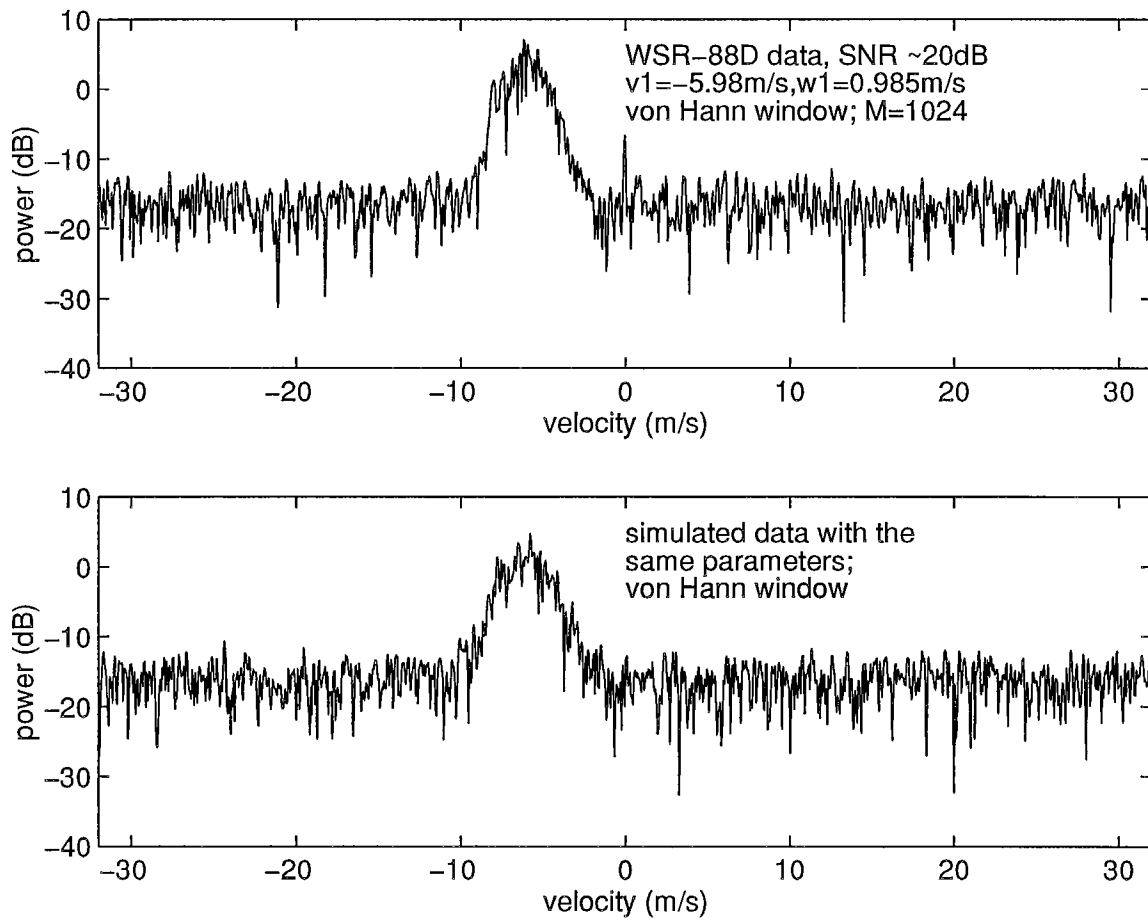


Fig. 2.3. A comparison of simulated weather spectrum with the spectrum of the data gathered from WSR-88D (WSR-88D data, courtesy: Frank Pratte, NOAA, FSL).

Here, the argument is in radians, and the velocity is in  $\text{m s}^{-1}$ . The symbol  $*$  represents a complex conjugate, and the symbol  $\hat{\phantom{x}}$  denotes an estimate. This is commonly called autocovariance processing. The other two spectral parameters (i.e., mean power,  $p$ , and spectrum width,  $w$ ) are estimated using the expressions given below. (see Doviak and Zrnic 1993 for details.)

$$\hat{p} = (1/M) \sum_{i=0}^{M-1} |E_i|^2, \quad (2.5)$$

and

$$\hat{w} = (\lambda/2\pi T\sqrt{2}) |\ln(\hat{p}/|\hat{R}(1)|)|^{1/2} \text{sgn}[\ln(\hat{p}/|\hat{R}(1)|)]. \quad (2.6)$$

In this study the computation of these three parameters is carried out in one program and is referred to as an autocovariance processor (program "pp.m").

When spectral coefficients are available and not the time series, the autocorrelation  $R(1)$  can be computed from the spectral coefficients directly, without a transformation to the time domain, using the relation,

$$\hat{R}(1) = (1/M) \sum_{i=0}^{M-1} |s_i|^2 \exp(j2\pi i/M). \quad (2.7)$$

In some of the algorithms discussed, there are situations where spectral coefficients are used for computing the autocorrelation (as well as the three spectral parameters) using the program "pps.m." This also is referred to as an autocovariance processor in this report, and no distinction is made between the two because both yield the same results.

### 2.3. Procedure for evaluation of algorithms.

The reflectivity, velocity, and the spectrum width are the three spectral parameters that need to be recovered for both the 1st and the 2nd trip echoes when they are overlaid. Of these three, velocity of the weaker signal is the most difficult to extract, and this is often the most important parameter of interest. Reflectivity, however, can be obtained from long PRT scan data, as is done in the WSR-88D radar. Spectrum width information is not used as often as the other two parameters. Thus, the recovery of velocity of the weaker signal decides the limit of usefulness of the algorithm. It is also observed during the course of the simulation study that the reflectivity of the weaker signal can be recovered over a larger dynamic range of overlaid signal power ratios than the velocity. Therefore, the error in the recovered velocity of the weaker signal is the parameter that is extracted in all the simulation runs. The errors in all other parameters (i.e., mean powers and widths) also are recorded over a large number of simulation runs. The commonly accepted error limits in the estimates are 1 dB for reflectivity, and  $1 \text{ m s}^{-1}$  for velocity and spectrum width. These limits are used in deciding the usefulness of the algorithms and in

comparing the different algorithms. It may be noted here that the reflectivity and the mean sample power are directly related but are not same. In all the simulations, the mean power is used and not the reflectivity, because the 1 dB accuracy required for the reflectivity estimate applies to the mean power estimate as well.

The error in the estimated velocity, as well as in the other parameters, depends on several factors, such as the spectrum width, noise level, window effect, number of samples in the time series, and the ability of the algorithm to recover the parameters. To separate these effects, and to evaluate the performance of the algorithm alone, first the number of samples,  $M$ , is taken to be large ( $M = 256$ ) in simulation, and the noise level is set to zero. The window effect is also not included in the simulated time series. The variance of the velocity estimate, due to the spectrum width, cannot be removed because it is intrinsic to the signal, but for large  $M$ , it is within the specified limits. The signal parameters varied in the simulation study are the overlaid signal power ratio,  $p1/p2$ , the velocity difference,  $(v1-v2)$ , and the spectrum widths of the two signals. For each set of parameters, several signal realizations were used to generate scattergrams of the error in the recovered velocity,  $v2$ , as a function of the variables of simulation. From these plots, limits of the algorithm were extracted. Later, to determine the practical limits of the algorithm, similar sets of simulations were run with  $M=64$ , which is about the maximum number of samples available in WSR-88D radar in the present working mode (vcp-11). In all simulations, the frequency is 3 GHz, and the PRT is 0.7812 ms. This choice gives an unambiguous range of 117.2 km and a Nyquist velocity of  $32 \text{ m s}^{-1}$ . In the presented data, the spectrum width can easily be normalized, with respect to the Nyquist velocity, to make inferences for a different Nyquist velocity.

Based on the results obtained on the performance of the algorithms (using  $M=64$ ), a comparison was made to select a most promising method to recover the velocity of the weaker signal.

## 2.4. Programs.

The software, MATLAB, has been used for all the simulation work. The software was selected for its compact programs and matrix manipulation capabilities. Several signal processing functions are also available in the package which is very convenient for simulation work. Efficient 2-D as well as 3-D plot routines are also handy in graphical presentation of the results.

The programs developed for the simulation study of the algorithms are listed below with a brief explanation. Only important ones are listed; a large number of programs for generating the data and graphics are not included.

Simulation and decoding programs.

1. `tsr1.m` Generates a simulated time series with the specified parameters, mean power, mean velocity, spectrum width, frequency, PRT, number of samples, and SNR.
2. `tsr2.m` Generates overlaid signal time series. 1st and 2nd trip parameters and the coding to be specified.

3. pp.m Autocovariance algorithm. Outputs power, velocity, and spectrum width, with time series as input.
4. pps.m Equivalent of autocovariance algorithm with spectra as input.
5. mfltr.m Smoothing or running average filter. Filters an input sequence with a specified filter length.
6. spc.m Peak sorting algorithm.
7. rndm.m Decoding algorithm for random phase coded signal.
8. piy2.m Decoding algorithm for  $\pi/2$  phase coded signal.
9. piy4.m Decoding algorithm for  $\pi/4$  phase coded signal.
10. msdz.m Decoding algorithm for a systematic code based on  $\exp(jn\pi k^2/M)$ .
11. testspc.m Program to test the peak sorting algorithm.
12. testrndm.m Program to test the random phase code algorithm.
13. testms2.m Program to test the  $\pi/2$  phase code algorithm.
14. testmsdz.m Test program for msdz.m
15. testms4.m Test program for the  $\pi/4$  phase code algorithm.
16. coder.m Program used for optimizing the random code sequence.
17. pps2.m Autocorrelation processor for lag 2 computed in the spectral domain.

### 3. PEAK SORTING METHOD

#### 3.1. Introduction.

This method requires a processor capable of the necessary computations in real time. Since no coding is employed at the transmitting stage, one has to depend on the available information about the signals to determine the mean velocities of the overlaid signals. The WSR-88D radar in the present configuration has a long PRT scan and a short PRT scan. The long PRT scan gives unambiguous reflectivity data over a 460 km range. This information can be used to assign the correct ranges to the estimated velocities of signals overlaid in the short PRT scan. That is, a comparison of powers associated with distinct spectral peaks, observed in the short PRT scan, with the powers from the long PRT scan, at ranges corresponding to  $\tau$  and  $(\tau+T)$  of the short PRT, is made to assign the velocity to proper ranges.

An assumption made in developing this algorithm is that the spectra have a Gaussian shape, which is an approximation for weather spectra. To recover spectral peaks with reasonable accuracy from a signal spectrum having considerable variance in each of its spectral coefficients, it is necessary to smooth the spectrum. However, smoothing the spectrum also smoothes the peaks and increases the width. The smoothing filter parameters have to be optimally chosen such that true peaks are not lost in the process of filtering and false peaks are kept to a minimum. The developed algorithm essentially locates and sorts the peaks in the spectral domain and assigns appropriate ranges to these velocities based on the data available from the long PRT scan. We assume that only 1st and 2nd trip signals are present in the spectra in developing the algorithm. It can easily be extended to a three or four trip signal overlay within certain restrictions.

#### 3.2. Conceptual development.

The basic idea behind the development of this algorithm is that if two weather signals having Gaussian shaped spectra are present in a time series, these two peaks can often be identified in the spectral domain by a human observer, provided they are distinct. When the two spectra overlap, peaks may not be distinguishable. But based on the a-priori information available from the long PRT scan (i.e., aliased velocities can be computed from long PRT data), a decision can be made to assign the same velocity to both signals. Of course, there is an amount of error in this assignment when the velocities are close but not the same. How close the velocities can be before they merge into a single spectrum depends on the relative power levels of the two signals.

The first task, in developing the algorithm, is to locate the peaks of the spectrum. While a human observer can often locate the peaks by observing the shape of the spectrum, automatic recognition needs a computational procedure to locate the peaks. To avoid the computer selecting a local peak (associated with statistical fluctuations) rather than the global peak (associated with peaks of assumed unimodal spectra), it is necessary to first smooth the spectrum so that random fluctuations are reduced. Based upon extensive experimentation, a weighted running average filter applied to the magnitude of spectral coefficients is chosen as the smoothing filter. Note that the smoothing process preserves the power in the spectrum only approximately, and hence, the spectrum may not give a correct mean power estimate after smoothing. However, this is not a

problem since the reflectivity data is obtained from the long PRT scan, and it is sufficient to have approximate power estimates to identify the ranges. More important criteria would be the selection of the smoothing filter width and the weights. The performance of the algorithm is dependent on these parameters to a large extent. An ideal choice would have matched Gaussian shaped weights for the filter. Although spectrum width is estimated in the long PRT scan and can be used to obtain matched filter coefficients, here we have adopted an approach which does not make use of the width information. The main reason is that signals with different widths are involved. For practical implementation, it is convenient to have a fixed width and weights for the filter, although it may not be the best in all cases. Another advantage of a fixed filter width is that its effect on the power and spectrum shape can be evaluated and compensated, if required. A near optimum filter of fixed width and shape can be obtained by an experiment on simulated weather signals with a median width of  $4 \text{ m s}^{-1}$ . The optimum filter parameters (i.e., number of coefficients and weights) are functions of the time series length,  $M$ , and the unambiguous velocity or the PRT. The requirement of smoothing is such that it should remove random perturbations while retaining the shape and distinct global peaks in the spectrum.

After smoothing, first the largest peak of the spectrum is located and several coefficients on both sides of the peak are selected such that the magnitude of the coefficients at the ends is approximately 0.8 times the peak value. Then a Gaussian shape is fitted (i.e., least squares fit) to these coefficients. Thus, the peak of the fitted Gaussian curve gives the mean velocity of the strongest of the signals. To find the next peak, the Gaussian fitted spectrum is subtracted from the original spectrum before the second peak is located. The subtraction significantly enhances the probability of locating the peak of the second signal. This process is repeated further to locate third and fourth peaks. If the long PRT scan indicates significant power returns from more than two trips, the velocities of these also might be recovered. But the reason for locating more than two peaks is for more reliable recovery of the velocity data of the first two trips and not for recovering third and fourth trip velocities. Also the largest powers are not necessarily associated with 1st and 2nd trip echoes. One or both could be from 3rd and 4th trip. The long PRT data is used for assigning the correct trip numbers. Of the three or four peaks recovered, only two with the largest powers associated with them are selected. Note that when the peaks are sorted in decreasing order, the associated powers are not necessarily in the decreasing order because power takes into account the width, but the peak does not. If the peak is spurious with large amplitude and narrow width, the power associated with it will be small and hence, will be eliminated by the algorithm.

A measure of the spectrum width is also obtained from the fitted Gaussian shape. It should be noted that the width parameter does not directly correspond to the spectrum width of the original signal because of smoothing. Alternatively, spectrum width can be computed from the long PRT data, and this procedure is adopted in the algorithm.

A point to note here is that the magnitude spectrum is used for processing, and the curve fitting is done with a Gaussian shape function,  $[\exp(-|v-v_m|^2/2w^2)]^{1/2}$ . However, the spectral shape of the signal may not match the Gaussian shape because of the smoothing filter which changes the shape of the spectra to some extent. Therefore, this is another reason for mismatch in the shape in addition to the variability of the shape of weather spectra. The choice of processing in the magnitude domain was based on the results obtained (not given here) with three different options: power spectra, magnitude spectra, and square root of magnitude spectra. For a mean

width of  $4 \text{ m s}^{-1}$ , processing in the magnitude domain performed the best. In the power domain, the ratio of two distinct peaks is the largest, and in the square root of magnitude domain it is the smallest. However, the width of the signal spectra is largest in the square root of magnitude domain and smallest in the power domain. For best performance, both ratio and width should be small, which is a conflicting requirement. Simulation studies showed that a compromise choice of magnitude domain performs the best for practical parameters.

The spectral processing steps are shown pictorially in Fig. 3.1, Fig. 3.2, and Fig. 3.3, in which a series of spectra are given at different stages of processing. In Fig. 3.1, two signals are taken with a power ratio of 10 dB, and the velocities are widely separated. The two spectra, with distinct peaks, can be seen clearly in Fig. 3.1(a). The smoothed spectrum is shown in Fig. 3.1(b), along with the Gaussian shaped fitted curve to the largest peak in the spectrum. The fitted curve is drawn with dashed lines. The spectrum in Fig. 3.1(c) is obtained after subtracting the fitted coefficients from the spectrum shown in Fig. 3.1(b). The dashed curve in Fig. 3.1(c) is a fitted curve to the second largest peak. Similarly, the steps are repeated in Fig. 3.1(d) and (e) to locate the 3rd and 4th peaks. The next two cases, Fig. 3.2 and Fig. 3.3, are for the same power ratio but for a different velocity separation (see figure for parameters). If the velocity separation is  $8 \text{ m s}^{-1}$ , the second peak is still recoverable. However, for a separation of  $4 \text{ m s}^{-1}$ , the two spectra merge into a single one and the algorithm is not able to recover the second peak correctly. There are also cases (not shown) where the perturbation in the Gaussian shape is large enough to generate a large false peak, which the algorithm will misclassify as the correct second signal.

The last task is to assign the velocities to the proper ranges. Here, several strategies can be adopted based on how much information is available from the long PRT scan. The present data acquisition procedure of WSR-88D collects about 16 to 17 samples per gate in the long PRT scan, and only reflectivity or the mean power is computed from these samples. If additional processing were done to recover the spectrum widths and aliased mean velocities, then the task of the peak sorting algorithm in the short PRT scan would be much easier. If not, we have to rely on only the mean power estimates to assign appropriate ranges to the recovered velocities. The probability of error can be significantly reduced if the additional processing is implemented. This is very important because locating the peak can fail if the spectrum shape does not conform to a Gaussian shape. For example, a perturbation in the spectral shape of a strong signal can contain more power than a weak signal that we are trying to recover, and the algorithm would select this perturbation as a signal rather than the weaker one. Such spurious peaks can be minimized if aliased velocity information is available from the long PRT scan. Another situation where the velocity information from long PRT data is useful is when the 1st and 2nd trip velocities are very close. The overlapped spectra will merge to produce a single peak, and these cases can be identified using the velocity data from the long PRT scan.

Since the scan rate of the antenna is the same for long or short PRT transmissions, the ratio of the number of samples for estimation equals the inverse ratio of the PRTs. Thus, the variance of the spectral parameters estimated using the long PRT scan data has a larger value than the variance of the data obtained with the short PRT. However, before deciding which data to use for spectral parameter estimation, it is important to look at the practical values. The typical number of samples available in the present WSR-88D scan is about 64 with the short PRT and about 16 in the long PRT scan. The standard error of the velocity estimate using 16 samples is about  $1.6 \text{ m s}^{-1}$ , for large SNR. (Doviak and Zrnicek 1993, Fig.6.5, p. 134.) For this calculation,

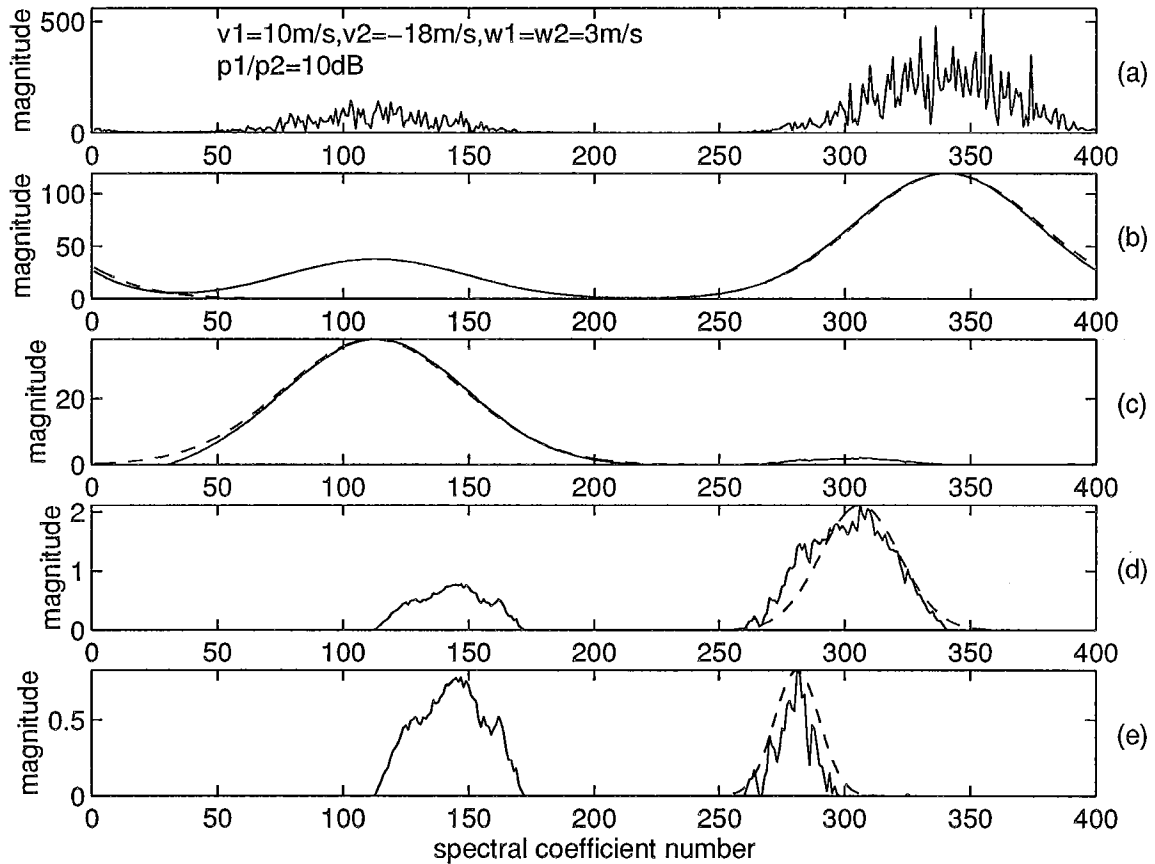


**Fig. 3.1.** Steps in the peak sorting algorithm; velocity separation is  $28 \text{ m s}^{-1}$ , and  $v_a=32 \text{ m s}^{-1}$ . (a) magnitude spectrum of overlaid signal, (b) smoothed spectrum after Gaussian weighted running average filter (continuous line) and the curve fitted Gaussian shaped spectrum for the largest peak (dashed lines), (c) spectrum after subtracting the strongest signal spectrum (continuous line) and the Gaussian shaped spectrum fitted to the second peak, (d) & (e) the same steps repeated for the 3rd and 4th peaks in the spectrum. Magnitude (y-scale) is the square root of the power.

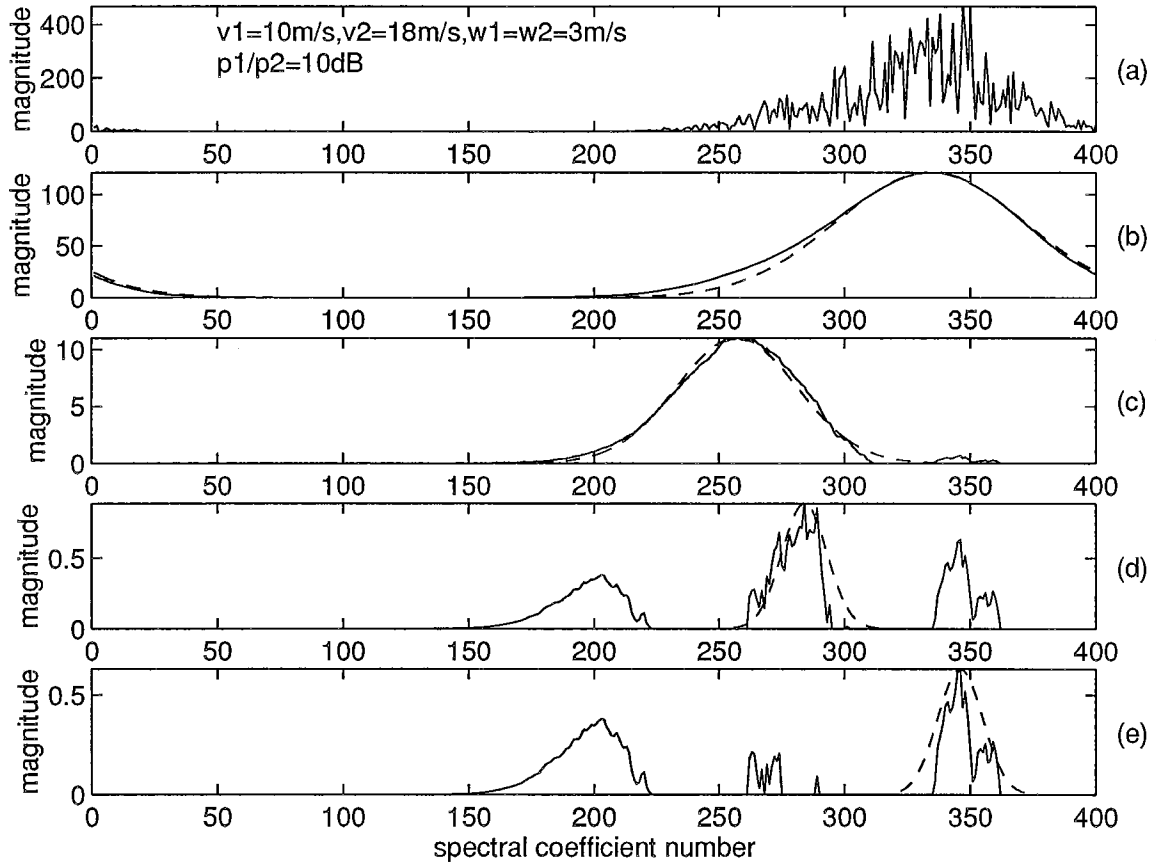


**Fig. 3.2.** Steps in the peak sorting algorithm. The steps are similar to those given in Fig. 3.1. The velocity separation is  $8\text{ m s}^{-1}$ .

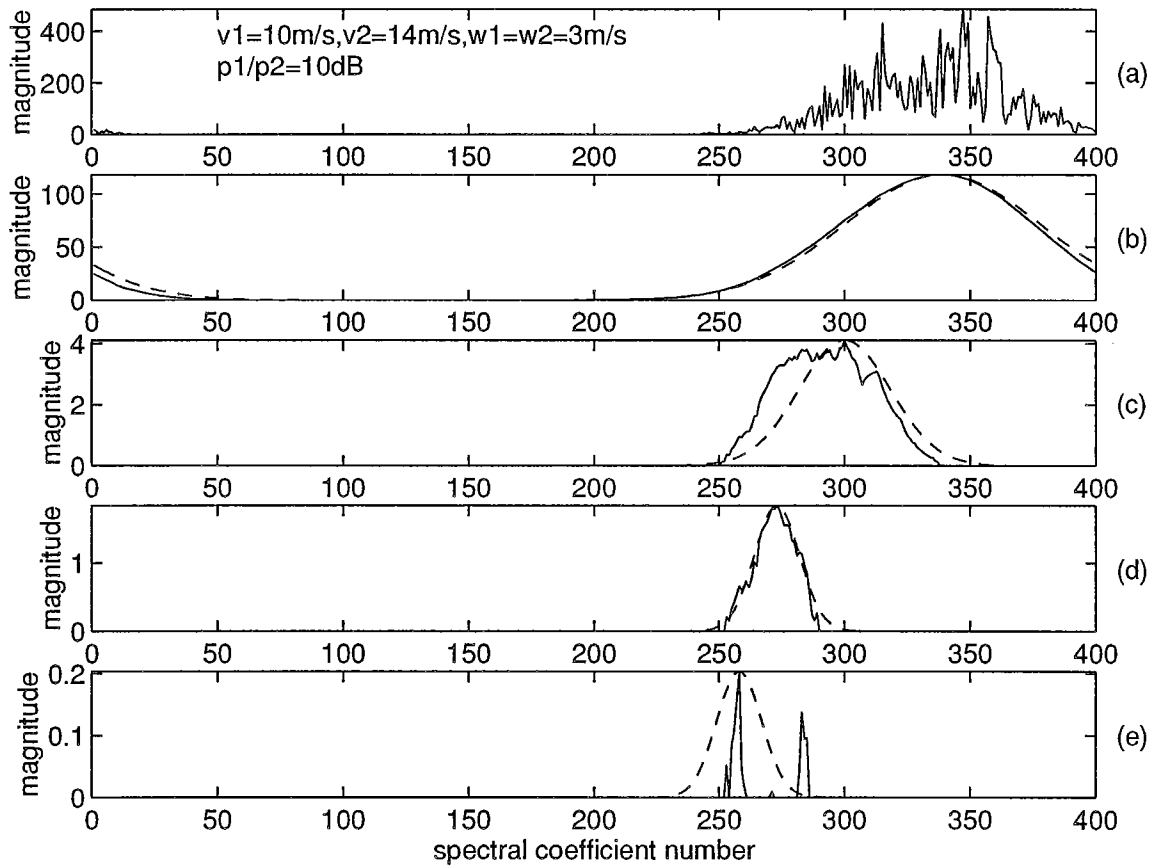


Fig. 3.3. Steps in the peak sorting algorithm. The steps are similar to those given in Fig. 3.1. The velocity separation is  $4\text{ m s}^{-1}$ .

we have assumed  $PRT = 3 \text{ ms}$  and a spectrum width of  $4 \text{ m s}^{-1}$ . This is quite adequate to determine aliasing interval alone, and correct the velocity data. The reflectivity and the spectrum width can be estimated from the long PRT scan.

### 3.3. The peak sorting algorithm.

The peak sorting algorithm is given below, step by step. It is assumed that the ground clutter, window effect, and noise are absent from the signal, and the time series consists of 1st and 2nd trip signals alone. The variables are the spectral parameters of the two signals. [*This algorithm uses the long PRT data. It is also assumed that all three spectral moments are estimated from the long PRT data.*]

<<-----START of the algorithm

1. Input time series  $E_i ; i=1,2,3,\dots M$ .
2. Compute magnitude of the spectral coefficients,  $|s_k| = |DFT\{E_i\}|$ .
3. Running average filter with Gaussian weights,  $SI_k = GWF\{|s_k|\}$ .
4. Locate the largest coefficient,  $S_m$  and select  $K$  coefficients around this peak.
5. Fit a curve  $S_m \{\exp(-|v-v_m|^2/2w^2)\}^{1/2}$  to these  $K$  coefficients.
6. Compute the mean power and mean velocity from this fitted curve.
7. Generate complete set of coefficients  $G_k$ , from the fitted curve and subtract from the smoothed spectrum  $SI_k$ .  $S2_k = SI_k - G_k$ .
8. Repeat steps 4 to 7 three more times with residual spectrum  $S2_k$  as the input or until no peaks are found. Rearrange powers in decreasing order and associate the corresponding velocities.
  - powers :  $pm1, pm2, pm3, pm4$  (decreasing order)
  - velocities :  $vm1, vm2, vm3, vm4$
9. Compute power and the probable velocities of 1st and 2nd trip signals from the long PRT data.
  - $vp1(i)=[v1, v1+2v_{al}, v1-2v_{al}, v1+4v_{al}, v1-4v_{al}]$ ,  $pw1$  - 1st trip.
  - $vp2(i)=[v2, v2+2v_{al}, v2-2v_{al}, v2+4v_{al}, v2-4v_{al}]$ ,  $pw2$  - 2nd trip.

[note: *This computation is actually done during the long PRT scan, and only the final data is passed on to the algorithm. The long to short PRT ratio is about 3 to 4 in WSR-88D, hence  $\pm 4v_{al}$  is used as the maximum velocity interval.*]
10. Match the power and the velocities with the recovered parameters to pick the

correct velocities for both the trips.

- a) if  $pw1 > pw2$ ,  
assign  $vp1(i)$  closest to  $vm1$ , to 1st trip.  
check for overlapped spectrum:  
if  $|v1-v2| < 1 \text{ m s}^{-1}$ , assign  $vp2(i)$  closest to  $vm1$  to 2nd trip  
else  
assign  $vp2(i)$  closest to  $vm2$  to 2nd trip.
- b) if  $pw2 > pw1$ ,  
assign  $vp2(i)$  closest to  $vm1$  to 2nd trip.  
Check for overlapped velocities:  
if  $|v1-v2| < 1 \text{ m s}^{-1}$  assign  $vp1(i)$  closest to  $vm1$  to 1st trip  
else  
assign  $vp1(i)$  closest to  $vm2$  to 1st trip.

11. Assign reflectivities and widths to 1st and 2nd trips from long PRT data.

<<<-----END of algorithm

The major CPU time in this algorithm is for the DFT, smoothing filter, and curve fitting. Step 9 uses autocovariance processing on two time series.

### 3.4. Simulation study and results.

The algorithm given in the previous section was programmed in MATLAB code, and extensive simulation runs were carried out to establish its usefulness. The test program generates two long PRT time series with a length of 16 samples, and estimates the spectral parameters of both using the autocovariance processor. Then, with the same input parameters, a short PRT time series with 64 samples is generated in which the two signals are overlaid. This time series is processed by the peak sorting algorithm to recover the mean velocities of the two signals. The nature of the algorithm is such that it either recovers the velocity correctly, or a wrong value is assigned. Therefore, it would be appropriate to assign a success rate rather than to evaluate the performance of the algorithm by the standard error in the recovered velocities. It was shown earlier (section 3.2) that the success of the algorithm depends on the velocity difference and also on the power ratios. It is a weaker function of spectrum widths. Therefore,  $p1/p2$  and  $(v1-v2)$  are taken as two variables, and the widths are kept constant in simulation. A typical width of  $4 \text{ m s}^{-1}$  is assigned to both signals, and for each set of parameters the simulation program was run 100 times. A successful recovery of velocity is assigned a value, 1, and 0 is assigned for failure. The ratio of the total number of ones to the number of trials, multiplied by 100, is taken as the percentage of success.

The rate of success in recovering the of velocity of the stronger signal is nearly 100 percent; hence it is not shown. The success rate for the weaker signal is shown in Fig. 3.4. The

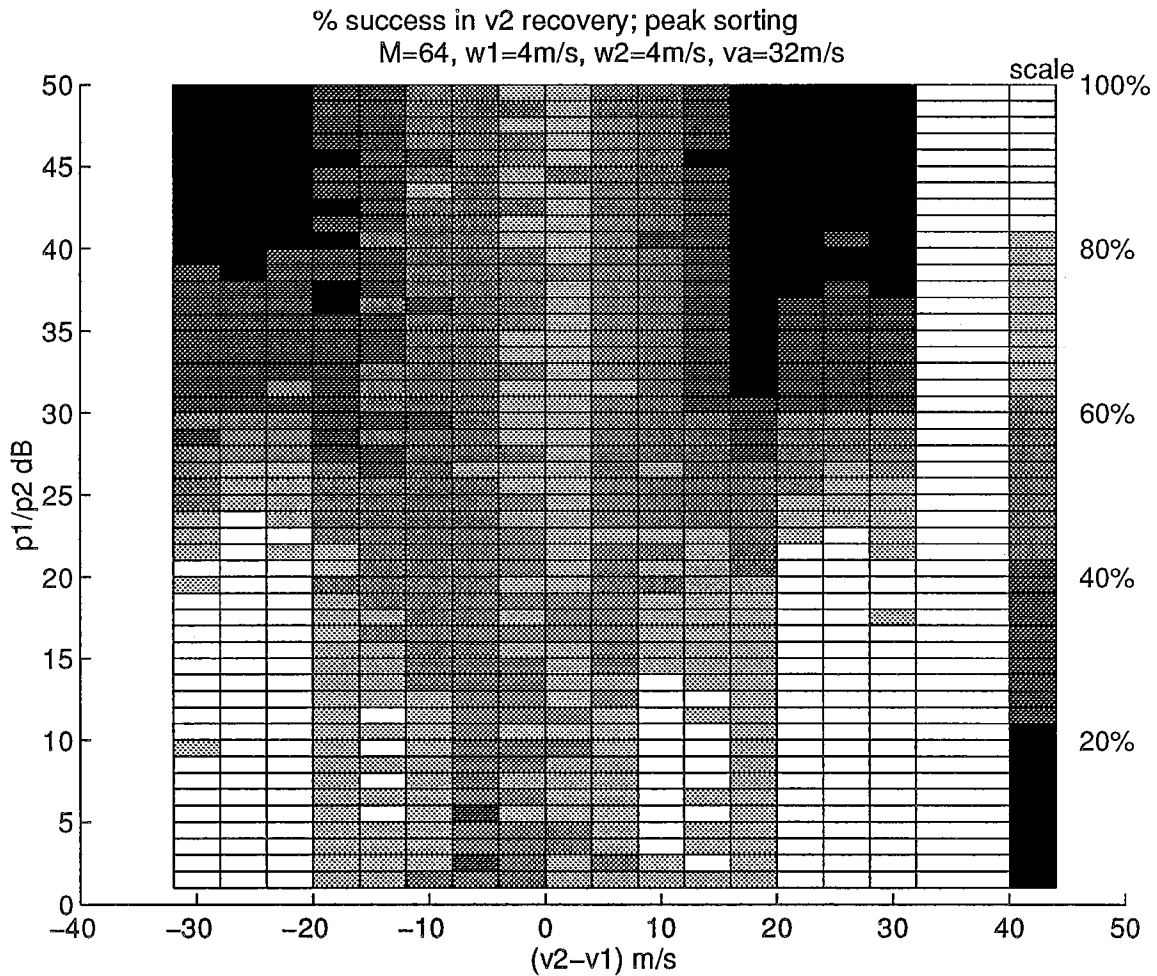


**Fig. 3.4.** Rate of success in the recovery of  $v2$  as a function of  $(v1-v2)$  and  $p1/p2$  for  $w1 = 4 \text{ m s}^{-1}$  and  $w2 = 4 \text{ m s}^{-1}$ . The peak sorting algorithm was used to recover the velocity,  $v2$ , from a simulated overlaid time series. Each rectangle is the percentage success obtained in 100 simulation runs with input parameters given along the axes. The gray shade scale at the right indicates the quantized value.

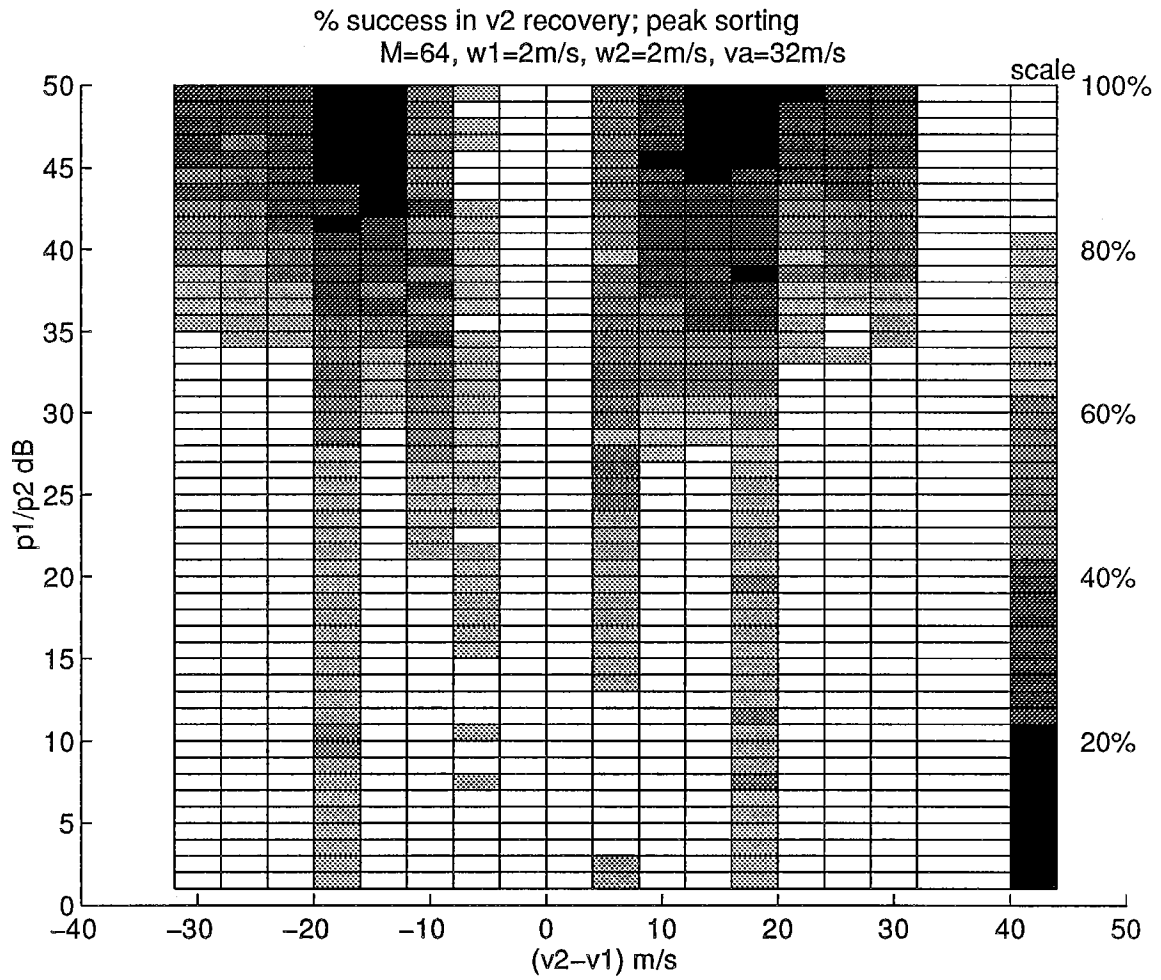


Fig. 3.5. Rate of success in the recovery of  $v2$  as a function of  $(v1-v2)$  and  $p1/p2$  for  $w1 = 2 \text{ m s}^{-1}$  and  $w2 = 2 \text{ m s}^{-1}$ . (similar to Fig. 3.4. for narrower spectrum width).

rate of success is quantized, and a gray shade is assigned to each cell. The gray scale at the right shows the values. A similar set of data generated for both signals with  $2 \text{ m s}^{-1}$  width is shown in Fig. 3.5, where the success rate is considerably higher. However, Fig. 3.4 is more representative of the results that can be expected in actual storms because  $4 \text{ m s}^{-1}$  is approximately the median width observed in severe storms (Doviak and Zrnic 1993, chapter 10). From Fig. 3.4, it can be concluded that approximately 50 percent success can be obtained if the power ratio is below 20 dB. This is not a significant improvement, nevertheless the velocity of at least the stronger signal is nearly always recovered. This accounts for at least 50 percent improvement in removing the purple haze in the first two-trip range interval. There is always an uncertainty in the recovered velocity of the weaker signal.

### 3.5. Conclusions.

The peak sorting technique presented in this section does not use coding. The radar is operated in the dual PRT mode, a long PRT scan followed by a short PRT scan, as done in the WSR-88D. The peak sorting algorithm uses the mean velocity and spectrum width estimates from the long PRT scan data, in addition to the reflectivity (or mean power) estimates. The long PRT scan data is used in assigning correct ranges to the recovered velocities based on the spectral power estimates. The algorithm is able to recover the velocity of the stronger of the 1st and 2nd trip signals nearly 100 percent of the time, and the weaker one if the velocity difference is large and the power ratio is less than 20 dB. There is an uncertainty in the recovered velocity of the weaker signal which cannot be removed easily. Therefore, we cannot use the weaker signal velocity confidently all the time.

Since the stronger signal velocity is always recovered correctly, the peak sorting algorithm can remove 50 percent of the purple haze from the 1st and 2nd unambiguous range intervals.

## 4. RANDOM PHASE CODING

### 4.1. Introduction.

The random phase method was first conceived for reducing the ground clutter contamination of the second-time-around weather echoes (Zrnic 1979; Laird 1981). Later, it was proposed as a method for separating the overlaid echoes (Siggia 1983). A detailed investigation was carried out by Zrnic and Mahapatra (1985), who also made a comparative study of the staggered PRT technique and the random phase technique.

In the random phase technique, the transmitted pulses are phase coded in a random sequence. The phase sequence is digitally stored and is used for recohering the return signals by appropriately correcting for the phase shifts incorporated during the transmission. The main idea behind the scheme is that when a sample sequence is phase shifted randomly, the resulting spectrum would be like a white noise spectrum. Thus, when a sample sequence is cohered for the 1st trip signal, the overlaid second and higher order trip signals would appear as white noise and would not bias the velocity estimate. However, the signal-to-noise ratio (SNR) would be degraded due to the overlaid power appearing as noise (In this case, effective SNR would be the ratio of the coherent signal power to the whitened signal power plus noise). Further, the mean signal power and the spectrum width estimates would be biased. The estimated power will be the sum of the power from both trips, and the width would be larger because of the larger noise level. The time series can be cohered for any of the overlaid signals, and its spectral parameters can be recovered, provided the SNR is sufficiently high for that trip signal. Obviously, in any given situation, mean velocity of only the strongest of the signals can be recovered if no further processing is done. Zrnic and Mahapatra (1985) have given a procedure for adaptively filtering the stronger signal to improve the effective SNR of the weaker signal.

In the adaptive filtering procedure, the coherent stronger signal is filtered out using a variable width notch rejection filter, and then the remaining part is cohered for the weaker signal. This effectively improves the SNR for the weaker signal, and if it is sufficiently high, the mean velocity of the weaker signal can be estimated accurately.

The method outlined in this section is similar to that reported in Zrnic and Mahapatra (1985), but with some modifications and additional steps, to further improve the SNR of the weaker signal. The algorithm requires significantly more computations than the present autocovariance processor.

The additional hardware required at the radio frequency (RF) stage is a phase shifter in the transmit path (at low power level), to control the phase of the transmitted pulse. The WSR-88D radar has a built in 8-bit PIN diode phase shifter, which is used for calibration purposes. Thus, the additional changes required are some circuits for synchronizing the code, so that the received samples can be cohered correctly.

A random number generator can be used to select any one of the phase shifts for each pulse, or a well designed fixed random code sequence can be used repeatedly. The second option is preferable because of its simplicity in implementation, although statistically speaking, the first one performs marginally better than the second.

The WSR-88D uses a long PRT scan and a short PRT scan (360° in azimuth at low

elevation angles and alternate radials for  $2^\circ \leq \theta_e \leq 6.5^\circ$ ). The long PRT scan data processing can include spectrum width computation as well, and the short PRT scan data can be used for velocity recovery alone. This reduces the computation required in the random phase algorithm. However, in this section, the random phase algorithm is developed as a **stand alone** method (without using the long PRT data) to recover the parameters of echoes from both 1st and 2nd trips.

#### 4.2. Random phase coding and spectral parameter estimation.

In a random phase coded radar, the whitened spectra does not bias the velocity estimate, but it does contribute to the variance of the velocity estimate in the same way as noise affects the estimate. Further, from the short PRT data, it is also required to estimate the mean power and spectrum width of the signals involved. In our discussions, we assume that two signals are overlaid, and we wish to recover the parameters of echoes from both trips. It is not necessary to assume the 1st and 2nd trip signals alone, but echoes could be associated with any two trip signals. If more than two trip signals are overlaid, decoding becomes more complex. The algorithm developed is for two overlaid signals. We have included a small section on the possible extension of the method to multiple trips later in this report, but no algorithm is given. The often encountered situation is the 1st and the 2nd trip overlay, and if this situation can be solved, the effective range would be doubled without sacrifice of the unambiguous velocity.

There are several ways to obtain spectral parameters from the sample time series. In order to select the best way which can work over a wide range of signal parameters, we first examine the properties of the random phase modulated spectrum and its effect on the estimated parameters. Weather signal strengths can span a dynamic range of 80 dB. Therefore, to ideally double the range of the radar, we should be able to recover parameters of both signals even when their power ratio is as large as 80 dB. Assuming that the noise level of the receiver is well below the weakest of the weather signals, we essentially have a situation where one of the signals is coherent, and the other is noise-like because of random phase modulation. Therefore, the theory of recovery of spectral parameters in the presence of noise will give us the limits of performance if no further processing is done. If we assume that the 1st trip signal power is  $p_1$  and the 2nd trip signal power is  $p_2$ , the ratio  $p_1/p_2$  gives the SNR for the 1st trip and  $p_2/p_1$  for the 2nd trip, when they are coherent. Obviously, in any given situation, if the minimum SNR required is 3 dB, parameters of only one of the signals can be recovered, or none if  $p_1/p_2$  is within  $\pm 3$  dB.

Generally, the mean power or reflectivity, the mean velocity, and the spectrum width are the three parameters estimated from the time series using autocovariance processing. Of these, the mean velocity is the limiting factor and is the most difficult to recover when the signals are overlaid. For the meteorological community, the reflectivity and velocity information are more important than the spectrum width. Therefore, we first discuss the recovery of velocity and then go on to the other two parameters.

The velocity is generally estimated from the phase of the autocorrelation of the signal for one pulse lag denoted by  $R(1)$ . In the autocovariance processor,  $R(1)$  is estimated from the time series samples. It can also be estimated from the power spectral coefficients. If  $s_k$  are the spectral coefficients obtained by DFT operation, the autocorrelation is expressed as

$$R(1) = 1/M \sum_{k=0}^{M-1} |s_k|^2 \exp(j2\pi k/M) . \quad (4.1)$$

If the spectral coefficient envelope is flat (i.e.,  $|s_k|$  is a constant), then  $R(1)$  would be zero. The random phase technique achieves this by whitening the spectrum. Therefore, the effectiveness of the random phase technique in removing the bias error in velocity estimate (i.e., in the argument of  $R(1)$ ) is determined mainly by the flatness of the spectrum that can be achieved. The bias error will depend on how small the  $|R(1)|$  is with respect to the  $|R(1)|$  of the other coherent signal, whose velocity we are trying to estimate. A measure of suppression of the overlaid signal for the velocity estimation can be obtained by calculating the ratio of magnitudes of  $R(1)$  before and after random phase modulation. Ideally, this ratio should be infinity. However, for finite length pseudo-random sequences, the achievable ratio is also finite and depends on the choice of the code sequence as well as the signal, especially its spectrum width. For a very narrow spectrum, it depends only on the code. The intrinsic suppression ratio of a code can be defined as the ratio of the mean power to the autocorrelation for lag one for the code itself. This is the same as the suppression ratio when the signal spectrum has a single coefficient (the spectrum of a single sinusoid). For a 64 length code, the best intrinsic suppression ratio that could be achieved is about 17 to 20 dB and is the upper bound for the suppression ratio. The upper bound is finite because we cannot achieve a perfectly flat spectrum. There are systematic codes which have perfectly flat spectra which are discussed later in this report (see Section 5). A simulation study shows that the suppression ratio decreases with increasing spectrum width (Fig. 4.1). In carrying out this simulation, first a search was made to obtain a random phase code with the largest intrinsic suppression ratio achievable practically. A random number generating program was used to generate the code (for  $M=64$ ) repeatedly, and its suppression ratio was computed. The code with the largest intrinsic suppression ratio was stored on the disk and was used in phase coding the weather signal and generating the scattergram shown in Fig. 4.1. With this fixed 64 sample pseudo-noise sequence having an intrinsic suppression ratio of 17 dB, the suppression ratio for the weather signal can lie anywhere between 4 to 25 dB, with a mean value between 8 and 10 dB. With longer code lengths, a small improvement can be obtained, as can be seen from the results of another simulation study shown in Fig. 4.2, for a 256 sample length random code. Therefore, autocovariance processing along with random phase coding is not sufficient to extract velocity over a wide dynamic range of overlaid signals.

Bias error in velocity is not the only problem when overlaid signal is present. While whitening removes the bias error, it introduces larger variance in the velocity estimate because of the overlapped spectrum. The acceptable variance is about  $1 \text{ m s}^{-1}$ , and to achieve this over a large dynamic range of the signal strengths, it is necessary to separate the signals. Adaptive filtering is one way of partially removing one of the signals, the stronger one, from the spectrum. Assuming the mean velocity of the stronger signal is known, a major part of the stronger signal can be removed by a notch rejection filter centered on the mean velocity. The remaining part, when cohered for the weaker signal, will have an improved SNR. It was shown by Zrnice and Mahapatra (1985) that only a part of the weaker signal remaining in the spectrum after notching

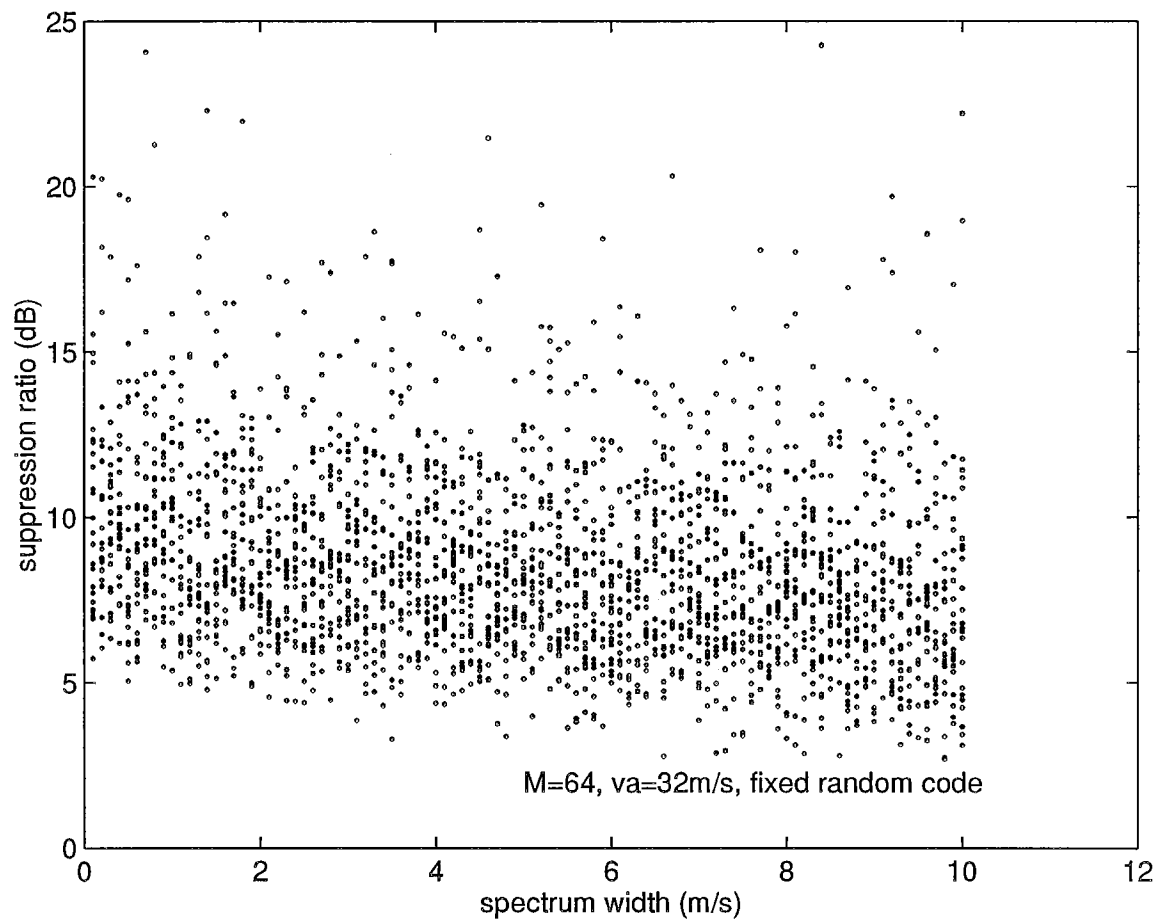


Fig. 4.1. Suppression ratio, the ratio of autocorrelation at lag 1 before and after coding expressed in dBs, obtained with simulated spectra and a 64 sample fixed random phase code as a function of spectrum width.

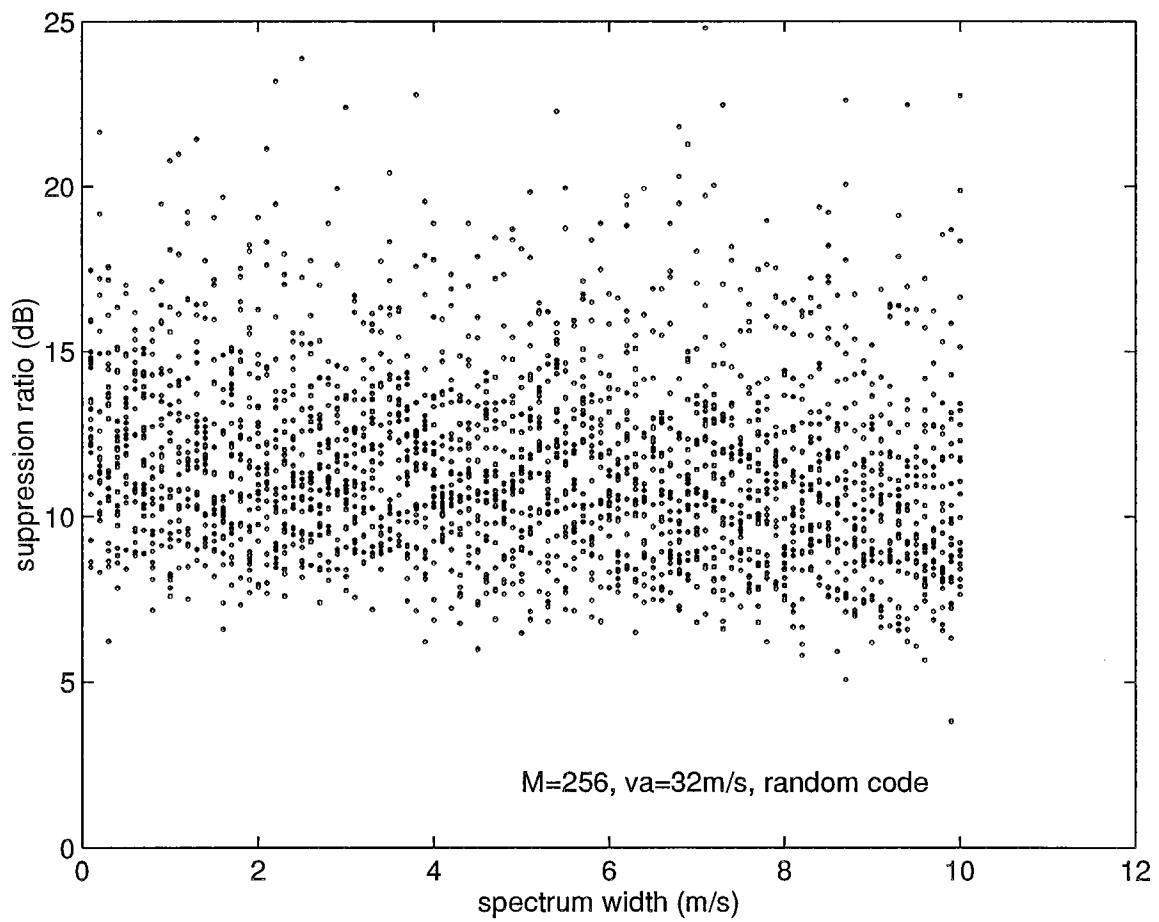


Fig. 4.2. Suppression ratio, as in Fig. 4.1, obtained with simulated spectra and a 256 sample random phase code.

becomes coherent. Thus, a self noise is generated by the notching process, and the residual of the stronger signal also turns into white noise due to random phase modulation.

To further improve the SNR of the weaker signal, one more step of processing is introduced. In this step, **the magnitude** of the spectrum, obtained after notching and cohering, is smoothed by a running average filter of sufficient length, and then thresholding is done to remove the noise floor. In a thresholding procedure, a constant threshold value is subtracted from all the coefficients. This requires a determination of the threshold value for each spectrum. Here, we adopt a new technique in which the magnitudes of two spectral coefficients, one at  $k$  and the other at  $(k+M/2)$ , are taken at a time, and the lower of the two is subtracted from both. This process is repeated for  $k=1,2,\dots,M/2$ , thus, 50 percent of the coefficients are zero. The resulting spectrum is a "thresholded" version of the weaker signal spectrum. From this spectrum,  $R(1)$  can be obtained, and the velocity can be estimated. This last step is termed smoothing and subtraction (S&S).

The S&S operation needs some explanation. The smoothing operation makes the spectrum flat when there is only white noise, and the signal appears as a raised portion above the noise envelope, provided the SNR is not too small. The subtraction removes the flat noise part of the spectrum. The smoothing could be carried out on the spectral coefficients raised to any power (i.e.,  $|s_k|^r$ ). While  $r > 1$  increases the ratio of maximum to minimum coefficient, as well as the fluctuations in the spectrum,  $r < 1$  decreases it. The best value of  $r$  is the one that reduces the fluctuations and increases the ratio of maximum to minimum coefficients. Obviously, these two are conflicting requirements, and we have to arrive at some compromise value of  $r$  which allows us to recover the weaker signal most successfully. From the results of a large number of simulation studies, the value of  $r$  was chosen to be 1.

It is instructive to examine how the white noise affects the spectral parameter estimates,  $p_2$ ,  $v_2$ , and  $w_2$ . In the absence of the 1st trip signal, the bias in  $p_2$  is exclusively due to the white noise power. The width estimate would be biased if eq. (2.6) is used. We could use an alternate width estimator that depends on the  $R(1)/R(2)$  ratio, which is not biased by the white noise (see Doviak and Zrnicek 1993, eq. 6.32). The autocovariance estimate of the velocity is unbiased but the variance,  $\text{var}(v_2)$ , increases with decreasing SNR.

The above discussion pertains to the white noise. In the case of random phase coded radar signal, the noise consists of the whitened 1st trip signal plus the self noise generated by the notch filtering process (assuming that the system noise is zero), which may have "white" and "non-white" part. The S&S process removes the smoothed "white" part and some part of the "non-white" noise which has the same magnitude envelope in the left and right half of the spectrum (we will refer to this part as the matched part). The part of the noise removed by the S&S process is largely the part that does not contribute to the autocorrelation  $R(1)$ , hence would not improve the  $\text{var}(v_2)$  significantly. In other words, the autocovariance method of  $v_2$  estimation automatically removes this part of the noise. Hence, the S&S step may not be necessary, as far as the velocity estimation is concerned. However, the width estimate would be significantly improved by this step. It may be noted that the alternate width estimator (Doviak and Zrnicek 1993, eq. 6.32), is unbiased in the presence of white noise alone. The S&S process removes the matched part of the "non-white" noise in addition to the "white" part, thus, improving the width estimate. Therefore, the S&S step is included in the algorithm. This step marginally improves the velocity recovery also (the recoverable limit of  $p_1/p_2$  is about 3 to 5 dB less without the S&S

step).

Some residual spectral power spread across the recovered spectrum that remain are actually not part of the weaker signal spectrum. These are due to the unevenness of the whitened spectrum, that may increase the error in the velocity estimate. To mitigate such errors, one more step is added. This step is needed only when the  $p1/p2$  and spectrum width are large, but is retained all the time. In this step, an approximate mean velocity is computed from  $R(1)$ , and then the spectral coefficients, over only a third of the spectrum centered on this approximate velocity, are used to compute a more accurate velocity estimate (by recomputing  $R(1)$ ). This, however, limits the recovery of spectrum width information when the actual spectrum width is large. It is a choice between overestimation and underestimation of spectrum width. The last step underestimates the width when the actual width of the weaker signal is large, and without the last step, the width is overestimated because of the residual spectral coefficients which do not belong to it.

How large the ratio  $p1/p2$  can be for which velocity  $v2$  can be recovered, depends on the SNR achieved after notch filtering. There are two parts to the noise remaining in the cohered spectrum after notching. One is the self noise, and the other is the residual of the stronger signal. With increasing notch width, the SNR due to the self noise decreases, whereas the SNR due the residual from the overlaid signal increases. Optimum width is the one for which largest "overall SNR" is achieved. This optimum point is a function of the width of the overlaid stronger signal as well as the ratio  $p1/p2$ . Fig. 4.3(a) is generated using an equation for the overall SNR (Zrnich and Mahapatra 1985, Eq. 30), for  $p1/p2=30$  dB. For a Gaussian shaped signal this equation can be expressed as

$$\text{overall SNR} = (1-n_w)^2 / \{ n_w(1-n_w) + [1 - \text{erf}\{v_a n_w / (w1\sqrt{2})\}](p1/p2) \}, \quad (4.2)$$

where  $n_w$  is the normalized notch width (normalized with respect to  $M$  or  $2v_a$ ), and  $\text{erf}\{\}$  is the error function. It shows that there is an optimum notch width for which SNR is the maximum, for a given spectrum width and  $p1/p2$ . Note that for a notch filter width larger than the optimum width, the SNR follows the asymptotic curve  $10\log_{10}\{(1/n_w) - 1\}$  dB, which is the SNR due to the self noise alone. The optimum notch width increases with increasing spectrum width and increasing  $p1/p2$  (Fig. 4.3b). However, for large spectrum widths the optimum notch width starts to decrease.

It is clear from Fig. 4.3(a) that for  $n_w = 0.5$ , the maximum SNR is 0 dB, thus is the upper limit for the  $n_w$ , assuming that SNR=0 dB is required for velocity recovery. This is about the optimum notch width for  $w1=4$  m  $s^{-1}$ . For larger spectrum widths SNR would be less than zero. The  $\text{var}(v2)$  for SNR=0 dB is between 1 and 2 m  $s^{-1}$  for spectrum widths between 1 and 8 m  $s^{-1}$  (Doviak and Zrnich 1993, Eq. 6.21). Although the residual 1st trip signal power decreases faster than the increase in the self noise power, as a function of notch width, the SNR due to the self noise alone puts a limit on the maximum usable notch width. In the random phase algorithm a notch width of  $M/2$  coefficients is selected which gives  $\text{var}(v2)$  within tolerable limit (i.e.,  $\text{sd}(v2) < 1$  m  $s^{-1}$ ) for  $M=64$  and  $w2=4$  m  $s^{-1}$ .

The SNR due to the residual overlaid power is a function of the spectrum width as well as the ratio  $p1/p2$ . We define the residual power ratio,  $R_p$ , as the ratio of the total power,  $p1$ , to the residual power after notching. The notch is centered on the peak of the spectrum. The  $R_p$  for

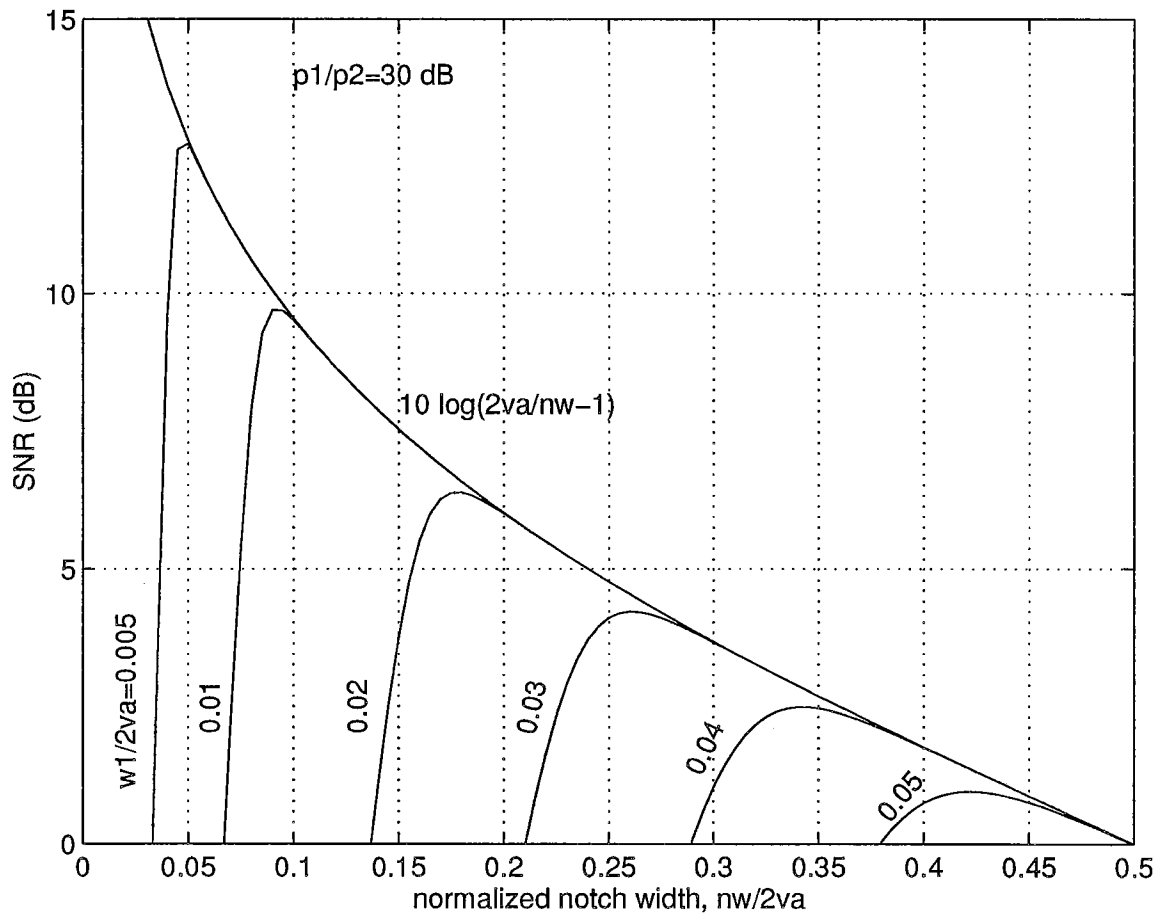


Fig. 4.3(a). SNR versus normalized notch width, computed using eq. 4.2.

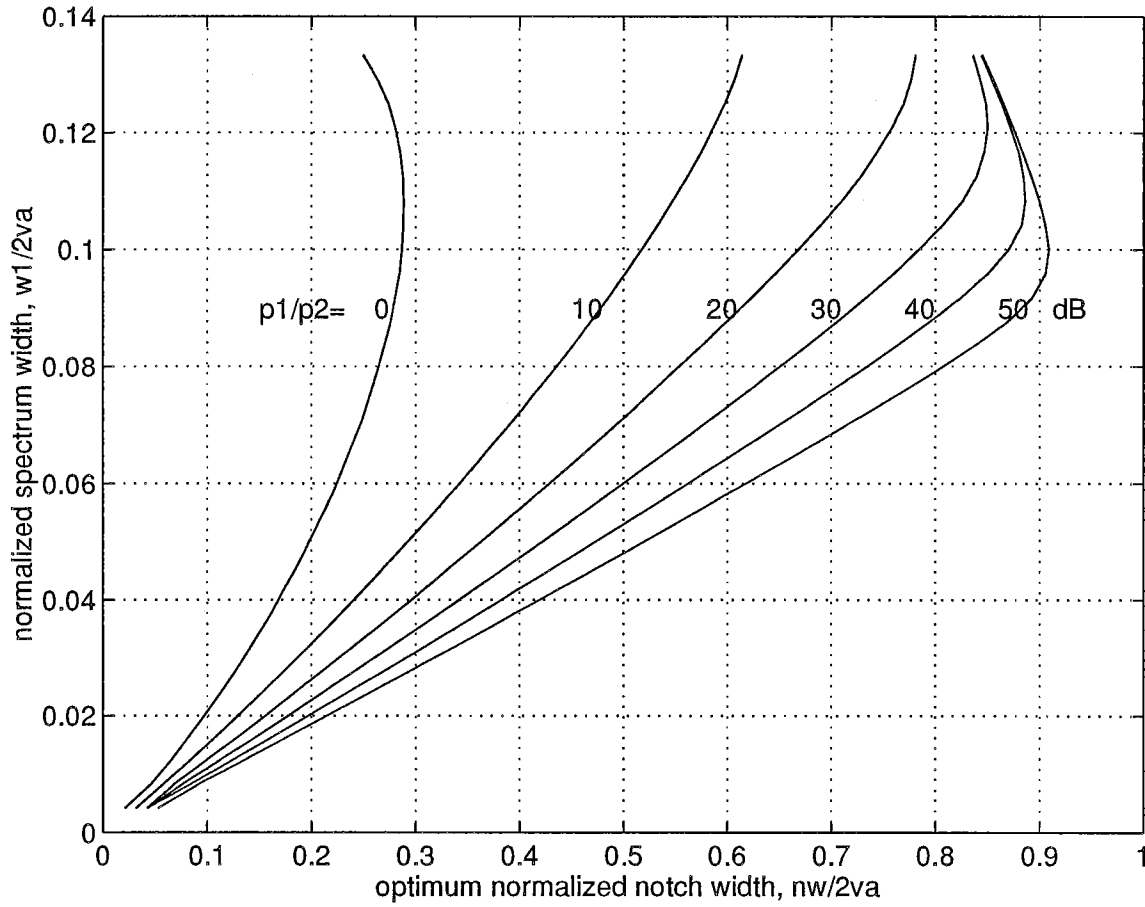


Fig. 4.3(b). Optimum notch filter width for which maximum SNR is achieved computed using eq. 4.2.

different notch widths is computed for a Gaussian shaped signal spectrum, and is shown in Fig. 4.4.

At the limit  $p1/p2=R_p$ , the overall SNR is about -7 dB for the weaker signal with  $M/2$  notch width ( $10 \log_{10}\{(1-n_w)^2/[1 + n_w(1-n_w)]\}$ ). Thus, the upper limit of  $p1/p2$  for which  $v2$  can be recovered is 7 dB below the  $R_p$  for  $n_w = 0.5$ . The S&S process improves the SNR by about 3 to 5 dB, which allows us to recover  $v2$  over 3 to 5 dB larger values of  $p1/p2$  than that given by  $(R_p-7)$  dB. For a given notch width, the SNR (eq.4.2) falls sharply for  $p1/p2>R_p$ , which increases the variance of the velocity  $v2$ . If the  $n_w$  is small, then SNR is larger for  $p1/p2<R_p$ , which gives lower variance of  $v2$ , but the upper bound of  $p1/p2$ , up to which velocity can be recovered is also lower. Hence an overall optimum  $n_w$  (assuming a fixed notch width) is the one for which  $\text{var}(v2)$  is the largest tolerable value; and this maximizes the extent of  $p1/p2$  for which  $v2$  can be recovered. In practice the limit  $p1/p2=R_p$  may not be achievable because it is actually dictated by the "whiteness" of the randomized spectra. The simulation studies have shown that one can achieve a limit fairly close to that expected.

By increasing the notch width, we can increase the limit of  $p1/p2$ . However, this improvement is at the expense of an increased variance in the recovered velocity. A simulation study, with  $n_w=0.75$ , showed that the limit for  $p1/p2$  is the same as that given in Fig. 4.4 (dashed curve), but with a  $\text{var}(v2)$  between 2 and 3  $\text{m s}^{-1}$  with  $M=256$  samples. For a practical value of  $M=64$ ,  $\text{var}(v2)$  is too large to be useful. For  $M=64$ , the notch width of  $M/2$  is nearly the optimum value.

Next, we turn to reflectivity or the mean power estimation. The total power is the sum of the powers of the two signals. Random phase modulation changes the distribution of power across the spectrum (whitens the spectra). It may be noted that the spectrum of the weaker signal, recovered using the steps explained in the previous paragraph, can be used for mean power estimation. But this does not give a very accurate mean power estimate because of the non-linear steps involved which do not preserve the power. The S&S are not operations that preserve the power in the spectrum. The processing loss, however, can be approximately determined and corrected. The processing loss is a function of the smoothing filter length and the "whiteness" achieved by random phase modulation. The variability in the correction is mainly because of the second factor.

Because of these reasons, an alternative approach is used to estimate mean power. Assuming that the random phase modulation produces a white spectrum, any small part of the spectrum, where the coherent signal is absent, can be used to estimate power. In this approach, a fourth of the spectral coefficients farthest from the mean velocity of the stronger signal are used to estimate the weaker signal power. When the stronger signal is coherent, this part has the least amount of power from the stronger signal. Weaker signal recovery is limited by the contribution of the stronger signal to this part of the spectrum. For a Gaussian spectrum with a width of 4  $\text{m s}^{-1}$ , the reflectivity of the weaker signal can be recovered even when the overlaid signal is as large as 88 dB above the weaker one. (See  $R_p$  versus spectrum width curve for  $3M/4$  notch width in Fig. 4.4.) This ratio degrades rapidly with the width of the spectrum. At 8  $\text{m s}^{-1}$ , it is about 26 dB. Comparing this limit to that for velocity recovery, it can be concluded that the velocity recovery is the limiting factor.

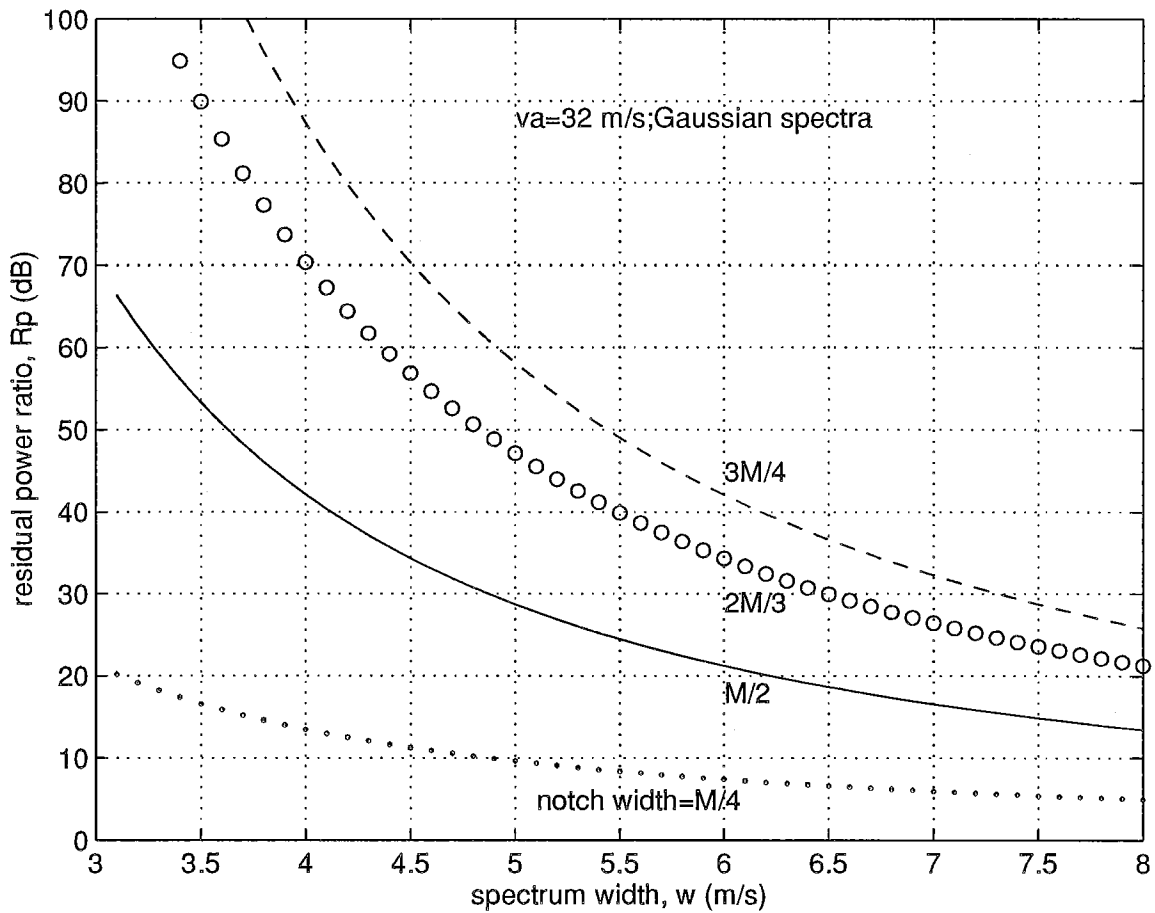


Fig. 4.4. The residual power ratio,  $R_p$ , as a function of notch filter width (in terms of the number of spectral coefficients  $M$ ) for Gaussian signal spectra.

At the outset, it appears that the variance of the reflectivity estimate using only a fourth of the coefficients would be larger than that obtainable with all the samples. However, this is not the case because the random phase modulation distributes the spectral power more or less uniformly over the spectrum, and information contained in all the spectral coefficients is embedded in each of the coefficients via the transformation. Therefore, the variance of the estimate is not degraded significantly by reducing the number of coefficients (degradation is not as much as that expected for  $M/4$  samples). For a large spectrum width of the stronger signal ( $wl$  large), the residual power from the stronger signal adds to the estimated power,  $p2$ , thus producing a bias error in the estimate. This can be calculated for a Gaussian signal and is shown in Fig. 4.5. If  $\pm 1$  dB is the allowable bias error in the  $p2$  estimate, the upper limit for the overlay ratio,  $p1/p2$ , for  $p2$  estimation, can be obtained from Fig. 4.5 at the 1 dB level. This limit is greater than 70 dB for a width of  $4 \text{ m s}^{-1}$ , and drops to about 20 dB for  $8 \text{ m s}^{-1}$ .

The mean power,  $p1$ , of the stronger signal can be taken as the total power in the spectrum when  $p1/p2 > 20$  dB. If  $p1/p2 < 20$  dB, the bias error in  $p1$  can be removed by subtracting the power  $p2$ . As far as the stronger signal parameters are concerned, the autocovariance processor is sufficient to recover all three parameters because  $p2$  is whitened. The performance will be the same as that of a signal in the presence of noise, with a  $\text{SNR} = p1/p2$ . When  $p1/p2 < 20$  dB, the variance of the velocity estimate,  $v1$ , increases and there is a bias error in width  $w1$ . The variance of  $v1$  is tolerable for  $M=64$  samples.

There are two ways to get accurate  $w1$  estimates with no bias error. One way is to estimate the bias error in width  $w1$ , using the autocovariance processor, and an empirical formula for the bias error correction can be derived and incorporated in the algorithm. Another way is to use the  $R(1)/R(2)$  ratio to estimate the width which is known to be unbiased (Doviak and Zrnic 1993, p. 138, eq. 6.32). However, this requires computation of  $R(2)$ , and also the width estimate has a slightly larger variance than the estimator using the  $p1/R(1)$  ratio (Doviak and Zrnic 1993, Eq. 6.27). In the algorithm presented in this report, the empirical error correction formula approach has been used because it is more accurate and needs less computation. To obtain the empirical correction formula, a large number of simulations were run with different widths and power ratios, and a polynomial fit to the error in the estimated  $w1$  was obtained, as shown in Fig. 4.6. The correction in terms of this polynomial fit is incorporated in the algorithm. Note that the error is a weak function of spectrum width,  $w1$ , but is a strong function of the power ratio; therefore, after removing the bias, the variance of the  $w1$  estimate is larger for lower  $p1/p2$ .

### 4.3. The choice of code.

As discussed in the previous section, the effectiveness of the random phase technique in removing the overlaid signal depends on the "whiteness" achieved by random phase coding, and the "whiteness" is a function of the code as well as the signal spectrum. The power removed by the S&S process gives us an idea of the effectiveness of the random phase technique. But this power does not contribute to the autocorrelation  $R(1)$ . Since the signal is not under our control, the best we can do is to select a code with as flat a spectrum as possible. A random number

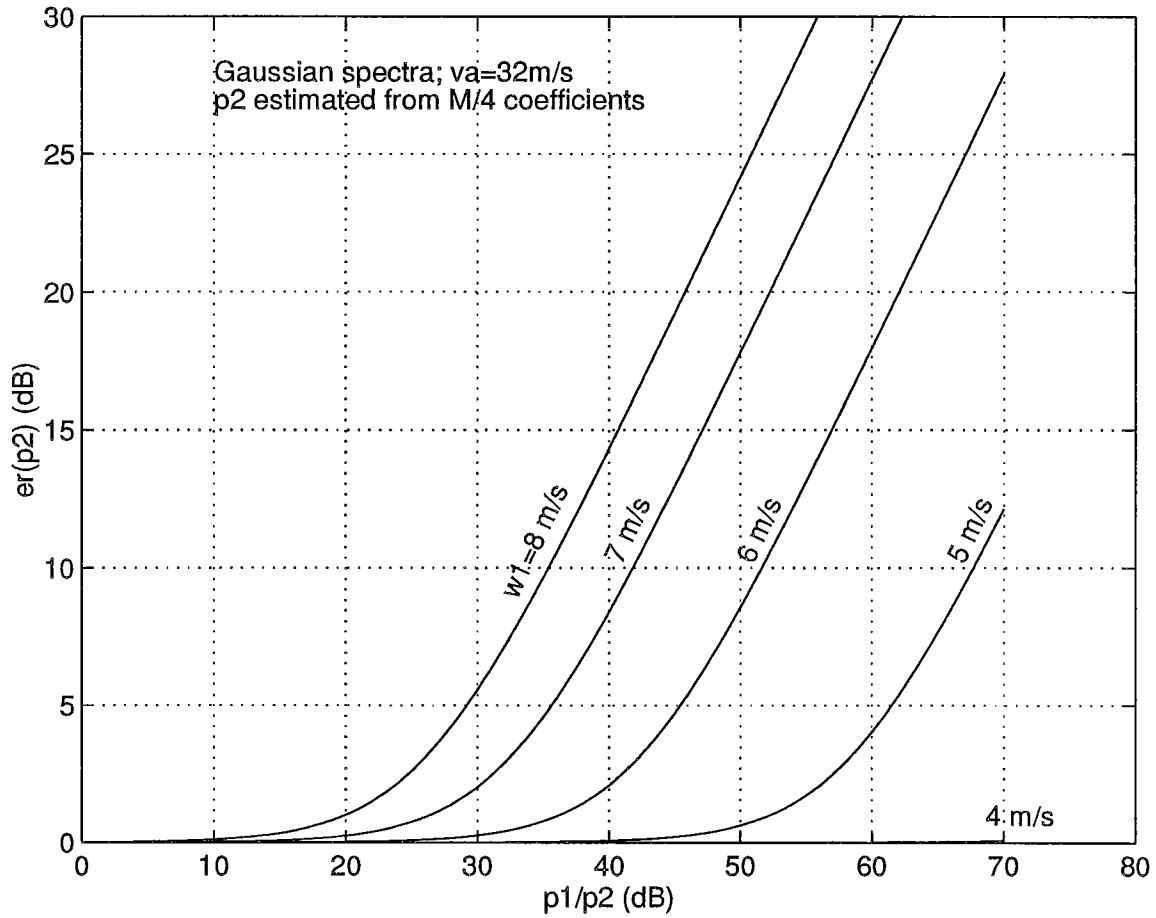


Fig. 4.5. Bias error in the mean power,  $p_2$ , of the weaker signal estimated from a fourth of the spectral coefficients farthest from the mean velocity of the stronger signal,  $v_1$ , shown as a function of overlaid power ratio  $p_1/p_2$ . Gaussian signal spectra is assumed. Spectrum width of the stronger signal,  $w_1$ , is shown as a parameter.  $M=64$ ;  $1 \leq w_1 \leq 8 \text{ m s}^{-1}$ .

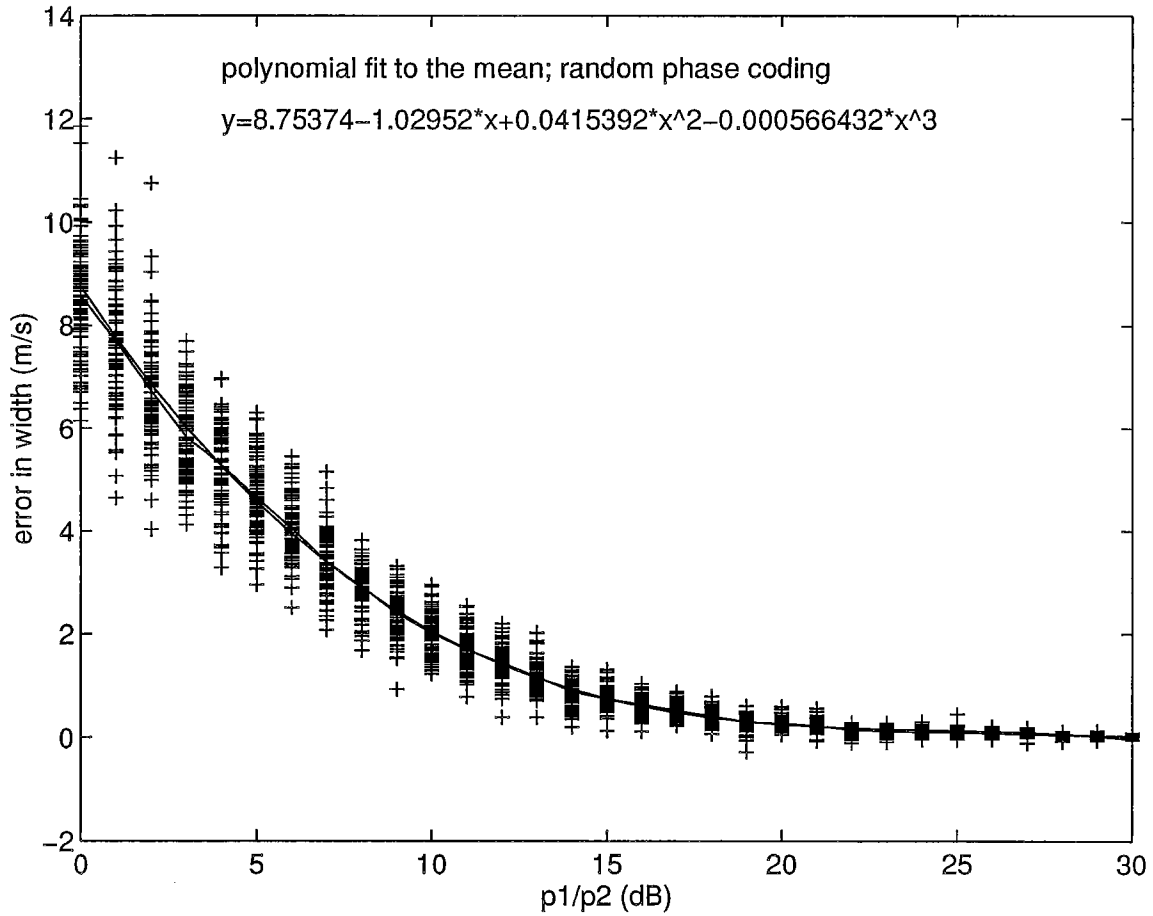


Fig. 4.6. Bias error in the spectrum width of the stronger signal estimated using autocovariance processing, shown as a function of overlaid power ratio,  $p1/p2$ . The + symbols show the error obtained in 20 simulations at each  $p1/p2$  value. The mean curve is shown with a continuous line. A polynomial fit to the mean curve is also shown in the figure for  $v_a=32 \text{ m s}^{-1}$ .

generating program was used to assemble a code. The resulting residual power after notch filtering, as well as power after smoothing and subtraction, were examined for the code alone. The ratio of powers before and after the S&S process, termed the intrinsic rejection ratio, is a measure of the whiteness of the code for the present purpose. It must be noted that the ratio also depends on the running average filter length; therefore, it is necessary to study the behavior of the code with respect to the filter length. A large number of simulations were run, and the one with lowest residual power after the S&S was selected as the best code. Further, this code was used repeatedly to whiten simulated weather spectra, and then passed through S&S operation to evaluate the rejection ratio for different realizations of the weather spectra..

Fig. 4.7 shows a sample spectrum of a 64 bit code before and after the S&S operation with a smoothing filter length of 9 coefficients. The intrinsic rejection ratio for this code is 22 dB. Fig. 4.8 shows the rejection ratio achieved for simulated weather spectra as a function of spectrum width. The scattergram shows that the mean rejection ratio is about 17 dB.

Fig. 4.9 illustrates the S&S process on a weather signal. The first spectrum is the signal spectrum, and the second one is the spectrum after random phase modulation. Note that the power is not uniformly distributed over all the spectral coefficients. When smoothed using a running average filter, the envelope is nearly flat. After subtraction, most of the power is removed as seen in the last spectrum.

#### 4.4. Some sample spectra and illustration of processing.

To illustrate the processing in the spectral domain, simulated weather spectra have been used. Figs. 4.10(a) through (h) show the steps involved in the processing. Figs. 4.10(a) and (b) show the spectra of signal "a" and "b" with indicated spectral parameters. Note that the y-axis is appropriately scaled to show the signal. Fig. 4.10(c) shows the spectrum of the overlaid signal with random phase modulation. Signal "a" is coherent, and "b" is whitened. The processing steps illustrate the recovery of the weaker signal "b" from this composite signal. Note that with a  $p1/p2$  ratio of 30 dB, the second signal is barely visible on the same scale. In the spectrum in Fig. 4.10(d),  $M/2$  coefficients centered on  $v1$  have been deleted or notched. Here, the randomized second signal is visible on an expanded y-scale. The spectrum in Fig. 4.10(e) is obtained after cohering the signal "b" which shows up above the noise level. Fig. 4.10(f) shows the same signal after smoothing with a filter length of 13 coefficients. Fig. 4.10(g) is after subtraction of the lower of the two magnitudes from both sides as explained earlier in the S&S procedure. Fig. 4.10(h) shows the final recovered spectrum after the unwanted part has been deleted. This is the last step in which a third of the spectrum centered around the approximate mean velocity, computed from the spectrum given in Fig. 4.10(g), is retained and the rest is deleted. Compare this last spectrum to the envelope of the spectrum given in Fig. 4.10(b). Except for the loss of some tail ends of the original spectrum, the signal has been recovered well. It can be used to estimate the autocorrelation and thus the mean velocity and the spectrum width.

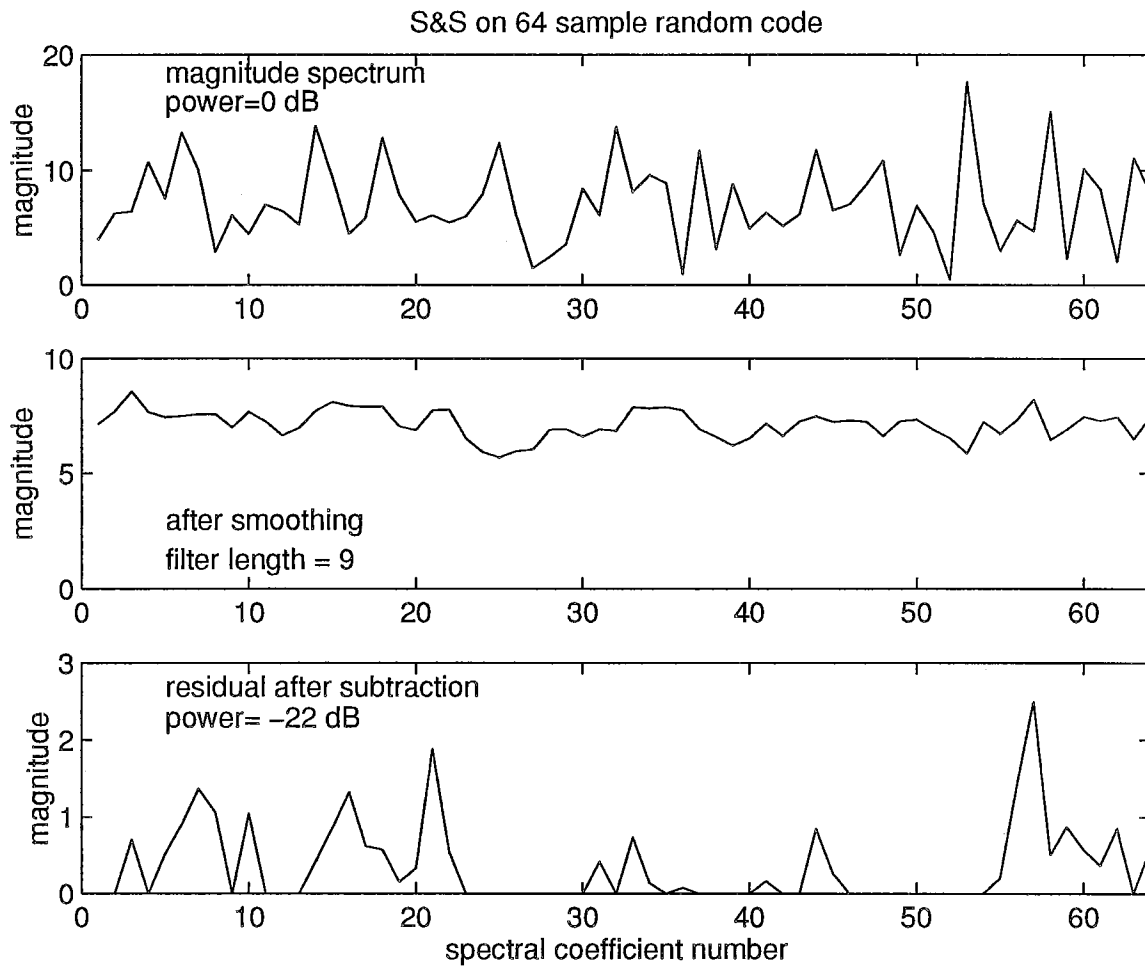


Fig. 4.7. The effect of smoothing and subtraction (S&S) on the spectrum of a 64 bit random code. The residual power after S&S is 22 dB below the original power.

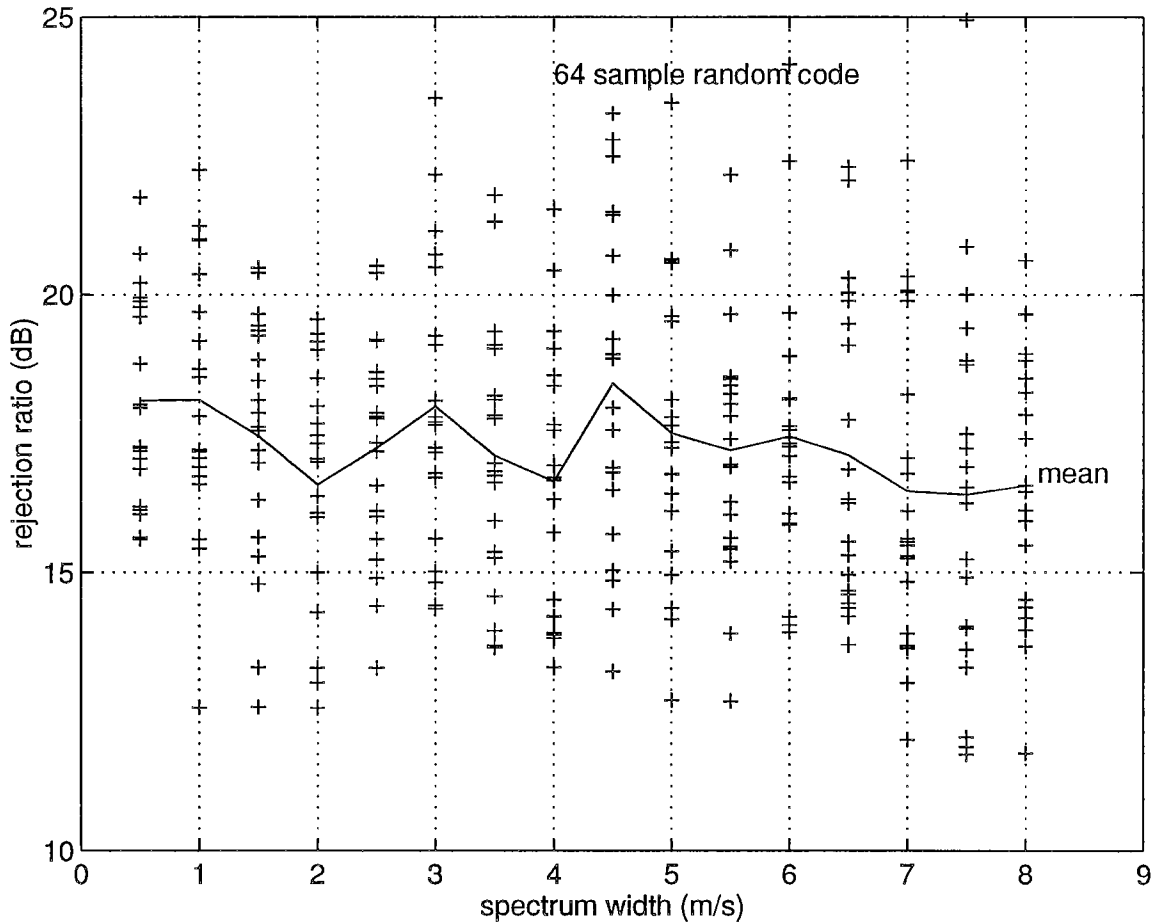
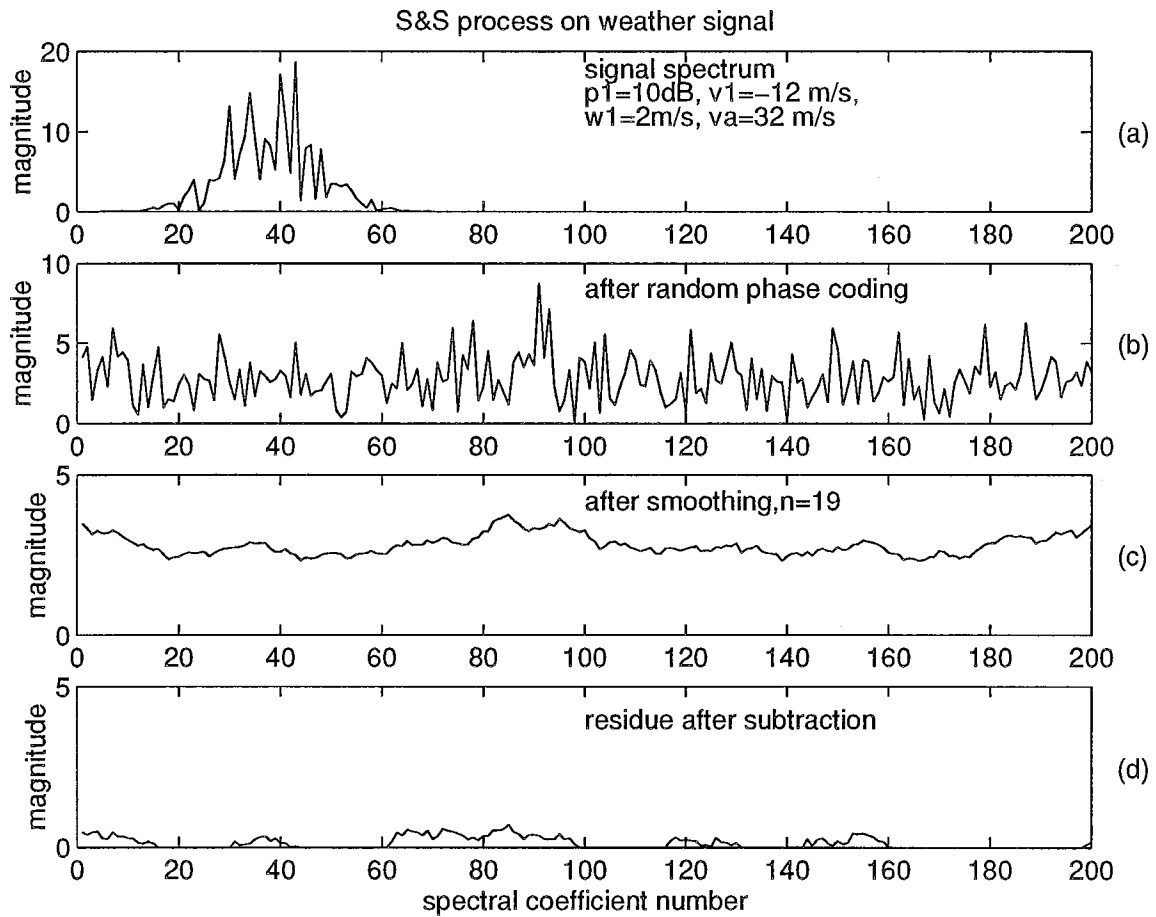
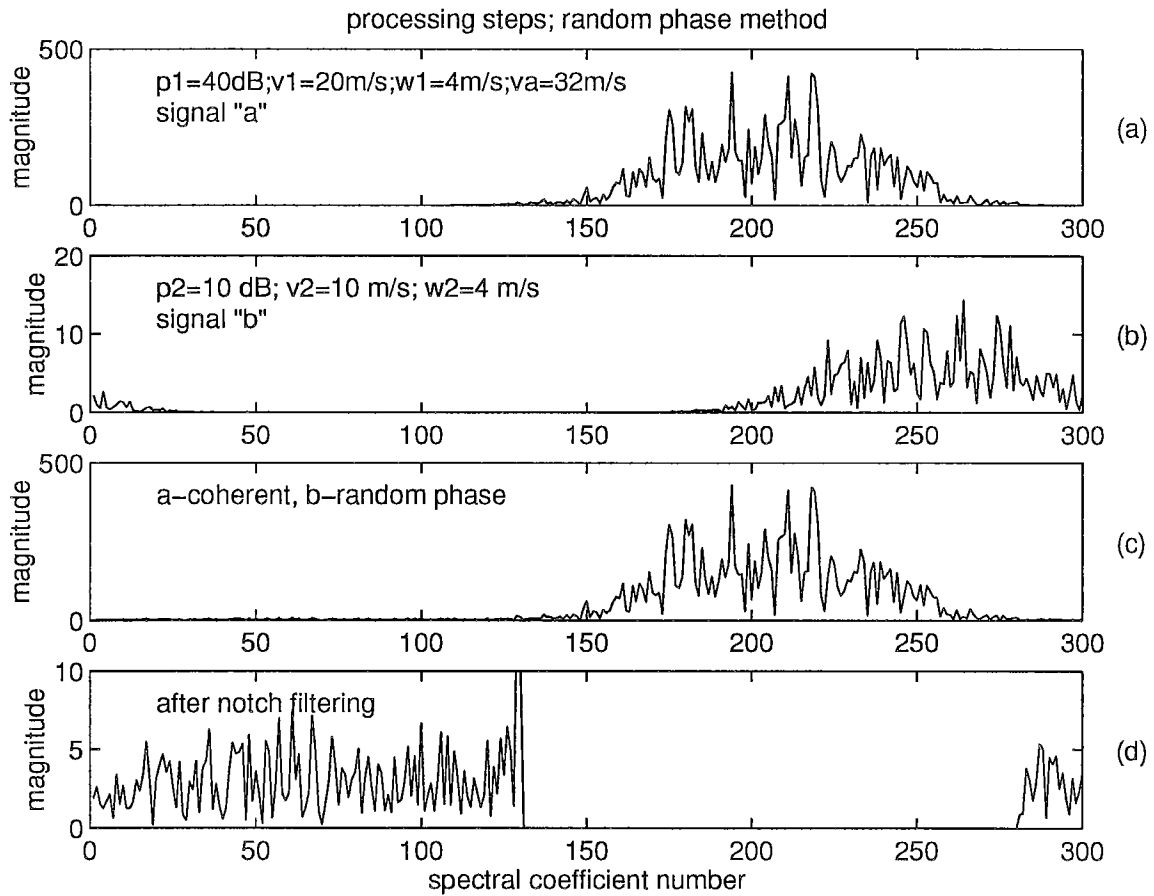


Fig. 4.8. The rejection ratio, the ratio of power in the random phase coded weather signal before and after the S&S process, expressed in dBs, as a function of width of the spectrum. Simulated weather signals are used with a 64 sample random phase code modulation ( $v_a = 32 \text{ m s}^{-1}$ ,  $n_w = 0.5$ ).



**Fig. 4.9.** The effectiveness of the S&S process on a weather signal. (a) simulated weather spectrum, (b) spectrum after random phase coding, (c) spectrum after smoothing, (d) spectrum after subtraction.



**Fig. 4.10.(a-d).** The processing steps in the random phase algorithm, using simulated signal. (a) & (b) strong and weak signal spectra separately, (c) spectrum of the signal from a random phase coded radar; one signal is coherent and the other is phase coded, (d) the spectrum after  $M/2$  coefficients centered on  $v_l$  are notch filtered.

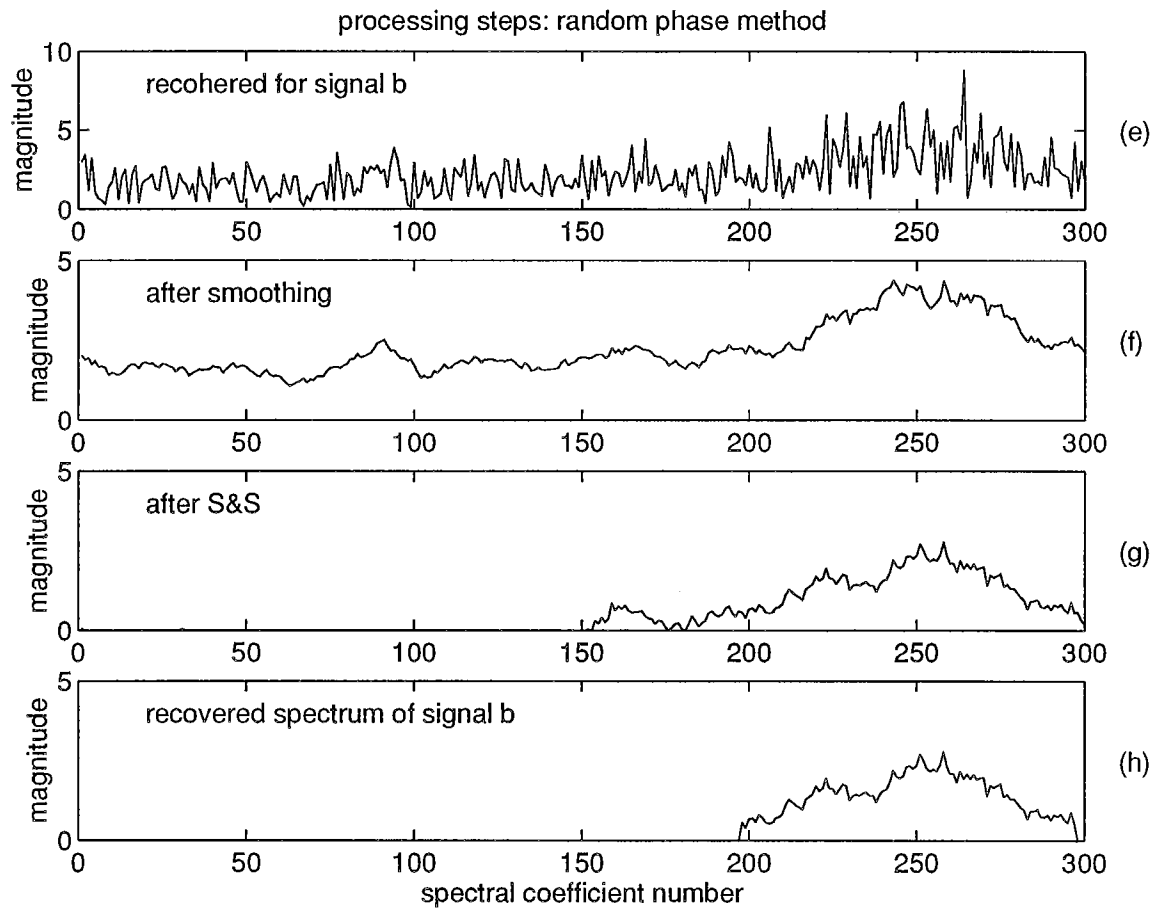


**Fig. 4.10.(e-h).** The processing steps in the random phase algorithm. (e) weaker signal is made coherent, (f) spectrum after smoothing, (g) spectrum after subtraction, (h) recovered spectrum after retaining only  $M/3$  coefficients around the approximate mean velocity,  $v_2$ .

For this illustration, a spectrum width of  $4 \text{ m s}^{-1}$  and a Nyquist velocity of  $32 \text{ m s}^{-1}$  was used. This is the median width encountered in severe storms. The recovery of the signal is not as impressive if we start with a wider spectrum for both signals.

#### 4.5. The random phase algorithm.

So far, the discussion has centered around the recovery of weaker signal parameters in the presence of a strong signal overlay. Several other aspects have to be considered for a practical algorithm. Assuming that we have only the 1st and 2nd trip signals present, we have to determine which one is stronger, to start the spectral processing. There is also the ground clutter in the 1st trip signal for low elevation scans which has to be removed. The ground clutter filtering is fairly straight forward because of the use of uniform PRT. The 1st trip signal in the time series is first cohered and then passed through a ground clutter filter. In the algorithm, this part is not implemented because ground clutter is not included in the simulated time series, but is required in a practical algorithm. After the ground clutter is filtered out, another time series is generated by cohering the 2nd trip signal. Now to determine which of the two trip signals is stronger, both are passed through the autocovariance processor, and the outputs of the autocovariance processor are mean powers,  $p1'$  and  $p2'$ , mean velocities,  $v1'$  and  $v2'$ , and spectrum widths,  $w1'$  and  $w2'$ . Of these,  $p1'$  and  $p2'$  are the same, and equal to the total power ( $p1+p2$ ). Depending on the power ratio, at least one of the velocities,  $v1'$  or  $v2'$ , is accurate. The spectrum widths, however, can be highly biased. Spectrum width of a whitened signal is as much as 0.7 to 0.8 times  $v_a$ . Note that this value is larger than the actual width of the white noise signal because it is estimated using the autocovariance algorithm which assumes Gaussian shape for the spectrum. (The correct width of the white noise spectrum is  $v_a/\sqrt{3}$ .) Therefore, the ratio  $w1'/w2'$  approaches  $1.25w1/v_a$  for large power ratio,  $p1/p2$ , and is equal to unity for  $p1/p2$  equal to unity. This is a convenient parameter for deciding which of the two signals is stronger. If one of the signals is 20 dB larger than the other, its parameters are accurately obtained from the autocovariance processor, and therefore, further processing needs to be carried out only to recover the other signal parameters. When the power ratio is less than 20 dB, the stronger signal parameters also get affected and need to be corrected, especially the mean power and the width.

The algorithm developed incorporates all these aspects and an appropriate logic to channel the computations. The computational steps with explanations are listed, and these can be easily translated into a computer program.

In simulating the time series, the assumptions stated in section 1.1 are made, and the algorithm given below is based on those assumptions. As stated earlier, *the algorithm does not use long PRT scan data*, and processing is done on the short PRT time series only. This algorithm is developed as a **stand alone** algorithm. In the lowest two elevation scans of the WSR-88D, the long PRT scan data can be utilized to compute  $p1$ ,  $p2$ ,  $w1$ , and  $w2$ , of the 1st and 2nd trip echoes. With this, many of the steps in the algorithm can be eliminated.

<<<-----START of algorithm

1. Input time series  $EI_k$ ;  $k=1,2, \dots M$ . (from short PRT scan)
  - ▶ 1st trip is coherent; 2nd trip is phase coded by a random phase sequence,  $\phi_k$ ;  $k=1,2,\dots M$ .
2. Cohere the 2nd trip signal.
  - ▶  $E2 = EI \exp \{-j \phi_k\}$
3. Autocovariance process  $E1$  and  $E2$  to get  $p1, v1, w1$  and  $p2, v2, w2$ .  
(output parameters are estimates; ^ symbol is omitted for convenience)
4. Compute  $w1/w2$  ratio.
  - ▶ if  $w1/w2 > 1$ , trip=2, 2nd trip is stronger - process  $E2$ .
  - ▶ if  $w1/w2 < 1$ , trip=1, 1st trip is stronger - process  $E1$ .
5. If  $w1/w2 > 1$ , interchange  $E1$  and  $E2$ , and all the parameters on line number 3.
  - ▶ with this interchange,  $E1$  is the time series with stronger signal coherent.
  - ▶ we need to recover  $p2, v2$  and  $w2$  of the weaker signal.[ Note: For the two cases in step 4, the processing steps 6 through 18 are the same with  $E1$  replaced by  $E2$ . This is accomplished by the interchange indicated in step 5. The trip numbers are restored in step 19.]
6. Compute spectrum of  $E1$ .
  - ▶  $SI' = \text{DFT} [ EI ]$
7. Notch  $3M/4$  coefficients centered on  $v1$  to get  $SI$  from  $SI'$ .
8. Compute mean power  $p$  from the remaining coefficients.  
Multiply  $p$  by 4 to get mean power  $p2$ .
9. Compute power ratio  $pr = 10 \log_{10}(p1/p2)$  dB.
10. If  $pr < 20$  dB, correct error in  $p1$  estimate.
  - ▶  $p1' = p1 - p2$
  - ▶ compute corrected power ratio  $pr = 10 \log(p1'/p2)$  (dB)
11. If  $pr < 20$  dB, correct the error in spectrum width  $w1$ .
  - ▶  $\text{err}(w1) = 8.75374 - 1.02952 pr + 0.0415391 pr^2 - 0.000566432 pr^3$   
This is polynomial fit to the error curve, with  $v_a = 32 \text{ m s}^{-1}$ .  
[For other values of  $v_a$  multiply all constants by  $(v_a/32)^{1.5}$  ]
  - ▶ corrected  $w1 = w1 - \text{err}(w1)$
12. Notch  $M/2$  coefficients centered on  $v1$  to get  $SI$  from  $SI'$ .

13. Cohere the weaker signal in  $S1$ .
    - ▶  $e1 = \text{IDFT} [ S1 ]$
    - ▶ if trip = 1,  $e2 = e1. \exp\{-j \phi_k\}$
    - ▶ if trip = 2,  $e2 = e1. \exp\{j \phi_k\}$
    - ▶ compute magnitude spectrum,  $q = | \text{DFT} [ e2 ] |$
  14. Apply smoothing filter to  $q$ .
    - ▶  $q = \text{SF}( q; m)$ ; (choose filter length  $m=9$  for  $M=64$ ).
  15. Subtract the residual stronger signal.
    - ▶  $a_k = \min \{ q_k, q_{(k+M/2)} \}$ ;  $k=1,2, \dots M/2$ .
    - ▶ subtract  $a_k$  from both  $q_k$  and  $q_{(k+M/2)}$ ;  $k=1,2, \dots M/2$ .
  16. Compute autocorrelation for 1 PRT lag,  $R(1)$  for  $q$ , and compute approximate mean velocity  $v2'$ .
  17. Delete coefficients outside  $M/3$  interval centered on  $v2'$ .
  18. Recompute  $R(1)$  and  $v2, w2$ .
  19. If trip = 2, interchange parameters  $(p1, v1, w1)$  and  $(p2, v2, w2)$
  20. Output the 1st and 2nd trip parameters and go to the next data set.
- <<<<-----END of algorithm

#### 4.6. Simulation and results.

To evaluate the performance of the algorithm given in Section 4.5, a test program was written which inputs a set of parameters for the 1st and the 2nd trip signals into the simulation program to generate an overlaid time series, and this time series is fed to the algorithm to recover the parameters. The recovered parameters are compared to the actual parameters of the two signals, which are computed individually by the autocovariance processor before mixing. It should be noted that the comparison is not done with the input parameters because there can be a difference between the input parameters and the autocovariance estimates for each realization due to several reasons such as aliasing, estimate variance due to spectrum width, etc. The above comparison separates these effects in evaluating the performance of the algorithm and gives us a measure of how good the estimates are with respect to the estimates normally obtained in the absence of overlaid signals.

A large number of simulations were conducted to determine the performance limits of the algorithm. Some sample scatter plots of the errors in the estimated parameters are given in Fig. 4.11 to 4.16. The power ratio,  $p1/p2$ , is varied over 0 to 70 dB, and the velocity difference,  $(v1-v2)$ , is randomly chosen for each simulation to be within  $\pm 28 \text{ m s}^{-1}$ . The unambiguous velocity,

$v_a$ , is taken to be  $32 \text{ m s}^{-1}$  with a PRT = 0.7812 ms. The velocities  $v1$  and  $v2$  are restricted to be less than  $v_a$  to avoid aliasing error appearing as estimation error. In Figs. 4.11 through 4.16, errors in  $v1$ ,  $v2$ ,  $p1$ ,  $p2$ ,  $w1$ , and  $w2$  are shown as a function of  $p1/p2$ . The spectrum widths are set to  $4 \text{ m s}^{-1}$  for both the signals. Each point on the plots corresponds to one simulation with  $M = 64$  samples. Note that the errors are computed with respect to the estimates obtained using the autocovariance algorithm on individual signals. This gives a false impression that for large  $p1/p2$ , the variance of  $v1$  estimate is zero (see Fig. 4.11, 4.13, 4.15). Actually, the variance is the same as that obtained with autocovariance processing in the absence of the overlaid signal. It can be observed that the error in the velocity,  $v2$ , (see Fig. 4.12) is the limiting factor as all other parameters can be recovered for larger  $p1/p2$  ratios. For  $4 \text{ m s}^{-1}$  width of the stronger signal,  $v2$  can be recovered up to about  $p1/p2 = 30 \text{ dB}$  with  $M = 64$ . The standard error is between 1 and  $1.5 \text{ m s}^{-1}$ .

Simulations were run with different values of  $w1$ , and the mean and standard deviations of the errors in recovered  $v2$  were computed and plotted for two values of  $M = 256$  and  $64$ . The standard error is higher for  $M = 64$  compared to that for  $M = 256$ . Fig. 4.17 shows standard deviation of error in  $v2$  as a function of  $p1/p2$  and  $w1$ , for  $M=256$ . It can be seen that the bounding value of  $w1$  and  $p1/p2$  which limit  $v2$  recovery is nearly that deduced from Fig. 4.4. A similar set of simulations were run with a notch filter width of  $3M/4$  in place of  $M/2$  in the algorithm, and the results are shown in Fig. 4.18. Again comparing this with Fig. 4.4 (dashed curve) for the limits of recovery of  $v2$  for  $3M/4$  notch width, we can see that the limit is indeed the theoretical value but with a higher standard error of about  $2 \text{ m s}^{-1}$ . Since  $M=256$  is not practical for the WSR-88D to maintain the present data rates, simulations were also run for  $M=64$ . The results are shown in Fig. 4.19. The standard error in  $v2$  is higher (about  $1.5 \text{ m s}^{-1}$ ) for  $M=64$ , with a notch width of  $M/2$ . At even higher notch widths and  $M=64$ , the error is not acceptable.

A somewhat improved algorithm would be one that adaptively sets the notch width based on the recovered  $w1$  and  $p1/p2$ . Both these parameters are accurately estimated in the region where  $v2$  is recoverable as per the limits given by Fig. 4.4. This is different from the adaptive notch width suggested in Zrnic and Mahapatra (1985), where notch width is selected based on  $w1$  alone. This, of course, would not increase the limit of  $p1/p2$  but can improve the standard error in the region of lower power ratios and narrower spectrum widths.

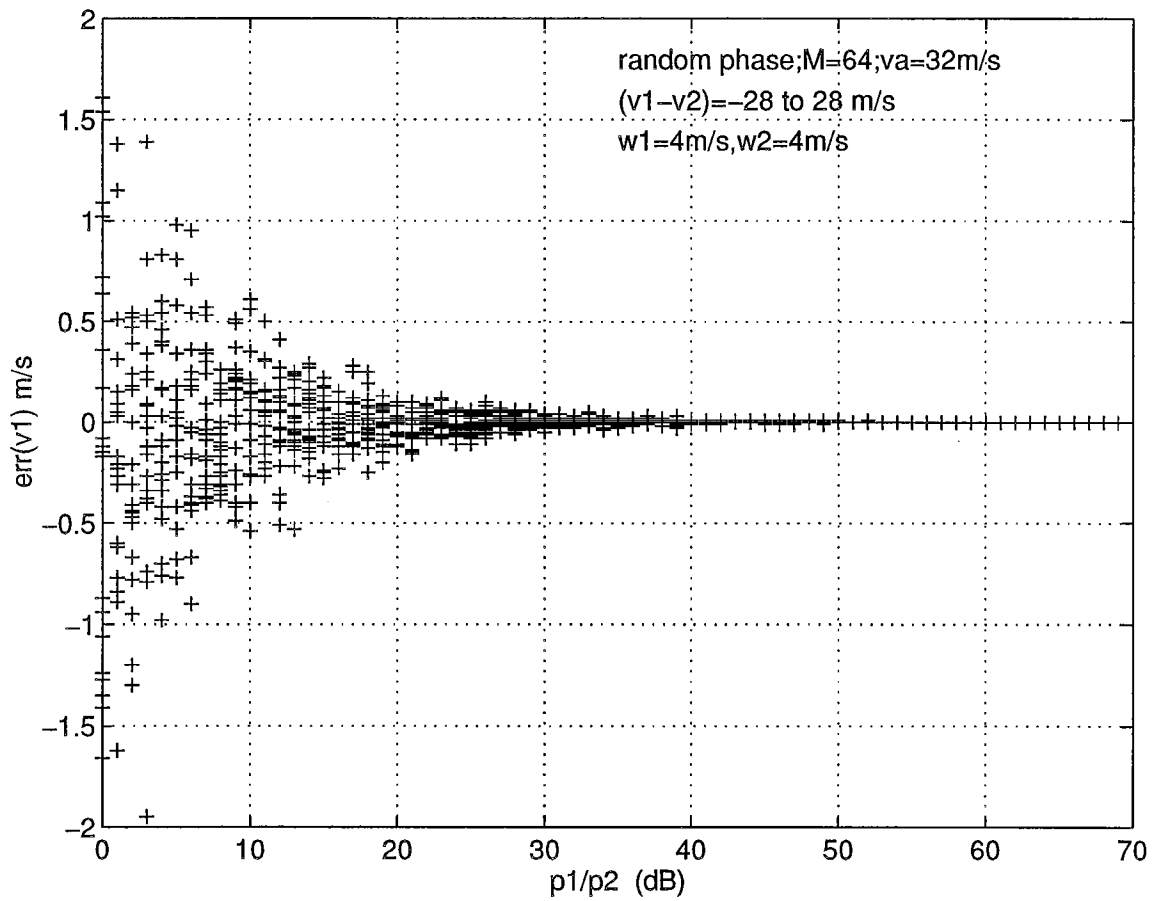


**Fig. 4.11.** Error in the mean velocity estimate,  $v_1$ , of the stronger signal using random phase coding and autocovariance processing. The velocity difference and  $p_1/p_2$  are varied over  $\pm 28 \text{ m s}^{-1}$  and 0 to 70 dB, respectively, in the simulation. The errors, in this as well as in the rest of the figures that follow, are with respect to the estimates using autocovariance processing of individual signals.

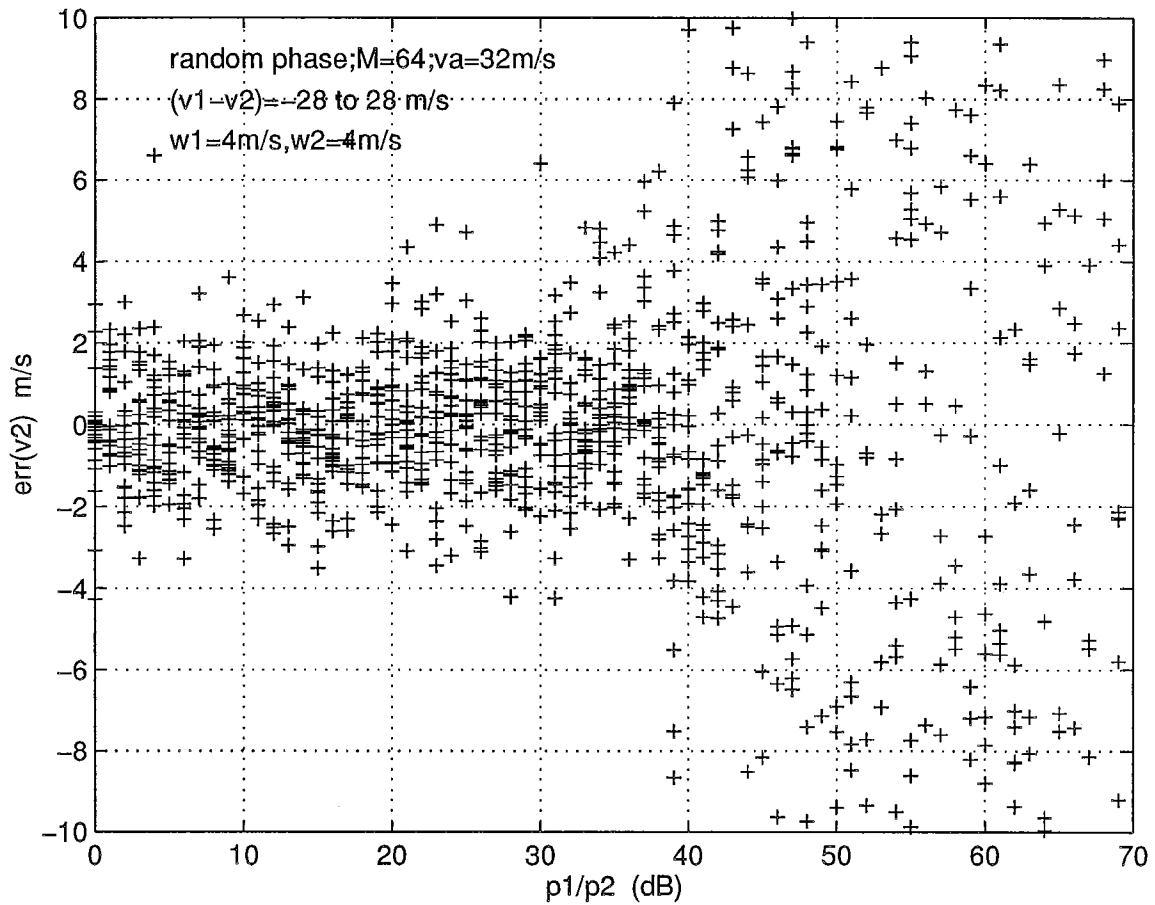


Fig. 4.12. Error in the mean velocity estimate,  $v_2$ , of the weaker signal recovered using random phase coding and decoding algorithm. The velocity difference and  $p_1/p_2$  are varied over  $\pm 28$  m s<sup>-1</sup> and 0 to 70 dB, respectively, in the simulation. The error is the difference between the recovered velocity and the velocity estimated using the autocovariance algorithm without the overlaid signal.

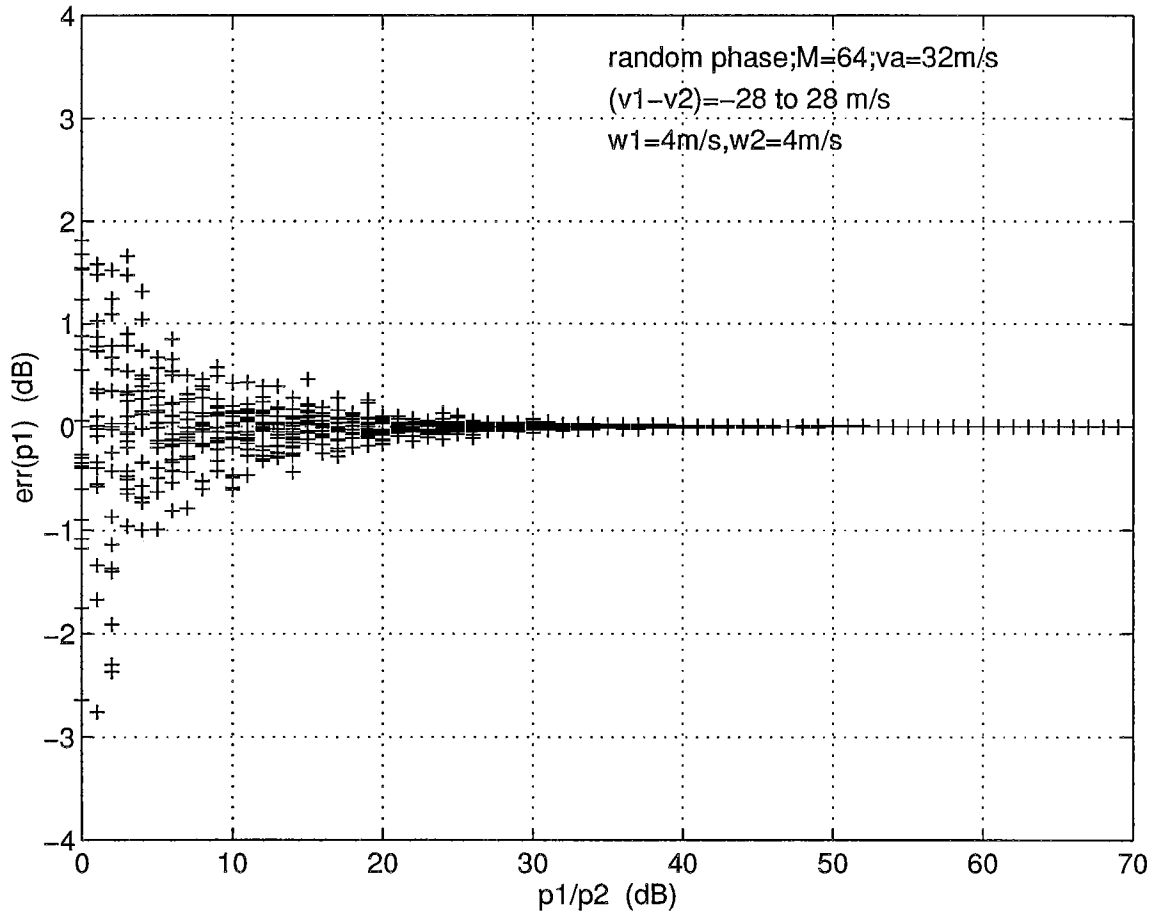


Fig. 4.13. Error in the mean power estimate,  $p_1$ , of the stronger signal using random phase coding and autocovariance processing. The velocity difference and  $p_1/p_2$  are varied over  $\pm 28\text{ m s}^{-1}$  and 0 to 70 dB, respectively, in the simulation.

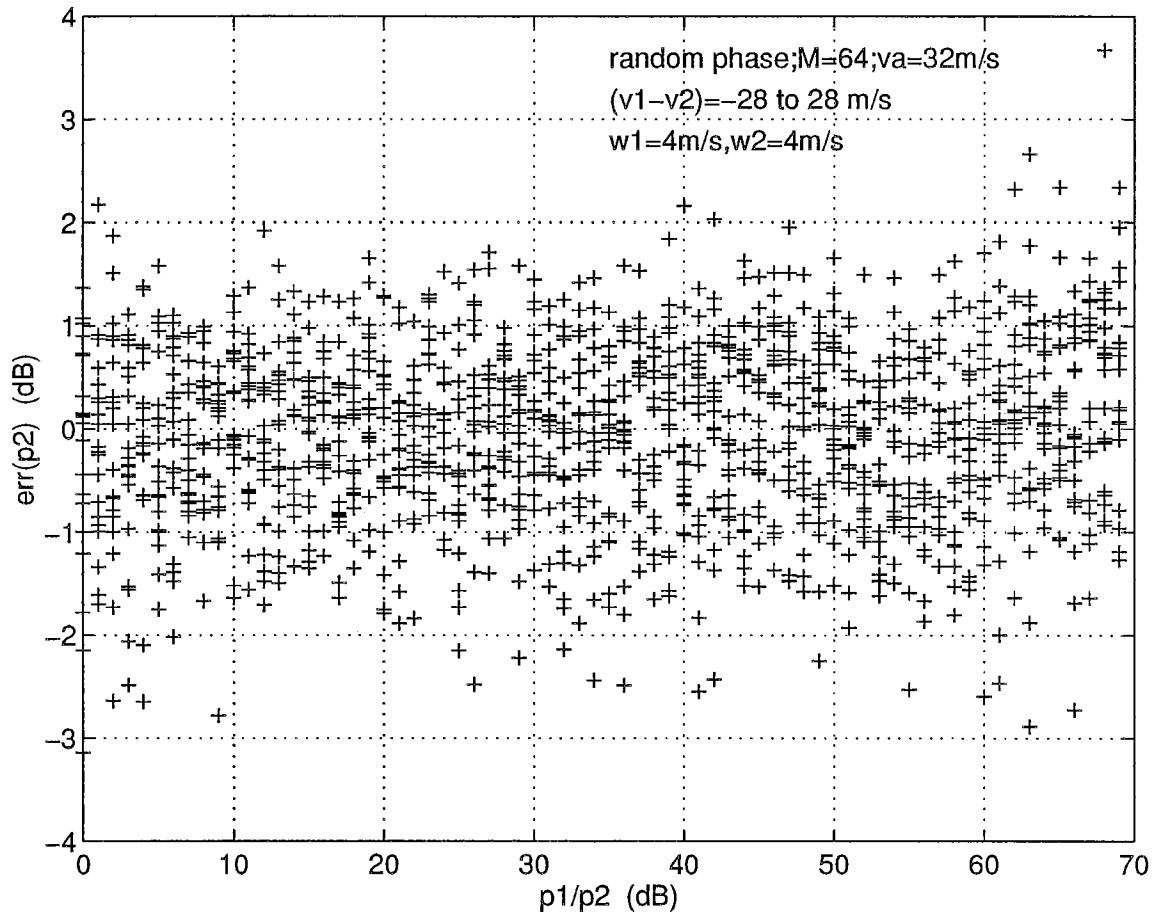


Fig. 4.14. Error in the mean power estimate,  $p_2$ , of the weaker signal recovered using random phase coding and the decoding algorithm. The velocity difference and  $p_1/p_2$  are varied over  $\pm 28 \text{ m s}^{-1}$  and 0 to 70 dB, respectively, in the simulation.

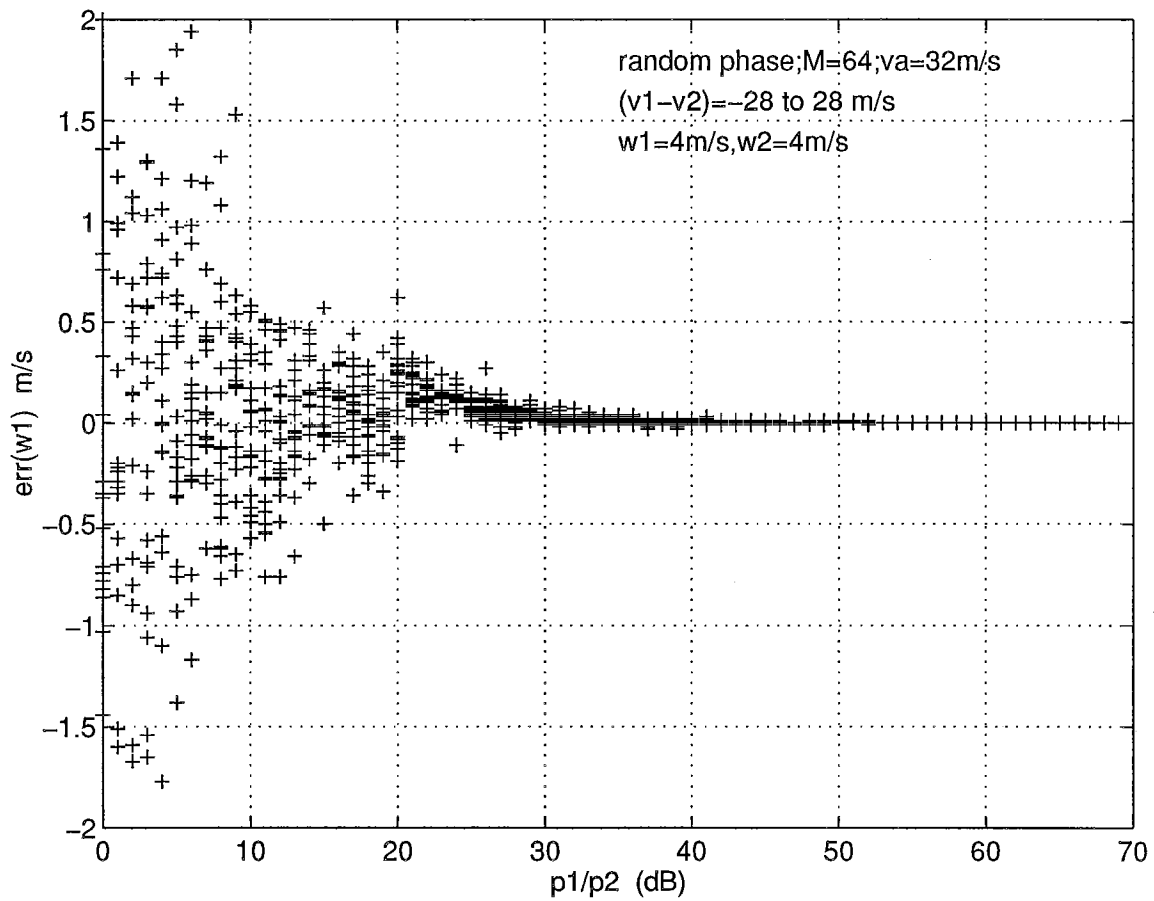


Fig. 4.15. Error in the spectrum width estimate,  $w_1$ , of the stronger signal using random phase coding and autocovariance processing. The velocity difference and  $p_1/p_2$  are varied over  $\pm 28\text{ m s}^{-1}$  and 0 to 70 dB, respectively, in the simulation. Bias correction is applied to the width estimate for  $p_1/p_2 < 20\text{ dB}$ .

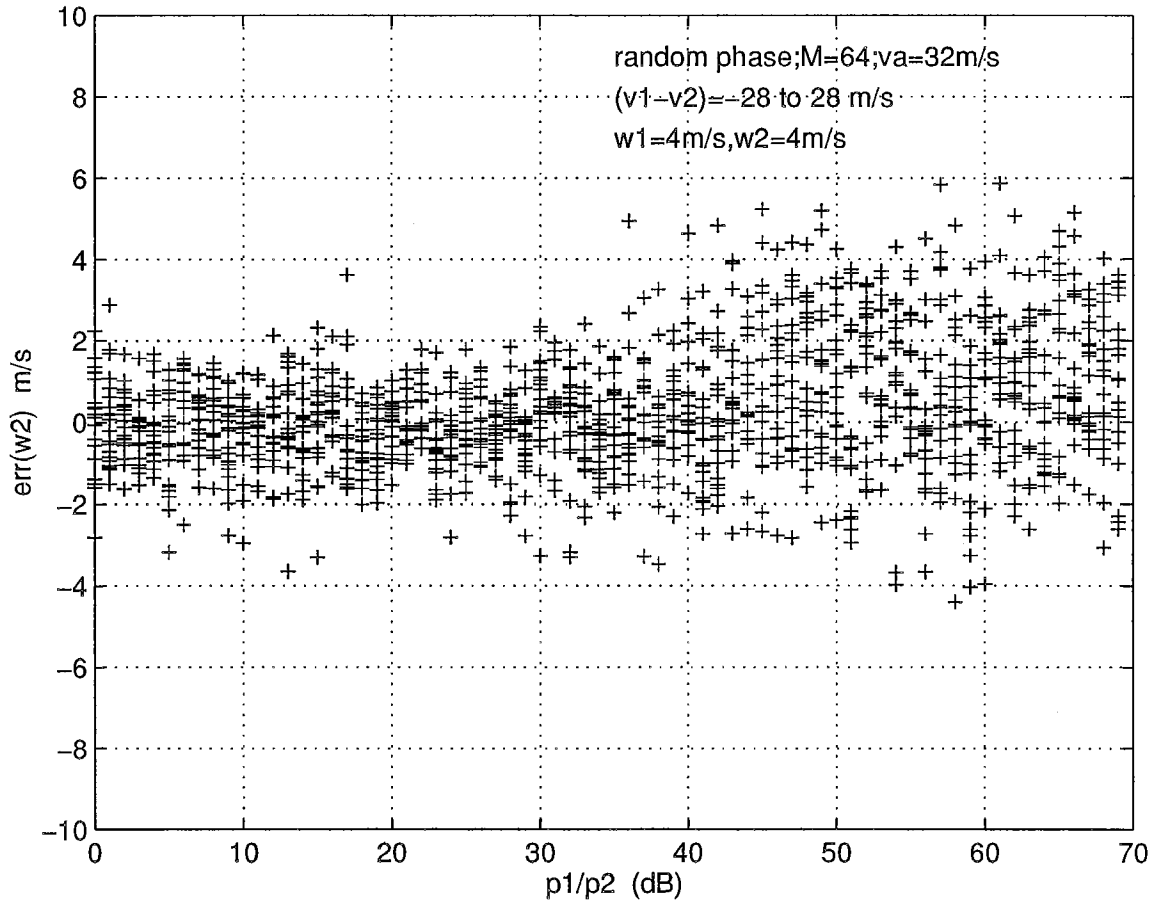
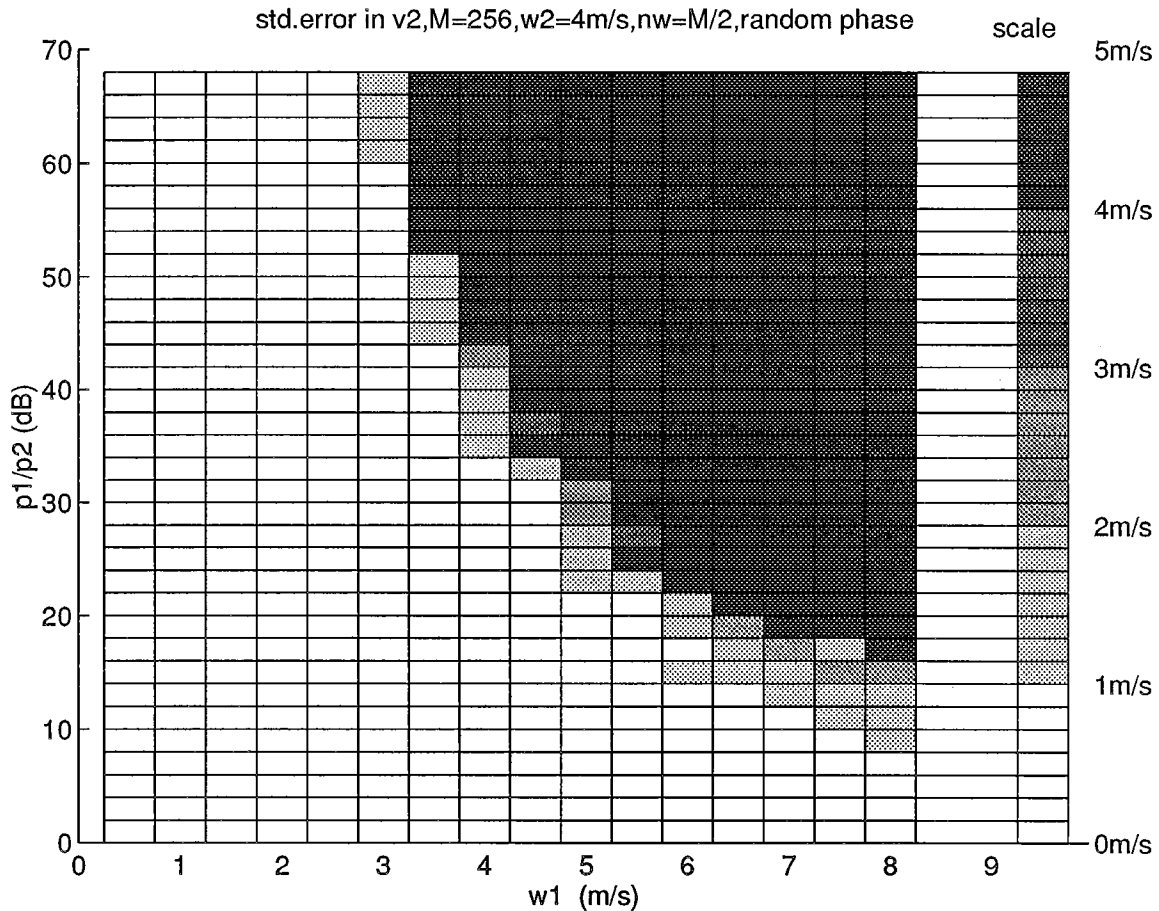
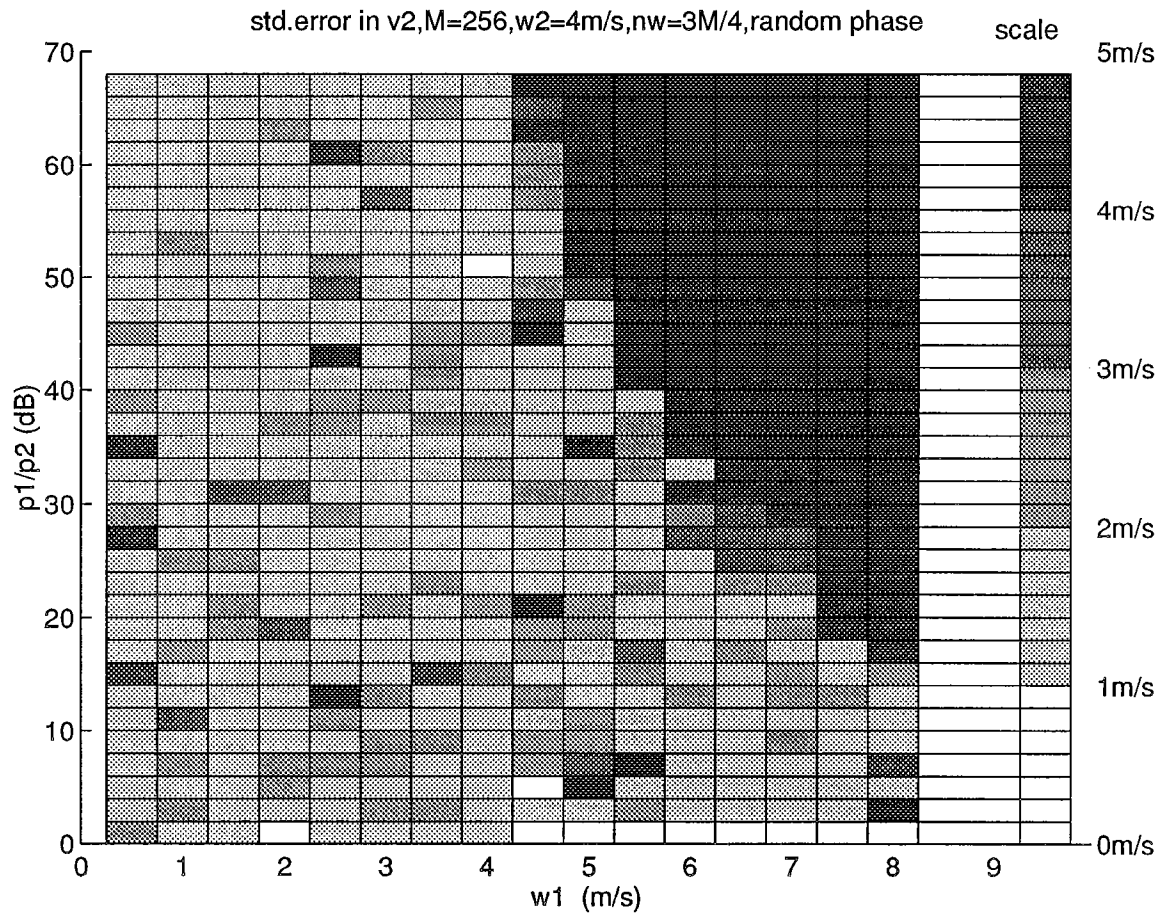


Fig. 4.16. Error in the spectrum width estimate,  $w_2$ , of the weaker signal recovered using random phase coding and the decoding algorithm. The velocity difference and  $p_1/p_2$  are varied over  $\pm 28\text{ m s}^{-1}$  and 0 to 70 dB, respectively, in the simulation.



**Fig. 4.17.** Standard deviation of the error in recovered velocity,  $v_2$ , of the weaker signal as a function of  $p_1/p_2$  and width,  $w_1$ , of the stronger signal, using the random phase code method. Each rectangle represents the standard deviation computed using 20 simulations with corresponding input parameters shown on the axes. The velocity difference is varied over  $\pm 28 \text{ m s}^{-1}$ . The quantization levels and the gray shades assigned to each level are shown on the right. The parameters shown on the top of the figure are kept constant for simulations.



**Fig. 4.18.** Standard deviation of the error in recovered velocity,  $v_2$ , of the weaker signal as a function of  $p_1/p_2$  and width,  $w_1$ , of the stronger signal, using the random phase code method. The simulations are carried out in the same way as for Fig. 4.17, with a  $3M/4$  wide notch filter in the decoding algorithm.

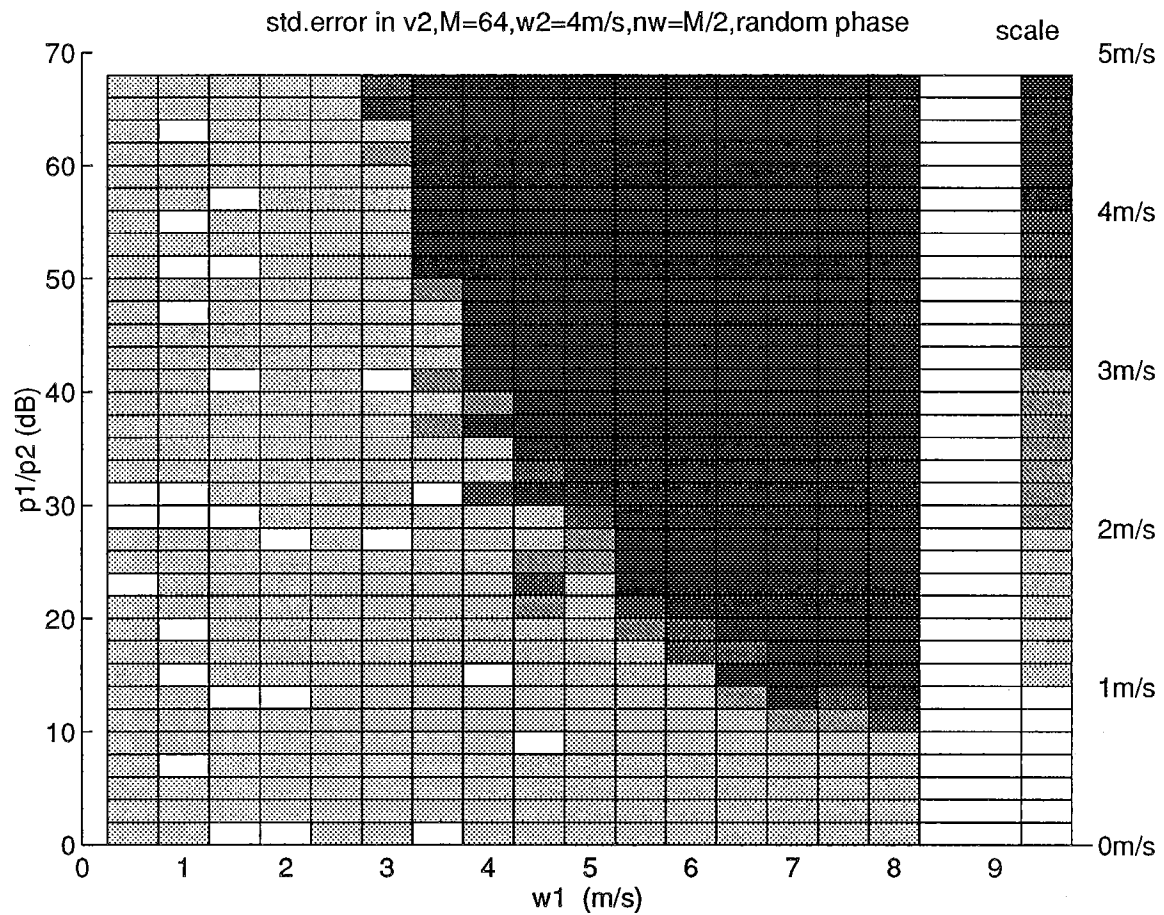


**Fig. 4.19.** Standard deviation of the error in recovered velocity,  $v_2$ , of the weaker signal as a function of  $p_1/p_2$  and width of the stronger signal, using the random phase code method. The simulations are carried out in the same way as for Fig. 4.17, with  $M=64$  samples.

#### 4.7. Possible extension to 3rd and 4th trips.

The algorithm presented in section 4.5 is specifically for recovering the spectral parameters of first and 2nd trips, with the assumption that higher order trip signals are absent. In fact, the algorithm is for any two overlaid trips. If the overlaid signal consists of 1st and 3rd trip signals instead of 1st and 2nd, the only change needed in the algorithm is to change the random code to that corresponding with the 3rd trip. If there is long PRT scan reflectivity data available, as in the case of WSR-88D radar, one can easily determine which of the two trips constitute the signal, and the code can be appropriately modified in the algorithm. Thus, the algorithm can work for any two trips.

When there are more than two trip signals overlaid, the decoding logic becomes more complex. It is required to cohere the time series for all the trip signals present (may be 3 or 4), and autocovariance process all of them to get corresponding spectral parameters,  $p(i), v(i), w(i); i=1,2,3,4$ , etc. Using the widths,  $w(i)$ , and powers,  $p(i)$ , a logic can be designed to determine the relative power levels of each of the signals. Once this information is obtained, the notch filtering and S&S process can be used to recover one signal at a time until all are separated. Although computationally more demanding than the algorithm for a two-trip overlay, it is a workable solution because when one of the signals is made coherent, all the other trip signals appear as white noise; that is equivalent to the situation of two overlaid trips, except that the noise power is from more than one trip signal. Just the S&S process without the notch filtering should be able to recover the signal parameters over a significant part of power ratios, if not as much as in the case of two-trip overlay. With long PRT data available, the determination of power levels of each of the trips is eliminated, and appropriate logic can be designed into the algorithm to recover mean velocities, one at a time, starting with the stronger signal.

#### 4.8. Conclusions.

In this chapter, an algorithm for recovery of spectral moments of two overlaid weather signals, from a random phase coded radar, has been presented. Various considerations that have gone into the development of the random phase coding scheme also have been discussed. Extensive simulation studies were carried out on the algorithm using simulated weather signals to establish the dynamic range of the power ratios over which the algorithm is effective. The main processing steps are the notch rejection filtering the stronger signal, recohering the weaker signal, and smoothing and subtraction of the noise floor.

## 5. SYSTEMATIC PHASE CODING.

### 5.1. Introduction.

Systematic phase coding is akin to the random phase coding except that the code is a periodic phase code instead of a random phase code. The phases of the transmitted pulses are switched in a regular sequence of discrete phase shifts to modify the spectrum of overlaid signal in such a way that its autocorrelation for one pulse lag is zero (Sachidananda and Zrníc 1986). Thus, the bias error in the velocity estimate due to the overlaid signal is removed. There are some advantages and disadvantages in this method compared to the random phase coding. A comparison is presented later in this report. In this section, we elaborate on the method and evolve a decoding procedure for the signal from a discrete phase coded radar. An algorithm is given which can be implemented on a radar. The only hardware change needed at the RF level is the addition of a phase shifter in the transmitter path at the low power stage. This is similar to the change required in the case of random phase coding, but the number of phase states required can be much smaller.

The method described here is an extension of the work reported in Sachidananda and Zrníc (1986). Their work mainly dealt with a switching sequence having a periodicity of 2 samples  $\{0, \pi/4, 0, \pi/4, \dots\}$ , although other switching sequences such as  $\{0,0,\pi/2,\pi/2,\dots\}$ ,  $\{0,0,0,\pi,\dots\}$ , etc. were also mentioned. In this report, these sequences will be referred to as the  $\pi/4$  seq., the  $\pi/2$  seq., and the  $\pi$  seq., respectively. Here, the same concept is used, but the  $\pi/2$  sequence, having a periodicity of 4 samples which has a better velocity recovery potential, is also explored. In this section, algorithms are given for the  $\pi/4$  and the  $\pi/2$  sequences. In the algorithm for the  $\pi/4$  sequence, the availability of long PRT data is assumed, and the algorithm for the  $\pi/2$  sequence is developed as a stand-alone algorithm which does not use the long PRT data, although the long PRT data can be used to reduce the computation. Because the  $\pi/4$  sequence has a periodicity of 2, there is a sign ambiguity in the recovered velocity which needs to be resolved using some a-priori information, and this information is obtained from the long PRT data.

The study of these two systematic codes and the random code, along with the development of algorithms for the recovery of spectral parameters, lead to a conceptual insight into the working of the codes and the recovery of the spectral parameters. The conceptual understanding allowed us to narrow our search for optimum codes and select an optimum phase code sequence which has outperformed all the other tested code sequences. This is the 3rd code described in this section. Extensive simulation studies were conducted, and the results are presented later in this section.

### 5.2. Systematic phase coding and spectrum modification.

The autocovariance processor estimates the autocorrelation for one PRT lag,  $R(1)$ , of the echo signal. The mean velocity is computed from the phase of the estimate,  $R(1)$ , using the

formula,

$$\hat{v} = (v_a/\pi) \arg\{ \hat{R}(1) \} . \quad (5.1)$$

Here, the symbol  $\hat{\phantom{x}}$  represents estimate, and  $v_a$  is the Nyquist velocity.

With a systematic phase code, the spectrum of one of the signals is modified such that its autocorrelation for lag 1 is zero. By cohering each signal in turns, both the velocities can be recovered without any bias due to the other signal. A condition under which autocorrelation is zero can be obtained from the well known relation between correlation coefficients,  $R(m)$ , and the power spectral coefficients  $|s_k|^2$ . For a discrete sample sequence, this relation is,

$$R(m) = \sum_{k=0}^{M-1} |s_k|^2 z^{km} ; \quad m=0,1,2,\dots,M-1 ; \quad z = e^{j2\pi/M} . \quad (5.2)$$

For  $m=1$ , this reduces to

$$\begin{aligned} R(1) &= \sum_{k=0}^{M/2-1} |s_k|^2 z^k + \sum_{k=M/2}^{M-1} |s_k|^2 z^k \\ &= \sum_{k=0}^{M/2-1} |s_k|^2 z^k - \sum_{k=0}^{M/2-1} |s_{(k+M/2)}|^2 z^k . \end{aligned} \quad (5.3)$$

Thus, if

$$|s_k| = |s_{(k+M/2)}| \quad \text{for } k=0,1,2,\dots,M/2-1, \quad (5.4)$$

we have  $R(1) = 0$ . This is one of the ways  $R(1)$  can be made zero. The  $\pi/4$  and  $\pi/2$  codes have this property of making the right and left halves of the spectrum identical, provided certain criteria are met by the uncoded spectrum. Thus the same information is contained in both halves of the spectral domain, and we can then filter half of the spectral coefficients containing the unwanted overlapped spectrum without losing information contained in the original uncoded spectrum (except  $v/2$ ). In the rest of this report we will refer to this (eq. 5.4) as the **matching property** of the coded spectrum. It is also possible to assemble several other codes that have this matching property. But the choice of the code also determines the method of recovering the spectral parameters.

One important fact to note here is that a good envelope matching in the left and right half of the spectrum, can be obtained using systematic codes, under conditions of narrow spectra ( $w/2v_a < 0.05$ ). This symmetry can be used in recovering the weaker signal spectrum or in cancelling the stronger signal.

### 5.3. $\pi/4$ phase coding.

#### 5.3.1. $\pi/4$ phase code and spectral moment estimation.

In the  $\pi/4$  coding scheme, the transmitted pulses are phase coded with a sequence,  $\{0, \pi/4, 0, \pi/4, \dots\}$ , and the return samples are phase shifted by a phase sequence,  $\{0, -\pi/4, 0, -\pi/4, \dots\}$ ,

so that the 1st trip signal is coherent. Because of the periodicity of  $2T$ , the 3rd trip signal also becomes coherent. The 2nd and 4th trip signals get modulated by a phase sequence,  $\{\pi/4, -\pi/4, \pi/4, -\pi/4, \dots\}$ . This modulation splits the 2nd and 4th trip spectrum into two parts; half the power in  $k^{\text{th}}$  spectral coefficient is shifted to a coefficient at  $(k+M/2)$ , where  $M$  is the number of samples collected for processing. This is shown in Fig. 5.1 for a Gaussian shaped spectrum. This coding scheme has been studied extensively by Sachidananda and Zrnic (1986), and a method for the recovery of the spectral parameters of the weaker signal also has been given in the paper. Therefore, we will confine our discussion to the development of the decoding algorithm, in the context of ambiguity mitigation in the WSR-88D. The algorithm is somewhat different from that given in the paper. We assume that only the 1st and 2nd trip signals are present, and the 1st trip signal is stronger. The stronger trip signal parameters can be estimated without much difficulty when phase coding is employed; hence, the discussion will be centered around the recovery of the weaker 2nd trip signal parameters.

First, we make the assumptions that (a) noise is zero and (b) each of the spectra involved have at most  $M/2$  non-zero coefficients. These two assumptions will be referred to as assumptions (a) and (b) in this report. The assumption of a Gaussian shape is not necessary for the method to work although this assumption is made in simulating the weather signal. The 1st and the 2nd trip parameters, viz., the mean power, the mean velocity, and the spectrum width, are designated by  $p1, v1, w1$  and  $p2, v2, w2$ , respectively. If we take the spectrum of the time series with the 1st trip signal coherent and the 2nd trip signal phase coded, the 2nd trip signal will have two spectra exactly separated by  $v_a$ . Half the power in the spectrum of the 2nd trip will be shifted exactly by  $v_a$ , and the shape of the spectrum is preserved in both halves. Now, the 1st trip signal in the spectrum can be completely removed by notch filtering or deleting exactly  $M/2$  coefficients centered on  $v1$ . Here is the importance of the assumption (b). If the assumption is not satisfied exactly, some residual power will remain in the spectrum which will affect the recovered parameters of the 2nd trip. This notch filtering leaves a replica of the 2nd trip signal with half the original power. Of course, depending on the velocity difference,  $(v1-v2)$ , the filtered spectrum would be the original, the one completely shifted by the Nyquist velocity, or part original and part shifted. Nevertheless, in all three situations, we can recover the mean velocity,  $v2$ , by an appropriate shifting operation to restore the split spectrum shape. But the recovered velocity will be the actual  $v2$  or  $v2$  shifted by the Nyquist velocity  $v_a$ , (i.e.,  $v2+v_a$  or  $v2-v_a$ , whichever is in the  $0^{\text{th}}$  aliasing interval corresponding to the short PRT). This is the main ambiguity that needs to be resolved. This ambiguity stems from the fact that the spectrum is split into two halves, and one half is deleted. In the process, the information on which half is the original signal is lost. Here, we make use of the long PRT scan data to resolve the ambiguity.

The long PRT time series is autocovariance processed to recover the aliased mean velocity of the 2nd trip signal. Now, using the Nyquist velocity of the long PRT, the possible mean velocities are computed and compared with the recovered velocities,  $v2$  and  $(v2 \pm v_a)$ , from the short PRT time series. Whichever is the nearest to the possible velocities is taken as the correct velocity,  $v2$ . The  $\pi/4$  decoding algorithm is developed based on these ideas and has the least amount of computation compared to all other algorithms given in this report.

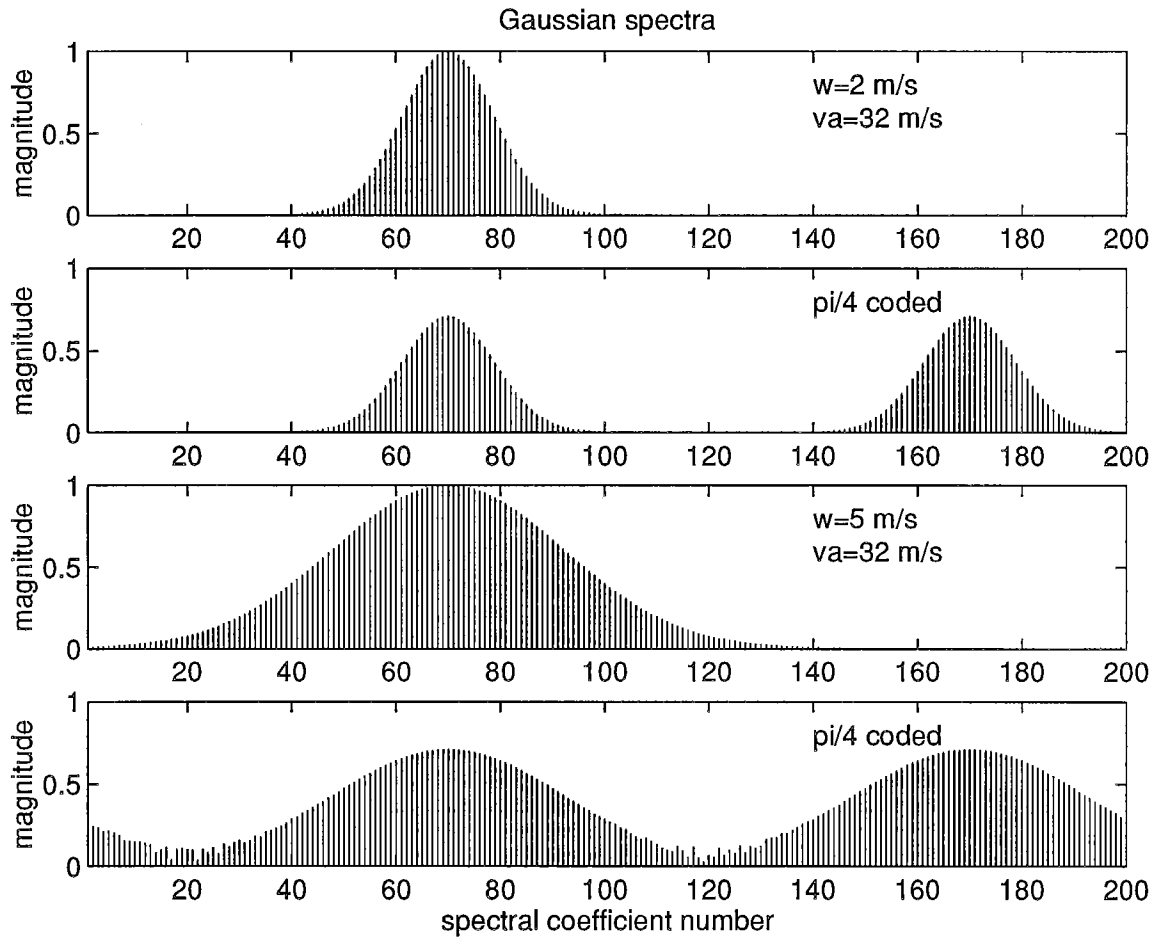


Fig. 5.1. The spectrum modification by the  $\pi/4$  phase code. Two cases are shown with narrow and wide Gaussian shaped spectra.

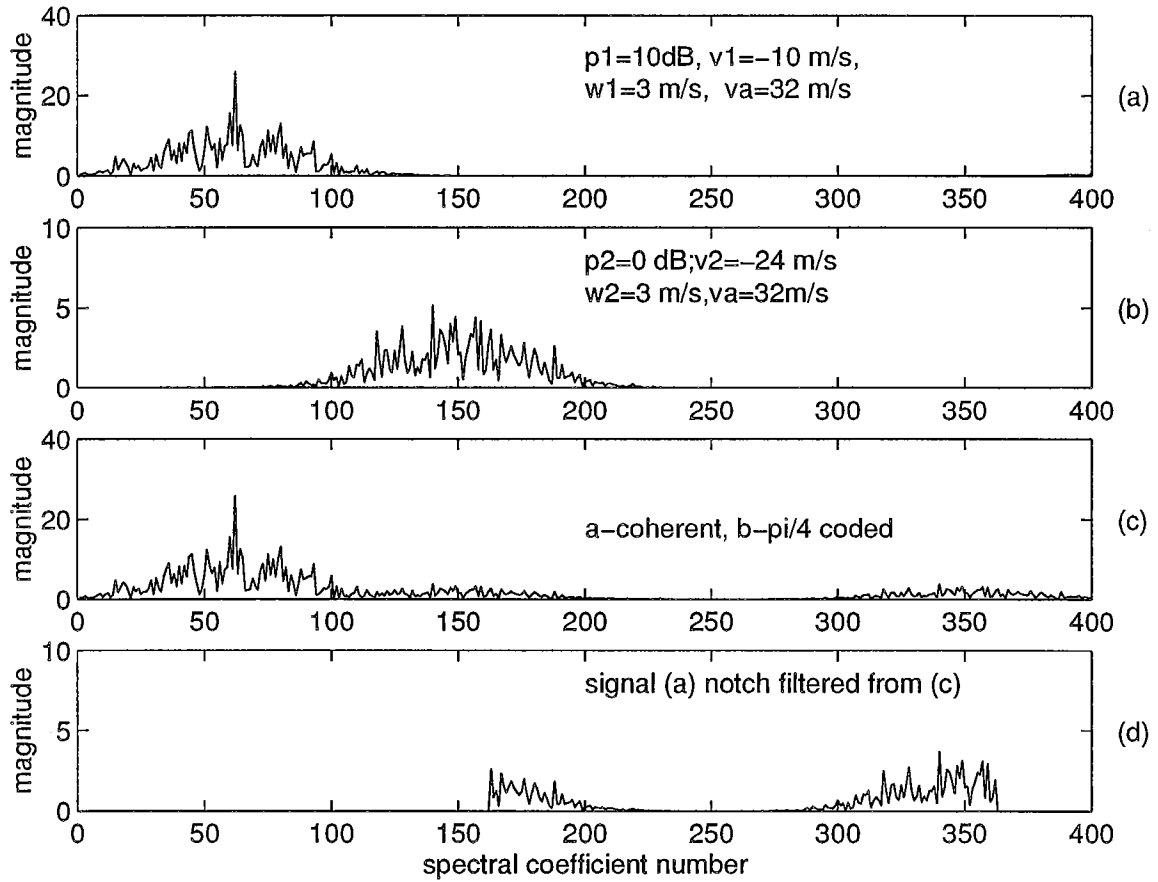


Fig. 5.2. The processing steps in the decoding algorithm for a  $\pi/4$  phase coded radar.

Fig. 5.2 shows the processing steps and the corresponding spectra at different stages of processing. The spectral parameters are shown in the figure. The spectra in Fig. 5.2(a) and (b) are the 1st and the 2nd trip signals, and Fig. 5.2(c) is the spectrum of the overlaid signal with the 1st trip coherent and 2nd trip phase coded. Note that the 2nd trip power is split into two parts. The spectra in Fig. 5.2(d) is obtained after deleting  $M/2$  coefficients centered on the  $v_1$  estimate. Note that the signal power is half the original power, and the 2nd trip signal spectrum shape is completely recovered, except for the  $\pm v_a$  shift.

The split shape has to be restored, and the restored spectrum has to be placed in the correct half of the spectral domain, if the mean velocity is to be computed using the autocorrelation,  $R(1)$ , for one PRT lag. However, a simpler procedure is to compute autocorrelation,  $R(2)$ , for lag 2 and use the formula,  $v_2 = (\lambda/8\pi T) \arg[R(2)]$ , for velocity computation. This does not require restoration of the split shape of the spectrum. The recovered velocity will be  $v_2$  or  $(v_2 \pm v_a)$ . The sign ambiguity is finally removed using the long PRT data.

When assumption (b) is not satisfied exactly, the residual 1st trip power in the spectrum after notch filtering produces a bias in the estimated mean velocity (in the random phase code the variance is increased). The bias becomes significant for large  $p_1/p_2$  ratios and large spectrum widths of the stronger signal.

The recovered mean velocities are usable only under certain conditions. It is shown in Sachidananda and Zrnic (1986) that the variance of the velocity estimate is highly dependent on the ratio of powers in the two trips and the velocity difference. It is also a function of the spectrum widths. Generally, the mean velocity of the stronger of the two signals can be recovered accurately. The recovery of the mean velocity,  $v_2$ , of the weaker 2nd trip signal in the presence of the stronger 1st trip signal overlay determines the limit of the algorithm.

### 5.3.2. The $\pi/4$ decoding algorithm.

In simulating the time series, the assumptions stated on page 4 are made. The algorithm given below is also based on those assumptions. *This algorithm makes use of the long PRT data.*

<<<-----START of algorithm

1. Input estimates  $p_1, v_1, w_1$  and  $p_2, v_2, w_2$  from the long PRT scan.
2. Input time series from short PRT scan.
  - ▶ 1st trip coherent; 2nd trip coded by a phase sequence  $\{\pi/4, -\pi/4, \pi/4, -\pi/4, \dots\}$ .
4. Determine from long PRT data which trip is stronger.
5. Cohere stronger trip signal and autocovariance process to estimate the mean velocity (assume  $v_1'$ ).
6. Compute spectrum,  $S$ .
7. Delete  $M/2$  coefficients around mean velocity,  $v_1'$ , of the stronger signal.
8. Compute  $R(2)$  and velocity of the weaker signal (assume  $v_2'$ ).
9. Compute  $(v_2' \pm v_a)$ , whichever is in the 0<sup>th</sup> aliasing interval.

10. Compute probable velocities from the aliased long PRT data.
11. Determine the velocity  $v_2'$  or  $v_2' \pm v_a$ , which is closest to one of the probable velocities.
12. Output  $v_1'$  and  $v_2'$ , the recovered velocities of 1st and 2nd trips.

<<<-----END of algorithm

### 5.3.3. Simulation and results.

The algorithm, given in section 5.3.2, was programmed in MATLAB code "piby4.m." In writing the code, it was assumed that the input is a time series from a  $\pi/4$  coded radar after ground clutter filtering. The 1st trip is coherent, and the 2nd trip is coded. The testing is done along the same lines as that for random phase coding. A test program was written which simulates two time series for the two trips with specified parameters and combines them to form an overlaid signal. Two long PRT time series with a reduced number of samples (reduction factor is made inversely proportional to the PRT's so that the dwell times for the short and long PRTs are nearly equal) are also generated to simulate the long PRT scan, and the estimated spectral parameters using a conventional autocovariance processor are fed into the algorithm as the long PRT data input. The recovered velocity of the weaker signal is compared to the correct velocity (computed using the pulse pair algorithm) and error statistics are generated from a large number of simulation runs with the parameters,  $p_1/p_2$ ,  $(v_1-v_2)$ , and spectrum widths,  $w_1$ . Spectrum width,  $w_2$ , of the weaker signal is kept constant at  $4 \text{ m s}^{-1}$ . The two PRT's are chosen to be 3 ms. and 0.7812 ms. The number of samples chosen is 64 for short PRT data and 16 for long PRT data. These are realistic values for the WSR-88D radar.

There are two steps in the recovery of the velocity  $v_2$ . First, determine the two candidate aliases,  $v_2'$  and  $v_2' + v_a$  or  $v_2' - v_a$ , whichever falls in the  $-v_a$  to  $+v_a$  interval. Second, determine which alias is correct based on the long PRT velocity data, which we refer to as the sign ambiguity resolution. To separate the effect of these two steps on the recovered  $v_2$ , first the long PRT data was not used in the simulation, and in its place, the correct velocity, as obtained from autocovariance processing the 2nd trip time series before combining, was supplied to the algorithm to remove the ambiguity. This gives us the performance of the spectral processing algorithm, assuming a perfect sign ambiguity resolution. The results from the simulation are shown in Fig. 5.3. Note that this result reflects the performance of only a part of the algorithm, which does not include the sign ambiguity resolution.

The region of recovery of  $v_2$  nearly corresponds to the limit given by the residual power ratio,  $R_p$ , (see Fig. 4.4.) for  $M/2$  notch width. The recovered velocity has the same variance as that of a signal without an overlaid 1st trip signal because the spectrum shape is completely recovered whenever condition (b) is satisfied. For larger widths, the residual power introduces a bias in the velocity estimate. The standard error shown in Fig. 5.3 is mainly the bias error, which is a function of the velocity difference.

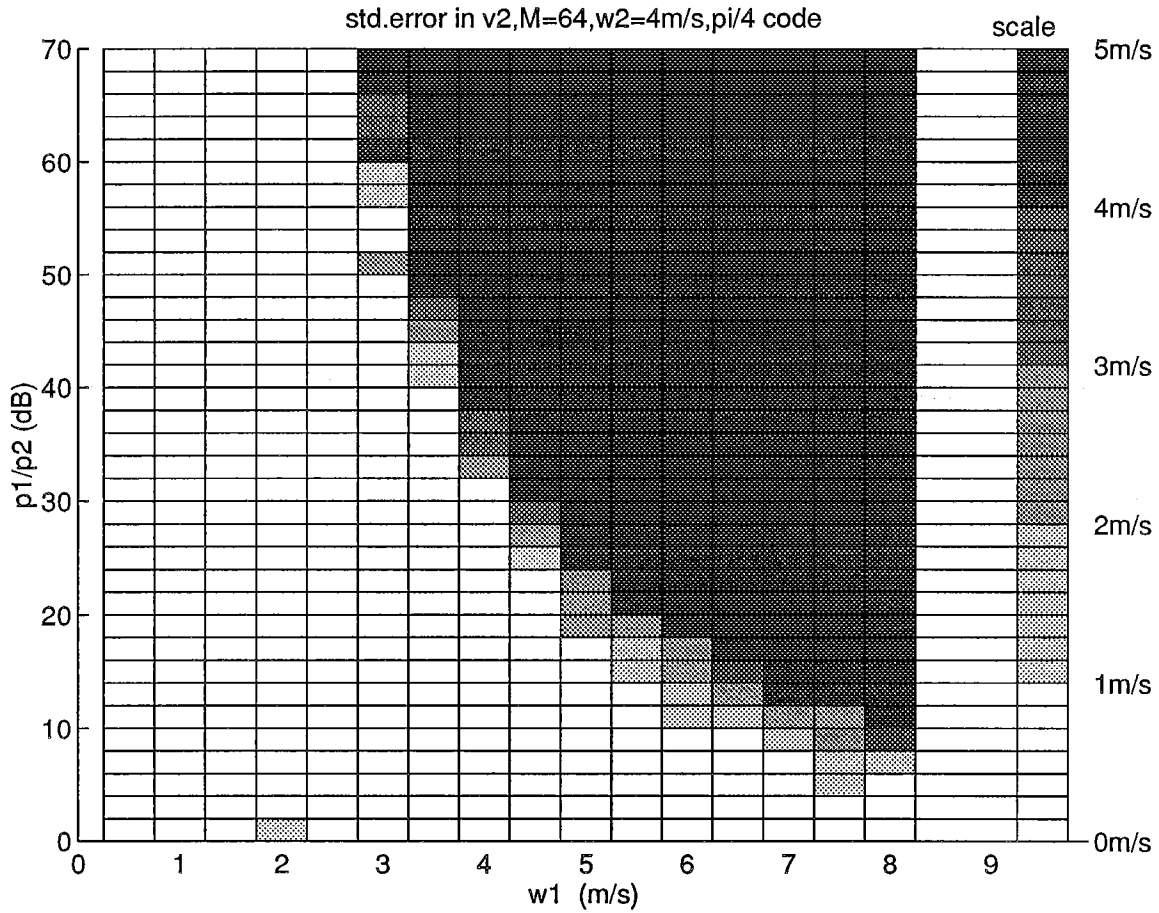


**Fig. 5.3.** Standard deviation of the error in recovered velocity,  $v_2$ , of the weaker signal as a function of  $p_1/p_2$  and width,  $w_1$ , of the stronger signal, using the  $\pi/4$  phase code method. Each rectangle represents the standard deviation computed using 20 simulations with corresponding input parameters shown on the axes. The velocity difference is varied over  $\pm 28 \text{ m s}^{-1}$ . The quantization levels and the gray shades assigned to each levels are shown on the right. The parameters shown on the top of the figure are kept constant for all simulations. [The long PRT data is not used in removing the sign ambiguity; instead, input data is used to remove sign ambiguity perfectly. Therefore, this figure reflects the performance of only a part of the algorithm which does not include the sign ambiguity resolution using long PRT data.]

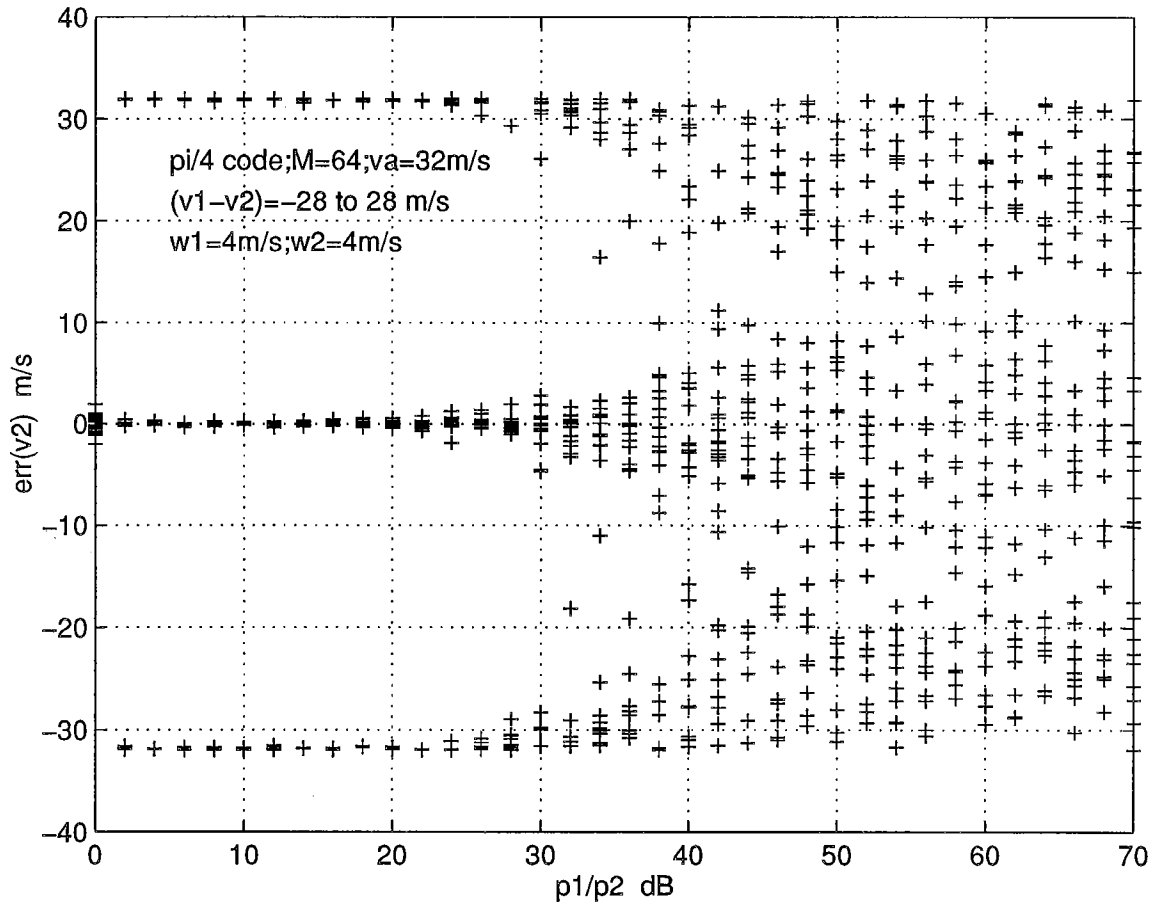


Fig. 5.4. Error in the recovered  $v_2$  using the  $\pi/4$  phase code method for  $w_l=4$  m  $s^{-1}$  width. The large error ( $\pm 32$  m  $s^{-1}$ ) for  $p_1/p_2 < 30$  dB in nearly 50% of the simulations is because of the failure of the sign ambiguity resolution using the long PRT data.

The performance of the second step in the algorithm, which selects the correct velocity alias based on the long PRT data, is dependent upon the ratio of PRTs. If the ratio of the long PRT and the short PRT is large, the number of velocity aliases increases, as well as the variance of these values, because of the reduced number of samples available for velocity estimation, and because the signal samples are less coherent, in the long PRT scan. The larger the ratio, the number of velocity aliases for comparison as well as the spread of the aliases will be larger. The probability of selecting the correct velocity also reduces with a larger PRT ratio. This effect is shown in the scatter plot (Fig. 5.4) of error in recovered velocity,  $v_2$ , when the second part is incorporated into the algorithm, with a PRT ratio of 3.84. The spectrum width of both signals is set to  $4 \text{ m s}^{-1}$  and  $p1/p2$ , and the velocity difference,  $(v1-v2)$ , are varied over 0 to 70 dB and -28 to 28  $\text{m s}^{-1}$ , respectively, for generating the scattergram. Note that for a spectrum width of  $4 \text{ m s}^{-1}$ , the velocity is recovered for  $p1/p2=30 \text{ dB}$ , but removing the ambiguity using the long PRT data is erroneous nearly 50 percent of the time for  $v2=4 \text{ m s}^{-1}$ . The success rate is higher for narrower widths and lower for higher widths. This makes the algorithm unsuitable for PRT ratios used in the WSR-88D radar.

Two other methods of resolving the sign ambiguity examined are, (a) power comparison, and (b) averaging  $R(1)$  estimate over four previous sample sets (Sachidananda and Zrnic 1986). These are discussed in the following paragraphs.

(a). The power comparison method: This method is based on two assumptions. The first one is that when two uncorrelated spectra overlap, the total power is the sum of the powers of the two signals. This assumption is not exactly true for each realization because the spectral coefficients can add or subtract depending on the phase. It is true only when applied to the expected value of the power. The second assumption is that when a signal is modulated by the  $\pi/4$  code, the splitting of the spectrum yields exactly same power in the two halves of the spectral domain. This again is exactly satisfied only if the spectra are narrow with at most  $M/2$  non-zero coefficients. For wider spectra the tail ends of the spectra overlap when modulated, thus making the powers unequal in the two halves.

In this method, the spectrum of the overlaid signal with 2nd trip signal coherent is divided into two parts ( $M/2$  coefficients each), one centered on estimated  $v_2$ , and the other, the remaining  $M/2$  coefficients (these are centered on  $v_2+v_a$  or  $v_2-v_a$ ). The power in these two halves is compared and the one with larger power is selected as the correct half in which the original signal resides. Since the assumptions are not exactly satisfied in practice for each realization of the weather signal, the method works only for low  $p1/p2$  ratios. A simulation study indicated that the largest  $p1/p2$  for which  $v_2$  sign ambiguity can be resolved is about 8 to 10 dB.

(b). Averaging  $R(1)$ : This method is based on the observation that the  $\text{var}(v_2)$  decreases with larger number of samples, and the velocity field is continuous. If the weaker 2nd trip signal is cohered and autocovariance processed to obtain the velocity,  $v_2$ , the standard deviation of the estimate would be within  $v_a/4$  with  $M=256$  for  $p1/p2$  up to 15 dB (Sachidananda and Zrnic 1986). This estimate of  $v_2$  is sufficient to remove the sign ambiguity. The required 256 samples are obtained by storing the previous four sample sets. These samples, of course, do not correspond to the same range cell, but are cells from previous radials at the same range. It is also possible to use data from the adjacent range cells along the same radial for the purpose. The assumption is that the velocities are continuous and hence will have nearly the same velocities

for all the resolution volumes around the volume under consideration. This procedure was proposed in Sachidananda and Zrnic (1986). Using this method sign ambiguity can be resolved if  $p1/p2$  is less than about 15 dB.

All the three methods of ambiguity resolution have limitations, and are unable to resolve the sign ambiguity fully in the region of low standard error in  $v2$ , shown in Fig. 5.3.

#### 5.4. $\pi/2$ phase coding.

##### 5.4.1. $\pi/2$ phase code and estimation of spectral moments.

In the  $\pi/2$  phase coding, the transmitted pulses are phase shifted in a sequence  $\{0, 0, \pi/2, \pi/2, \dots\}$ , and the return samples are phase shifted in the sequence  $\{0, 0, -\pi/2, -\pi/2, \dots\}$  so that the 1st trip samples are coherent. The 2nd trip signal phase code sequence is shifted by one PRT, and hence, does not cohere but gets modulated by a phase sequence  $\{\pi/2, 0, -\pi/2, 0, \dots\}$ . If the 2nd trip echo is made coherent by appropriately correcting the phase shifts, the 1st trip signal gets modulated in a similar way.

It may be noted that because of the periodicity of 4 in the sequence, one of the first four trip signals can be made coherent at a time, and the other three will be modulated such that their autocorrelation at lag 1 is zero. This allows us to recover the mean velocity of at least the strongest of the signals, even when more than two trip signals are present. However, this applies to autocovariance processing alone. If spectral processing is carried out, the algorithm becomes complicated. In this report, we assume the presence of 1st and 2nd trip signals alone in developing the algorithm. The same algorithm with some changes in the decoding procedure can be applied for any two overlaid signals, not necessarily the 1st and the 2nd. However, there must be some mechanism to determine which two of the first 4 trip signals are present in the time series. (e.g., a long PRT scan.) This information is also needed to identify the data where more than two signals are present.

An examination of the spectrum of the signal modulated by a phase sequence  $\{\pi/2, 0, -\pi/2, 0, \dots\}$  shows that the power in the  $k^{\text{th}}$  spectral coefficient gets distributed equally among the four spectral coefficients at  $k, k+M/4, k+M/2, \text{ and } k+3M/4$ . Thus, in the modulated spectrum, the  $n^{\text{th}}$  coefficient is a vectorial sum (with appropriate phase shifts) of the contribution from the four coefficients separated by  $M/4$  in the original unmodulated spectrum. This is shown mathematically in the following paragraphs.

Let the phase sequence be represented by  $\phi_i = \{\pi/2, 0, -\pi/2, 0, \dots\}$ , and let  $E_i$ ,  $i=0, 1, 2, 3, \dots, M-1$ , be the time series complex samples of a signal. The spectral coefficients,  $a_k$ , of the unmodulated signal,  $E_i$ , are given by

$$a_k = 1/M \sum_{i=0}^{M-1} E_i z^{-ik}, \quad (5.5)$$

and  $E_i$  can be written as the inverse transform of  $a_k$ , as

$$E_i = \sum_{m=0}^{M-1} a_m z^{im}. \quad (5.6)$$

The spectral coefficients of the modulated signal can be expressed as

$$\begin{aligned} b_k &= 1/M \sum_{i=0}^{M-1} E_i \exp(j \phi_i) z^{-ik} \\ &= 1/M \sum_{i=0}^{M-1} \sum_{m=0}^{M-1} a_m z^{im} \exp(j \phi_i) z^{-ik} \\ &= 1/M \sum_{m=0}^{M-1} a_m \left\{ \sum_{i=0}^{M/2-1} j z^{2i(m-k)} (-1)^i + \sum_{i=0}^{M/2-1} z^{(2i+1)(m-k)} \right\}. \end{aligned} \quad (5.7)$$

The first summation over index,  $i$ , has a non-zero value only for  $m=k+M/4$  and  $m=k+3M/4$ , and the second summation over index,  $i$ , has non-zero value only for  $m=k$  and  $m=k+M/2$ . The values are  $j/2$  for the first two and  $1/2$  and  $-1/2$  for the second two, respectively. Therefore, we can express the coefficients of the coded spectra in terms of the uncoded spectra using the following relation:

$$b_k = 1/2 \{ a_k + j a_{(k+M/4)} - a_{(k+M/2)} + j a_{(k+3M/4)} \}. \quad (5.8)$$

This is an important equation which gives us the property of the modified spectrum.

If the unmodulated spectrum is narrow and has at most  $M/4$  non-zero coefficients  $a_k$  (assumption (b)), it can be shown using the result (5.8) that the equation (5.4), or the matching property, is exactly satisfied, making  $R(1) \equiv 0$ . If the non-zero spectral coefficients span  $M/2$ , two of the four coefficients contribute to  $b_k$ , and one of the coefficients is much larger than the other, thus making  $|b_k|^2$  nearly equal to  $|b_{(k+M/2)}|^2$ . If the non-zero coefficients span more than  $M/4$ , the condition (5.4) is not satisfied exactly, resulting in a small residual value for  $R(1)$ . This residual value is mainly due to the non-zero coefficients outside the  $\pm M/4$  interval centered on mean Doppler. Therefore,  $R_p$  for a  $M/2$  notch width is a measure of the suppression of  $R(1)$  that can be achieved by phase coding (See Fig. 4.4.). It can be seen that  $R(1)$  is suppressed by as much as 40 dB for spectrum width of  $4 \text{ m s}^{-1}$ , and  $v_a = 32 \text{ m s}^{-1}$ . The suppression deteriorates rapidly for larger widths. If we assume  $8 \text{ m s}^{-1}$  as the largest width encountered in storms, the worst case suppression is about 15 dB, if  $v_a$  is chosen to be  $32 \text{ m s}^{-1}$ .

Fig. 5.5 shows two Gaussian spectra and the corresponding modulated spectra for two different widths. Note that the spectrum splits into four identical parts separated by one quarter of the unambiguous interval or  $M/4$  coefficients. For narrow widths (1 to  $3 \text{ m s}^{-1}$ ), the four parts overlap but the magnitudes of the coefficients spaced by  $M/2$  are still nearly equal. If the width

is larger than  $3.5 \text{ m s}^{-1}$ , the significant coefficients span more than  $M/2$ , and their complex addition causes the coefficients,  $b_k$  and  $b_{k+M/2}$ , to differ in magnitude.

Implementation of this scheme is simple. The only hardware change required is the addition of an electronic phase shifter with two phase states (0 and  $\pi/2$  radians), in the transmit path, at the low power stage. The received time series is first phase corrected to cohere the 1st trip signal and then passed through a clutter filter. After the clutter is filtered, the time series can then be cohered for the 2nd trip by appropriately shifting the phases of the samples. An autocovariance processor can be used to recover the mean velocities of the stronger signal. The recovery of weaker signal parameters needs further processing in the spectral domain. The development of the algorithm is discussed in the next section.

#### 5.4.2. The algorithm development.

When the 1st and 2nd trip spectra overlap, the  $k^{\text{th}}$  spectral coefficient is a sum of the individual spectral coefficients,  $a_k$  and  $b_k$ , of the 1st and 2nd trip signals, respectively. Thus,  $R(1)$  can be written as (see eq. 5.3)

$$\begin{aligned} \hat{R}(1) &= \sum_{k=0}^{M-1} |a_k + b_k|^2 z^k \\ &= \sum_{k=0}^{M-1} \{ |a_k|^2 + |b_k|^2 + 2 \operatorname{Re}[a_k b_k^*] \} z^k \\ &= \hat{R}_a(1) + \hat{R}_b(1) + \hat{C}_{ab}(1). \end{aligned} \quad (5.9)$$

To estimate  $R_b(1)$ ,  $R_a(1)$  is made zero by phase code modulation. The expected value of the cross term,  $C_{ab}(1)$ , is zero because the two signals are uncorrelated. However, with a finite number of samples for estimation,  $C_{ab}(1)$  will be nearly zero only if the spectra do not overlap, or if there are sufficient numbers of non-zero product terms  $[a(k).b(k)^*]$  with uniformly distributed phases, when the spectra overlap. The phases are random because the signals are uncorrelated, but the number of terms is directly proportional to  $M$  and the spectrum overlap. When spectrum widths,  $w1$  and  $w2$ , are the same, and the spectra perfectly overlap, the number of terms available for averaging (i.e., an equivalent number of independent samples; see Doviak and Zrnic 1993, p. 128) is proportional to  $(Mw2/2v_a)$ . Thus, for narrow spectrum widths of perfectly overlapped spectra,  $M$  has to be large to make  $C_{ab}(1)$  small (Sachidananda and Zrnic 1986). The cross terms are the main contributors to the  $\operatorname{var}(v2)$ . Since  $M$  cannot be made arbitrarily large, the only way to recover  $v2$  accurately is to separate the spectra before estimating the autocorrelation. In the following, a procedure is developed to separate the spectra.

The following assumptions are made in evolving the procedure: (a) noise is zero or SNR is infinity and (b) the spectrum is narrow (i.e., the Nyquist velocity is chosen large enough so that non-zero spectral coefficients span at most  $M/2$  coefficients). The effectiveness of the method depends on how well these assumptions are satisfied by a weather signal. It is also assumed that

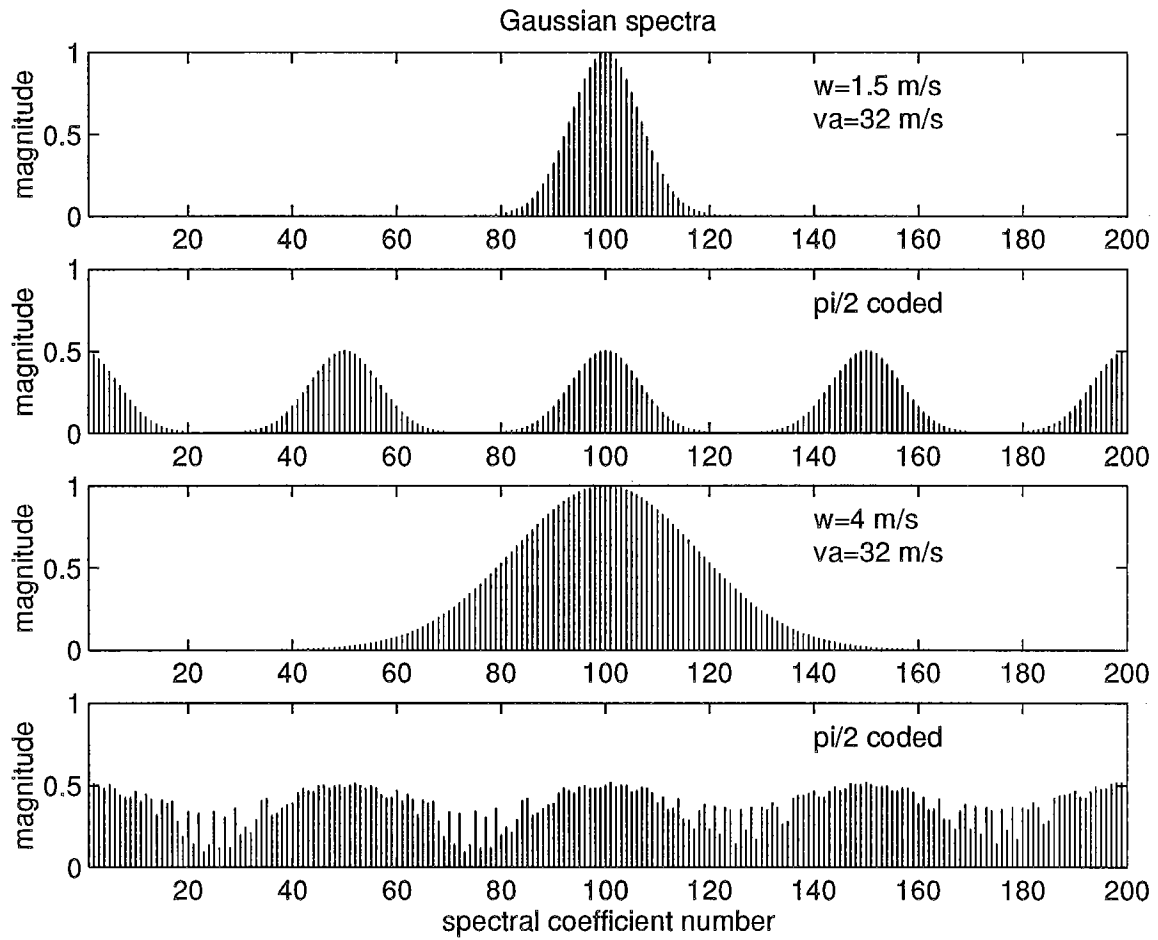


Fig. 5.5. The spectrum modification by the  $\pi/2$  phase code. Two cases are shown with narrow and wide Gaussian shaped spectra.

velocity aliasing is absent. Note that this assumption is not necessary for the algorithm to work. The algorithm recovers the aliased velocity if there is velocity aliasing.

In this procedure, the time series with the 1st trip coherent is taken, and  $R(1)$  is computed which gives the mean velocity,  $vI$ , of the 1st trip accurately (i.e.,  $sd(vI) < 1 \text{ m s}^{-1}$ ), because the weaker 2nd trip is phase modulated by the  $\pi/2$  code. A discrete Fourier transform (DFT) of the time series gives the spectrum. To recover the 2nd trip signal, a major part of the 1st trip spectrum is deleted to improve the ratio of overlaid powers.  $M/4$  coefficients centered on  $vI$  are deleted, and then remaining spectrum is cohered for the 2nd trip signal. Note that notching a major part of the coherent 1st trip spectrum also removes 1/4 of the power of the 2nd trip spectrum. When the 2nd trip signal is cohered, not all the 2nd trip signal becomes coherent because of notching. Only half the 2nd trip signal becomes coherent; the remaining 1/4 of the 2nd trip signal and the residual 1st trip signal are phase modulated. The power is distributed in four equal parts (as explained earlier) which do not contribute to the autocorrelation,  $R(1)$ . There is a net improvement in the ratio,  $p1/p2$ , after this operation. If this improvement is sufficient, one could recover the mean velocity of the 2nd trip signal at this stage. However, further improvement can be made in the  $p1/p2$  ratio using the following steps before computing the autocorrelation.

To remove the residual 1st trip signal power, we use the magnitude equality of the left and right half of the modulated spectrum. At this stage, the magnitude of the spectral coefficient alone is retained (phase is discarded). Two coefficients at  $k$  and  $k+M/2$  are taken, and the lower of the two is subtracted from both the coefficients. This process is continued for  $k=1$  to  $M/2$ . The resulting spectrum has mostly the coherent 2nd trip signal, and a small part of the unwanted 1st trip signal which biases the velocity estimate. To remove this bias, first an approximate velocity is estimated from the autocorrelation,  $R(1)$ , and then only  $M/3$  coefficients are taken centered on the approximate velocity to compute the accurate velocity. This last step is useful when the assumptions (a) and (b) mentioned earlier (in section 5.3.1) are not satisfied exactly.

These processing steps are illustrated in a series of spectra shown in Figs. 5.6(a) through (h). Figs. 5.6, (a) and (b) show the 1st and 2nd trip signal spectra. The spectral coefficient magnitude, obtained from DFT operation, versus the coefficient number, is plotted. The corresponding velocity scale is 0 to  $-v_a$  for the left half and  $+v_a$  to 0 for the right half. A simulated 400 sample time series is used for generating the spectra, and the parameters of the spectra are indicated. The next two, Fig. 5.6(c) and (d), show the effect of phase coding on the spectra. In Fig. 5.6(c), the 1st trip is coherent, and the 2nd trip signal is modulated, and in Fig. 5.6(d), it is the reverse. Since the 1st trip is stronger, the spectrum in Fig. 5.6(c) is chosen for recovering the mean velocity of the weaker 2nd trip signal. The spectrum, after  $M/4$  coefficients centered on  $vI$  are deleted, is shown in Fig. 5.6(e). In the next figure, Fig. 5.6(f), the 2nd trip signal is cohered. This spectrum has some residual, modulated 1st-trip signal. This is partially (major part) removed by subtracting "the lower of the two" from both sides of the spectrum as explained in the preceding paragraph. The result is the spectrum in Fig. 5.6(g). The last spectrum, Fig. 5.6(h), is obtained by deleting the undesirable coefficients outside the  $M/3$  coefficients centered on the recovered approximate mean velocity, computed using the autocorrelation  $R(1)$  of the spectrum in Fig. 5.6(g). In this example, the ratio  $p1/p2$  is 10 dB.

A similar sequence of steps are illustrated in the next figure, but the power ratio is 50 dB and the spectrum width is  $2 \text{ m s}^{-1}$  ( $v_a=32 \text{ m s}^{-1}$ ;  $wI/2v_a=0.03125$ ) which satisfies the

assumptions made earlier in evolving the procedure. As can be seen in Fig. 5.7(a) through (h), the recovery of the weaker signal is dramatic. Note that the weaker signal is not visible in Fig. 5.7(c) and (d); nevertheless, it is recovered in the end. However, when the spectrum width is large ( $w/2v_a > 0.0625$ ), having significant residual power, the recovery of the weaker signal is not always successful. In fact, the recovery of the weaker signal depends on the residual overlaid power.

The processing steps in Fig. 5.6(f) and (g) need some explanation. Here, the magnitude of the spectral coefficients is used and not the power. The magnitudes of the  $k^{\text{th}}$  and  $(k+M/2)^{\text{th}}$  coefficients in Fig. 5.6(f) are identical (according to eq. 5.8) if the contribution is from the 1st trip alone. If they are unequal, at most one of them has a contribution from the 2nd trip (because they are separated by  $M/2$ , and the widths are narrow). Thus, if the signal is from the 1st trip alone, the process of "subtraction of the lower of the two from both the coefficients" completely deletes both the coefficients. When they are unequal, the larger of the two retains some power.

There is an underlying assumption made in this that the larger coefficient contains the 2nd trip signal power. This is not always true for all  $k$  because the magnitude also depends on the relative phase of the two components constituting the coefficient. However, an examination of the probability of the larger coefficient containing the 2nd trip signal shows that it is always greater than 0.5. To show this, let "a" and "b" be the complex spectral coefficients of the 1st and 2nd trip signals. We have to compute the probability of  $|a+b| > |a|$ . Since the two signals can be assumed to be uncorrelated, the relative phases of  $a$  and  $b$  can be assumed to be uniformly distributed over 0 to  $2\pi$ . A simple analysis gives the probability as

$$\mathcal{P} \{ |a+b| > |a| \} = 1/2 + (1/\pi) \sin^{-1}( |b/2a| ) ; \quad |b/2a| < 1 . \quad (5.10)$$

The asymptotic value as  $|b/a| \rightarrow 0$  is 1/2, and for  $|b/a| > 2$ , it is unity. Therefore, the larger the  $|b/a|$  ratio, the better will be the recovery of the weaker signal. The notching of  $M/4$  coefficients helps the recovery in two ways, (a) it equalizes the magnitudes of the 1st trip signal in the right and left half of the spectrum and (b) it improves the  $|b/a|$  ratio.

### 5.4.3. The $\pi/2$ decoding algorithm.

In simulating the time series, the assumptions stated in page 4 are made. The algorithm given below is also based on those assumptions. *This algorithm does not use long PRT data.*

<<<-----START of  $\pi/2$  algorithm

1. Input time series  $EI_i ; i=1,2, \dots M.$ 
  - ▶ transmitter phase switching sequence  $\psi_i = \{ 0, 0, \pi/2, \pi/2, 0, \dots \text{etc.} \}$
  - ▶ note : the time series must start with 1st phase code 0 for correct decoding.
  - ▶ 1st trip is coherent; 2nd trip is phase coded by a sequence  $\phi_i = \{ \pi/2, 0, -\pi/2, 0, \dots \text{etc.} \}$

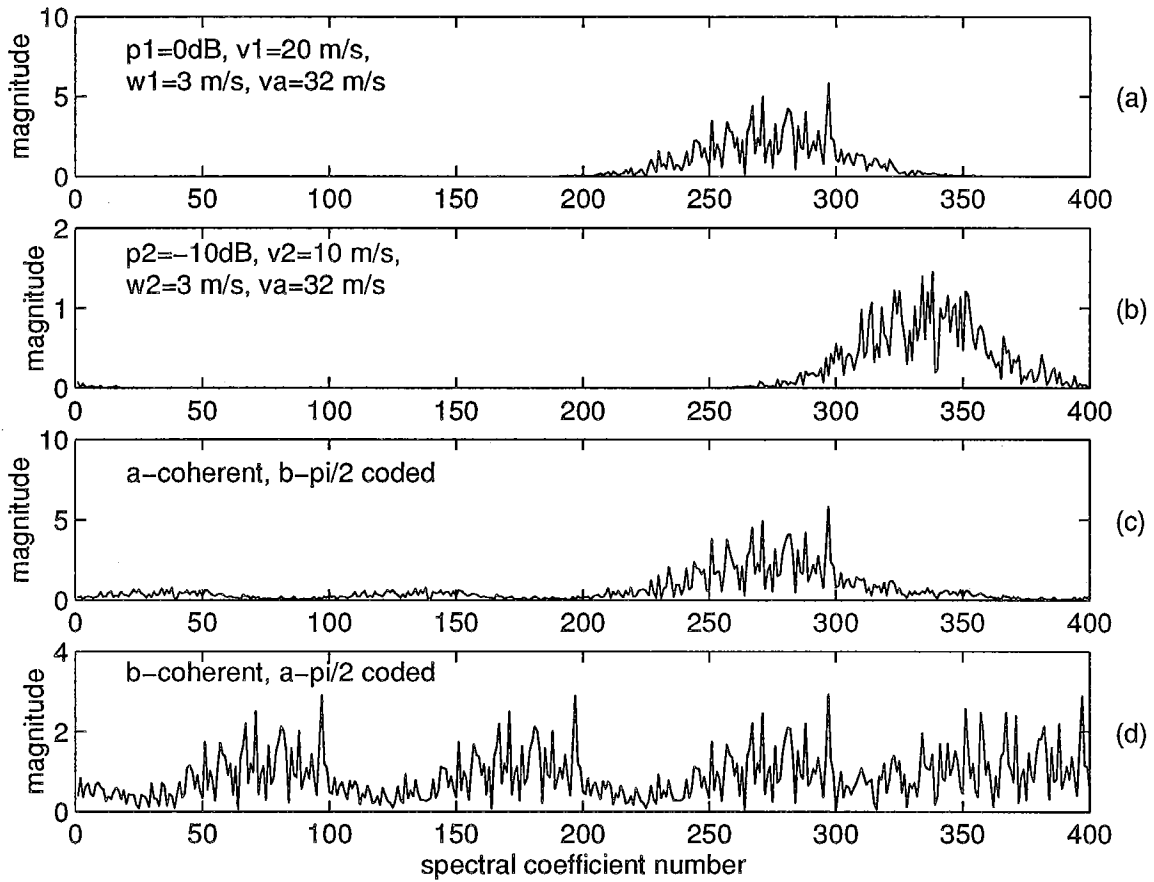


Fig. 5.6.(a-d). The processing steps in the decoding algorithm for a  $\pi/2$  phase coded radar.  $p_1/p_2 = 10$  dB.

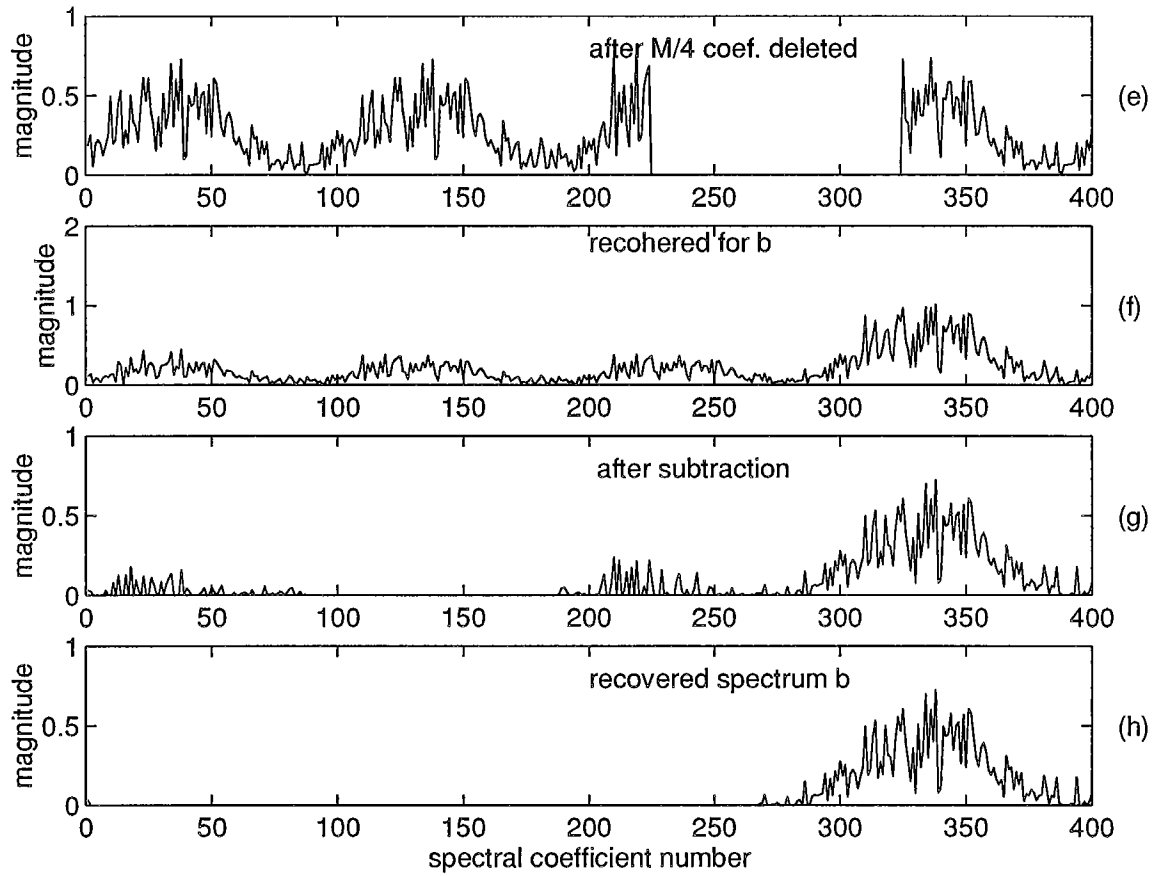


Fig. 5.6.(e-h). The processing steps in the decoding algorithm for a  $\pi/2$  phase coded radar,  $p1/p2= 10$  dB.

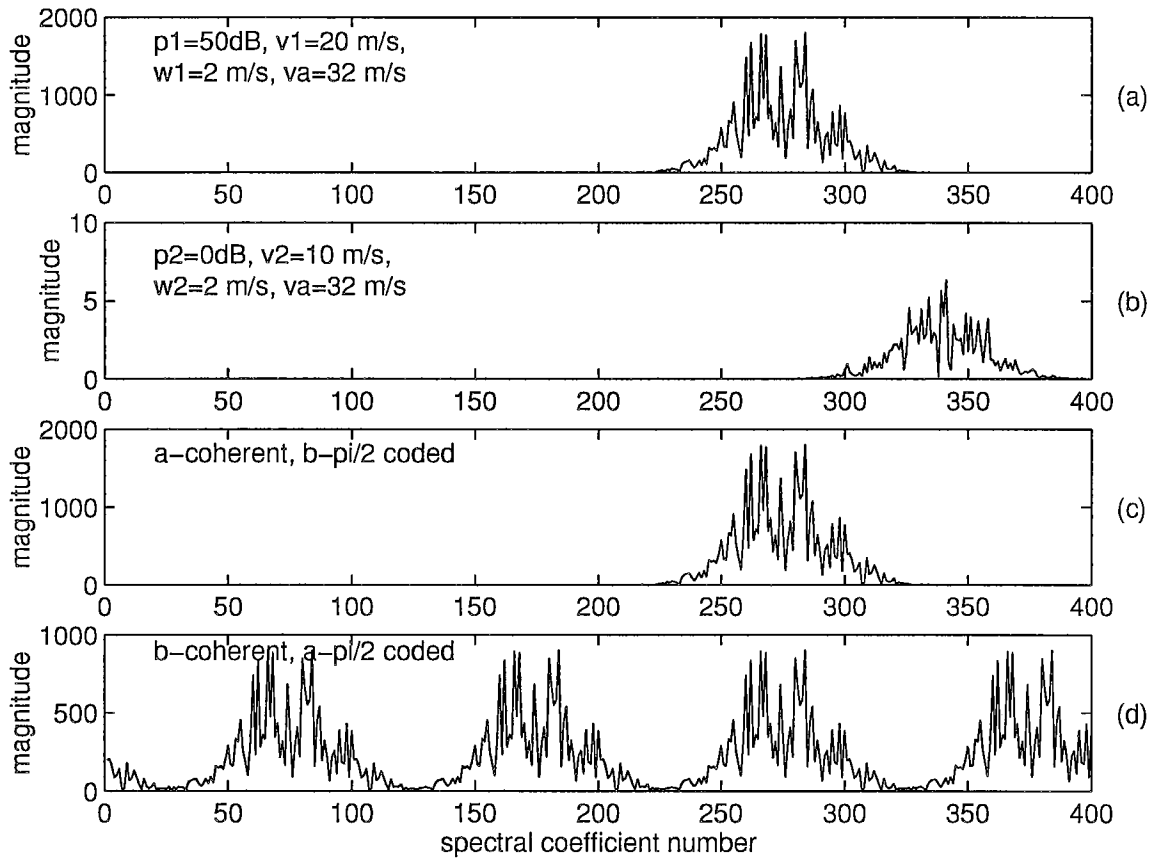


Fig. 5.7.(a-d). The processing steps in the decoding algorithm for a  $\pi/2$  phase coded radar.  $p_1/p_2=50\text{ dB}$ .

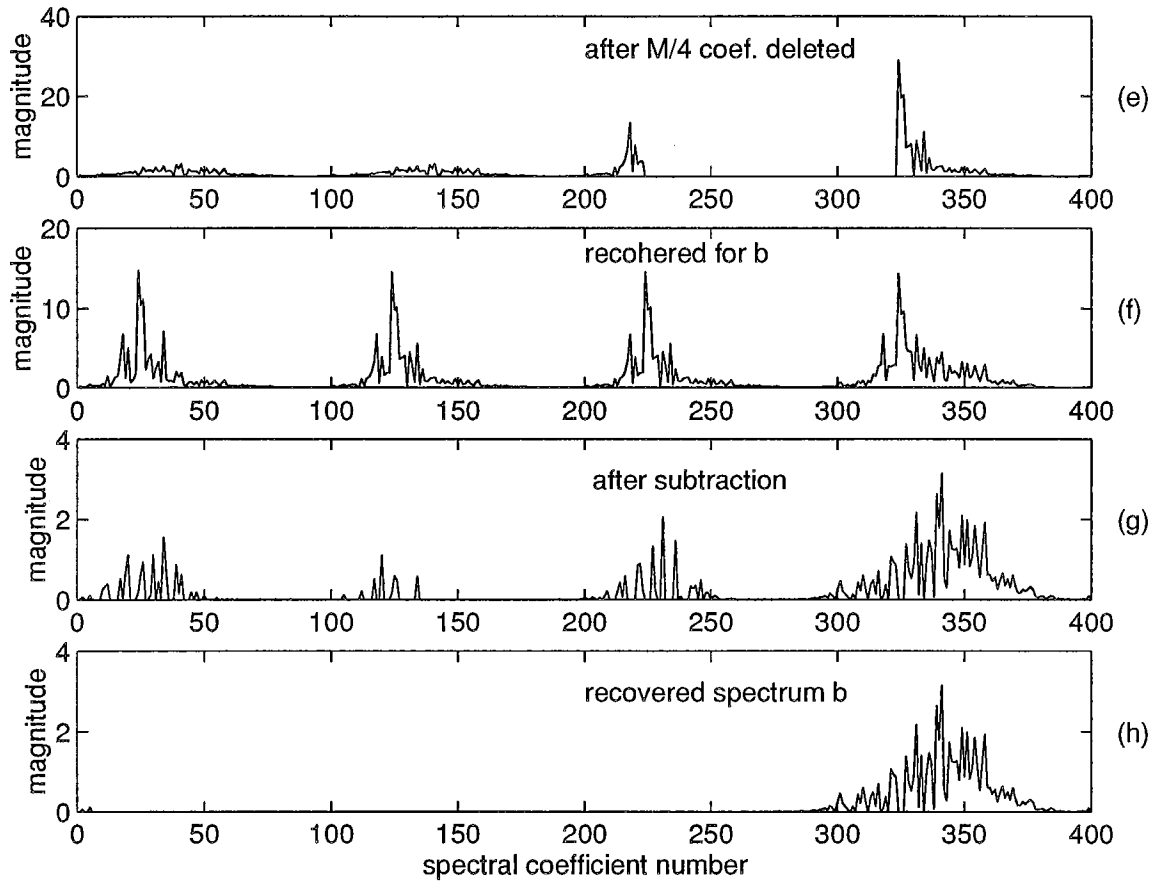


Fig. 5.7.(e-h). The processing steps in the decoding algorithm for a  $\pi/2$  phase coded radar.  $p1/p2=50$  dB.

2. Cohere the 2nd trip.
  - ▶  $E2 = E1 \cdot \exp(-j \phi_i)$
3. Autocovariance process  $E1$  and  $E2$  to get  $p1, v1, w1$  and  $p2, v2, w2$ .  
(the output parameters are estimates;  $\wedge$  is omitted for convenience.)
4. Compute  $w1/w2$  ratio.
  - ▶ if  $w1/w2 > 1$ , trip=2, 2nd trip is stronger - process  $E2$ .
  - ▶ if  $w1/w2 < 1$ , trip=1, 1st trip is stronger - process  $E1$ .
5. If  $w1/w2 > 1$ , interchange  $E1$  and  $E2$ , and all the parameters on line number 3.
  - ▶ with this interchange,  $E1$  is the time series with stronger signal coherent.
  - ▶ we need to recover  $p2, v2$  and  $w2$  of the weaker signal.
6. Compute spectrum of  $E1$ .
  - ▶  $SI' = \text{DFT} [ E1 ]$
7. Notch  $3M/4$  coefficients centered on  $v1$ . Compute mean power  $p$  from the remaining coefficients. Multiply  $p$  by 4 to get mean power  $p2$ .
8. Compute power ratio  $pr = 10 \log_{10}(p1/p2)$  (dB.)
9. If  $pr < 20$  dB, correct error in  $p1$  estimate.
  - ▶  $p1' = p1 - p2$
  - ▶ compute corrected power ratio  $pr = 10 \log(p1'/p2)$  (dB)
10. If  $pr < 20$  dB correct the error in spectrum width  $w1$ .
  - ▶  $\text{err}(w1) = 8.75374 - 1.02952 pr + 0.0415391 pr^2 - 0.000566432 pr^3$   
This is polynomial fit to the error curve, with  $v_a = 32 \text{ m s}^{-1}$ .  
[For other values of  $v_a$  multiply all constants by  $(v_a/32)^{1.5}$  ]
  - ▶ corrected  $w1 = w1 - \text{err}(w1)$
11. Notch  $M/4$  coefficients centered on  $v1$  from  $SI'$  to get  $SI$ .
12. Cohere weaker signal in  $SI$ .
  - ▶  $e1 = \text{IDFT} [ SI ]$
  - ▶ if trip = 1,  $e2 = e1 \cdot \exp(-j \phi_i)$
  - ▶ if trip = 2,  $e2 = e1 \cdot \exp(j \phi_i)$
  - ▶ compute magnitude spectrum,  $q = | \text{DFT} [ e2 ] |$
13. Subtract the residual of the stronger signal.
  - ▶  $a_k = \min \{ q_k, q_{(k+M/2)} \}$ ;  $k=1, 2, \dots M/2$ .
  - ▶ subtract  $a_k$  from both  $q_k$  and  $q_{(k+M/2)}$ ;  $k=1, 2, \dots M/2$ .

14. Compute autocorrelation for 1 PRT lag,  $R(1)$  from  $q$ , and compute approximate mean velocity  $v_2'$ .
15. Delete unwanted coefficients outside  $M/3$  coefficients centered on  $v_2'$ .
16. Recompute  $R(1)$  and  $v_2, w_2$ .
17. If trip = 2, interchange parameters  $(p_1, v_1, w_1)$  and  $(p_2, v_2, w_2)$
18. Output 1st and 2nd trip parameters and go to next data set.

<<<-----END of algorithm

#### 5.4.4. Simulation and results.

To evaluate the performance of the algorithm, a simulation study was performed along the same lines as that for random phase coding in section 4. A test program was written which inputs a set of parameters for the 1st and 2nd trip signals into the simulation program to generate a overlaid time series, and this time series is processed by the algorithm to recover the parameters. These recovered parameters are compared with the parameters of the two signals, computed individually by the autocovariance processor before adding. The window effect, the effect of noise, and the ground clutter filtering are not included as in the random phase case, so that the comparison among the various methods is based on the basic capability of the method alone.

A large number of simulations were carried out to characterize the performance. Some sample scatter plots of the errors in the estimated parameters are in Fig. 5.8, Fig. 5.9, and Fig. 5.10. The power ratio,  $p_1/p_2$ , is varied over 0 to 70 dB, and the velocity difference ( $v_1-v_2$ ) is randomly chosen for each simulation to be within  $\pm 28 \text{ m s}^{-1}$ . The unambiguous velocity,  $v_a$ , is  $32 \text{ m s}^{-1}$  with a PRT = 0.7812 ms. The velocities,  $v_1$  and  $v_2$ , are restricted to be less than  $v_a$  to avoid aliasing error. The spectrum widths are set to  $4 \text{ m s}^{-1}$  for both signals. Each point on the plots corresponds to one simulation with  $M = 64$  samples. It can be observed that the error in the velocity  $v_2$  (see Fig. 5.8) is the limiting factor since the power,  $p_2$ , can be recovered over a much larger dynamic range of  $p_1/p_2$  (Fig. 5.9). For  $4 \text{ m s}^{-1}$  width of the stronger signal,  $v_2$  can be recovered up to a limit of about  $p_1/p_2=20 \text{ dB}$ , with  $M = 64$ . The standard error is somewhat larger than  $1 \text{ m s}^{-1}$  at  $p_1/p_2=20 \text{ dB}$ . Although the error in  $v_2$  appears as random in the scatter plot (see Fig. 5.8) for large  $p_1/p_2$  ratios, there is, in fact, a systematic bias error, unlike in the case of random phase coding. This bias error is caused by the residual of the 1st trip signal that is not removed by the subtraction procedure. The spectral processing procedure could be employed to remove this residual power, but involves more computation. The random appearance of error in Fig. 5.8 is because the velocity difference was varied over all possible values. If ( $v_1-v_2$ ) is kept constant, the scatter plot will show the bias error clearly. However, to evolve a bias correction mechanism, a large number of simulations have to be run with different parameters, and from these results, empirical error correction formulae can be generated. By estimating this systematic bias, which is a function of  $p_1/p_2, w_1$ , and ( $v_1-v_2$ ), and correcting the error, we can

extend the recovery limit to about  $p1/p2 = 35$  dB for  $w1=4$  m s<sup>-1</sup> and  $M=64$ . In the presented algorithm, this bias correction has not been implemented.

Results of simulations, where in addition to  $p1/p2$  and  $(v1-v2)$ ,  $w1$  is also a parameter, are summarized in Fig. 5.11. The spectrum width of the weaker signal,  $w2$ , and the number of samples,  $M$ , are kept constant ( $w2=4$  m s<sup>-1</sup>;  $M=64$ ). The standard error in the estimated velocity  $v2$  is quantized for plotting, and a gray shade is assigned to each level. The scale on the right shows the quantization levels. If 1 m s<sup>-1</sup> is the acceptable limit for the error, the recovery region is approximately that given by the theoretical limit shown in Fig.4.4 for notch width of  $M/4$ . If bias correction is implemented, the recovery limit can be extended nearly up to the limit corresponding to the  $M/2$  notch width in Fig.4.4. Note that in the region of recovery, the standard error is very small. This is because when  $w1$  is small, the spectrum is accurately recovered, and when  $w1$  is large, the assumption that the spectrum is confined to  $M/2$  coefficients only is not satisfied, producing a bias error.

Given the fact that the  $\pi/2$  coding splits the spectrum into four equal parts shifted by  $M/4$  coefficients, and that there is a definite phase relationship among the four components, it is possible to devise other methods of recovering the mean velocity of the weaker signal. For example, we can select one quarter of the spectrum farthest from the mean velocity of the stronger signal, and compute the mean velocity and mean power of the weaker signal. This part of the spectrum has the least amount of power from the stronger signal. If  $v2$  is the estimated velocity of the weaker signal, the correct velocity will be one of the four values  $\{v2, v2 \pm v_d/2, v2 \pm v_d, v2 \pm 3v_d/2\}$ ; select the four which are in the 0<sup>th</sup> aliasing interval}. To select the correct value from these four, a comparison of phase difference (taking one of them as a reference) among the spectral coefficients at three of these four locations farthest from  $v1$  can be used. Obviously, the limitation will be the contamination from the stronger signal at these locations and would be equivalent to a notch width smaller than  $3M/4$  used for velocity recovery. The performance of this method is likely to be comparable to the one that is given in this section.

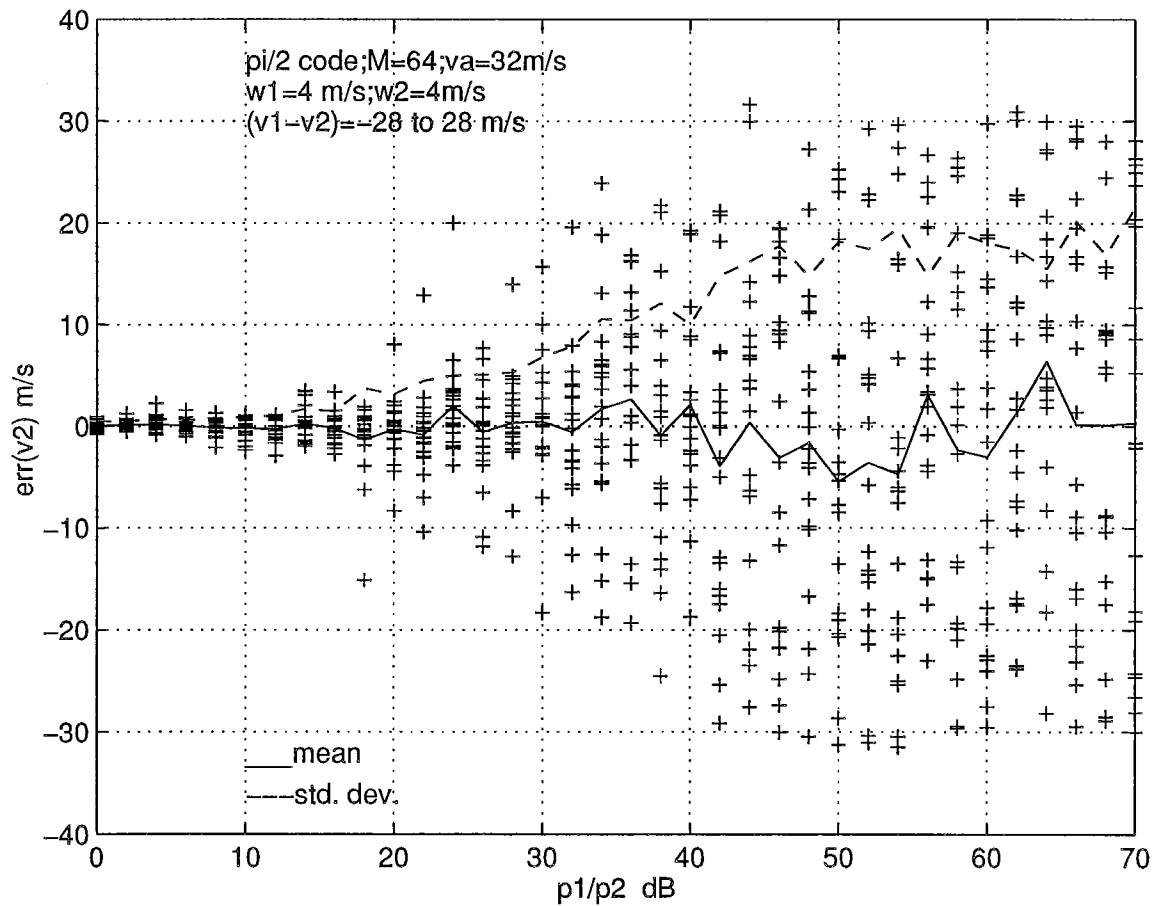


Fig. 5.8. Error in the mean velocity estimate,  $v_2$ , of the weaker signal recovered using the  $\pi/2$  phase coding method. The velocity difference and  $p_1/p_2$  are varied over  $\pm 28\text{ m s}^{-1}$  and 0 to 70 dB respectively, in the simulation. The error is the difference between the recovered velocity and the velocity estimated using the autocovariance algorithm without the overlaid signal.

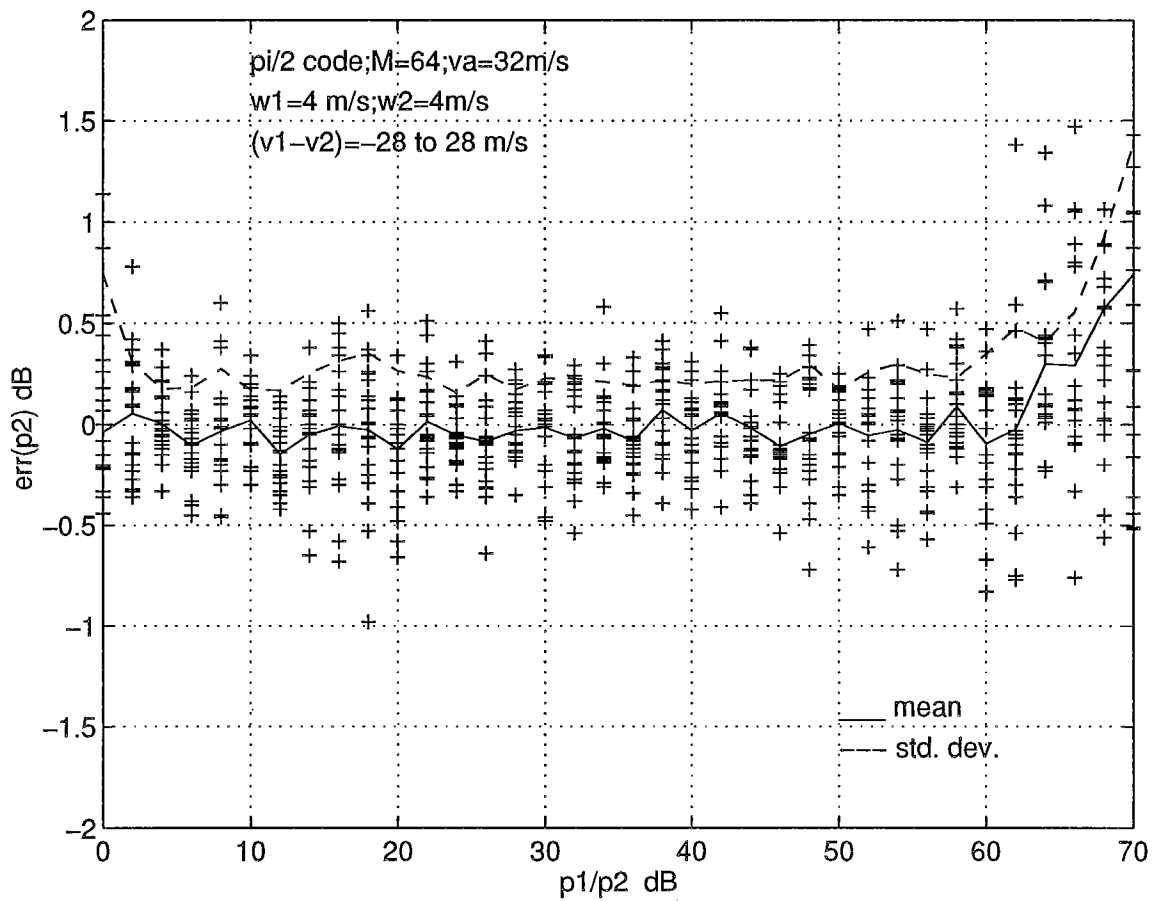


Fig. 5.9. Error in the mean power estimate,  $p_2$ , of the weaker signal recovered using the  $\pi/2$  phase code method. The velocity difference and  $p_1/p_2$  are varied over  $\pm 28 \text{ m s}^{-1}$  and 0 to 70 dB, respectively, in the simulation.

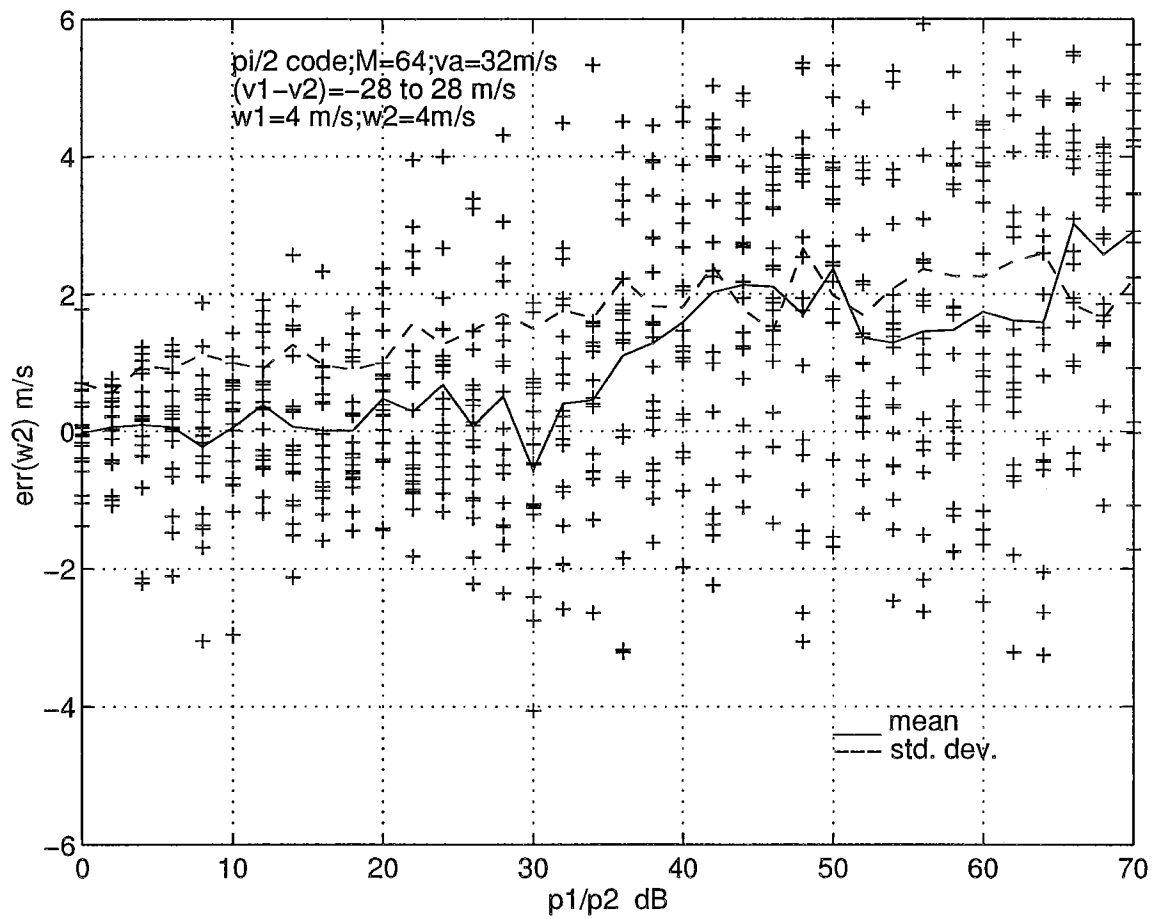
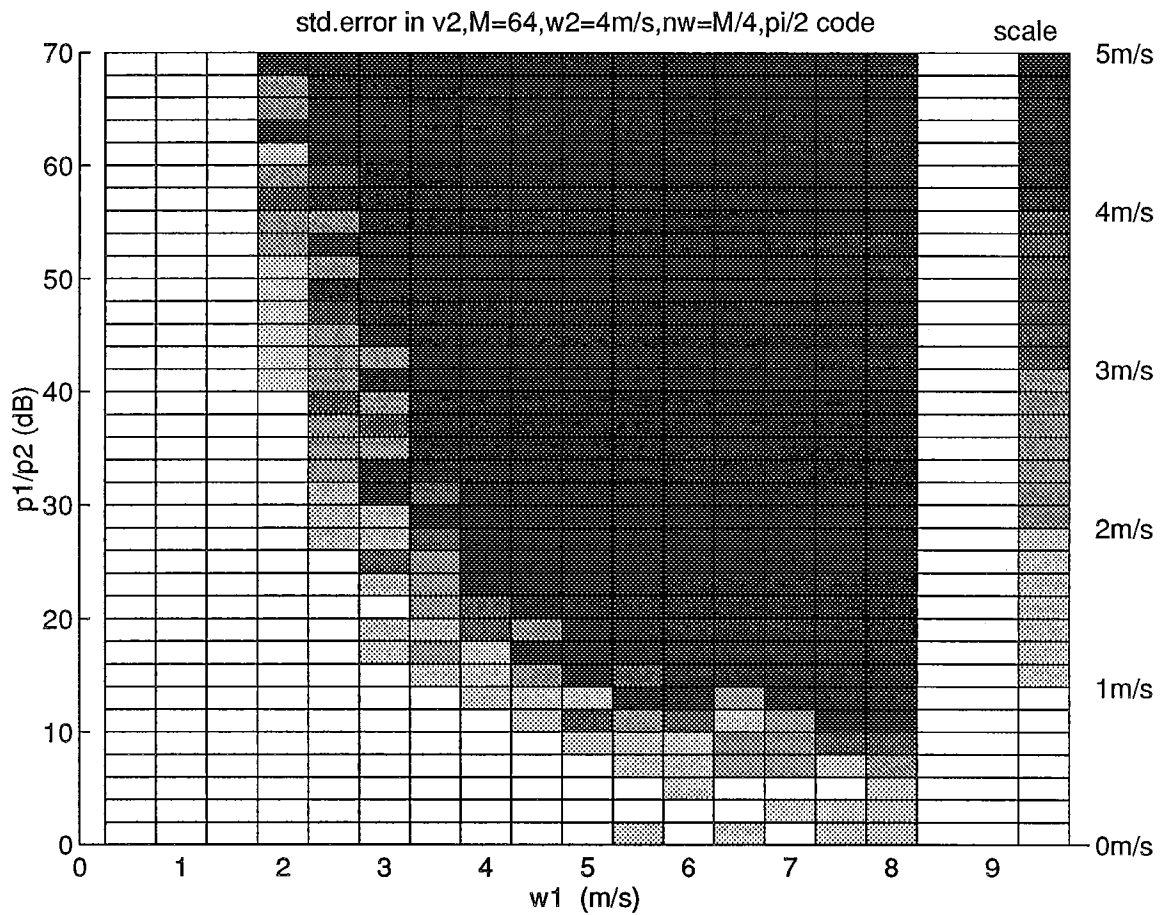


Fig. 5.10. Error in the spectrum width estimate,  $w_2$ , of the weaker signal recovered using the  $\pi/2$  phase code method. The velocity difference and  $p_1/p_2$  are varied over  $\pm 28\text{ m s}^{-1}$  and 0 to 70 dB, respectively, in the simulation.



**Fig. 5.11.** Standard deviation of the error in recovered velocity,  $v_2$ , of the weaker signal as a function of  $p_1/p_2$  and width,  $w_1$ , of the stronger signal, using the  $\pi/2$  phase code method. Each rectangle represents the standard deviation computed using 20 simulations with corresponding input parameters shown on the axes. The velocity difference is varied over  $\pm 28 \text{ m s}^{-1}$ . The quantization levels and the gray shades assigned to each level are indicated on the right, and the fixed parameters are at the top of the figure.

## 5.5. Optimizing the systematic code.

The three phase coding algorithms presented so far give us some insight into the working of phase coding techniques. The phase coding seeks to modify the spectrum of one of the overlaid signals so that the spectral parameters of the other can be recovered by appropriate processing techniques. Conceptually, all three methods have been reported in the literature; however, the algorithms developed and presented in this report show improved performance because of larger notch width and some additional spectral domain processing steps introduced in the algorithms. Specifically, the subtraction process in the  $\pi/2$  coding technique and smoothing and subtraction (S&S) procedure in random phase technique are the important ones. The improvement in the recovery of velocity, due to the S&S step, is equivalent to an increase of the weaker signal by 3 to 5 dB. The noise power removed by the S&S step is roughly same as the noise that does not contribute to  $R(1)$ . Therefore, the S&S step can be eliminated from the random phase algorithm, if the width is not required to be estimated. The effectiveness of the autocovariance processor is limited by the "whiteness" of the noise or the "matching property" of the modulated spectra. This leads us to the possibility of further improvement in the performance by selecting a phase code with better "whitening" or the "matching" property. In this, section we explore this possibility and arrive at a better phase code.

### 5.5.1. Conceptual development.

The performance of each method is summarized in a plot of  $sd(v_2)$  as a function of overlaid power ratio,  $p_1/p_2$ , and spectrum width,  $w_1$ , of the stronger of the two overlaid signals. This we refer to as  $err(v_2)$  plot in  $\{p_1/p_2; w\}$  space in the rest of the report. All the results of the simulation study of the four algorithms presented so far indicate that the region of  $\{p_1/p_2; w\}$  space, where the velocity of the weaker signal can be recovered, is demarcated by the  $R_p$  for the notch width used in the algorithm (See Figs. 4.19, 5.3, & 5.11). This suggests that the limiting factor is the residual stronger signal power after notch filtering. Therefore, to increase the region of recovery, it is necessary to increase the notch width.

The  $\pi/2$  and  $\pi/4$  schemes have fixed notch widths dictated by the code itself; therefore, the region of recovery in the  $\{p_1/p_2; w\}$  space is also fixed. The error in the velocity is small in the region of recovery, and as the  $p_1/p_2$  increases for larger widths, the velocity has a bias error. In the  $\pi/2$  scheme, this bias can be removed to some extent by a bias error correction scheme or further processing in the spectral domain to increase the region of recovery. Even with this correction, the upper bound is that of the  $M/2$  notch width. For the  $\pi/4$  code, the sign ambiguity is the main problem that limits the recovery.

In the case of the random phase technique, the error in  $v_2$  has no bias, and the standard deviation of the error is a function of the SNR that can be achieved after notch filtering and cohering. A larger notch width decreases the residual power and increases the region of recovery in the  $\{p_1/p_2; w\}$  space, but at the same time reduces the SNR (due to increased self noise), producing a larger standard error in the velocity estimate. There are two components to the noise power; one is the residual part of the stronger signal, and the other is the part of the weaker signal power that does not cohere (self noise) because of notch filtering.

Now, given a notch width and spectral parameters of the weather signal, the residual of the stronger signal power in the spectrum is fixed. Therefore, the scope for further improvement is in maximizing the coherent part of the weaker signal, and in improving the whiteness and the matching property of the residual noise. Since we do not have control on the weather signal the best we can do is to select a phase code that allows us to cohere maximum amount of the power from the original spectrum, and make the spectrum of the residual stronger signal power as white as possible at the same time ( or make it as identical as possible in the left and right half of the spectrum). There is an upper limit for the whiteness that can be achieved for weather signals if the random phase coding is used (see Fig.4.8). But there is a possibility of achieving a significantly larger rejection ratio using the systematic code, where a better match between the left and right half of the spectrum can be obtained. The phase coding essentially redistributes the power in the spectral domain. A well designed code allows reconstruction of the signal spectra from the filtered and cohered spectra, with a largest possible self SNR (SNR due to self noise alone). In this, the distribution of phase of the individual components making up the coefficient plays an important role. The two requirements viz., restoring the spectrum, and minimizing the residual noise via notch filtering, are conflicting which suggests that the optimum code is a compromise.

A systematic phase code that has the property of zero cyclic autocorrelation for all lags except zero lag is given by Chu (1972). This property is the same as that of the spectrum of the code being perfectly flat, or all spectral coefficients having the same magnitude. The code is given by the expression

$$C_k = \exp( jn\pi k^2/M ) \ ; \ k=0,1,2,\dots \quad (5.11)$$

where  $n$  is prime to  $M$  (i.e.,  $M$  not divisible by  $n$ ). In fact, for  $M$  even, any odd number,  $n$ , will produce a flat spectrum and zero autocorrelation, for all lags except zero. The phases progress in a quadratic fashion with the smallest step size determined by  $(n\pi/M)$ , but appear as random when reduced to  $(0-2\pi)$ . If  $n$  and  $M$  are even, only a few of the spectral coefficients are non-zero, and they have equal magnitude. Few sample code spectra are shown in Fig. 5.12 for  $n=1,4,8$  and 11, with  $M=64$ . Note that for odd  $n$ , the spectrum is flat, and for even  $n$ , some of the coefficients are zero. If  $M$  is divisible by  $n$ , only  $M/n$  coefficients are non-zero. For  $n=1$  and 11, the spectra differ only in phase.

If a weather signal is modulated by this phase code, the resulting spectrum is the convolution of the code spectrum and the signal spectrum. Thus, if  $n/M=1/8$ , the spectrum of the coded signal would have 8 peaks separated by  $M/8$  coefficients, with one of the peaks at the same location as the original uncoded spectrum. To be able to cohere the weaker signal and recover the velocity, we require at least two of these peaks retained in the spectrum after notch filtering. This will put an upper limit on the maximum notch filter width that can be used for a given  $n/M$ . The SNR due to self noise decreases as a function of increasing notch width, hence the standard error in the velocity estimate also limits the maximum usable notch width. In a practical situation the lower of the two is to be selected. It is important to note that the functional dependence of the self SNR on  $n_w$  is different from that given by eq. (4.2), because the signal is not whitened by the code, but is systematically modified. After notch filtering and

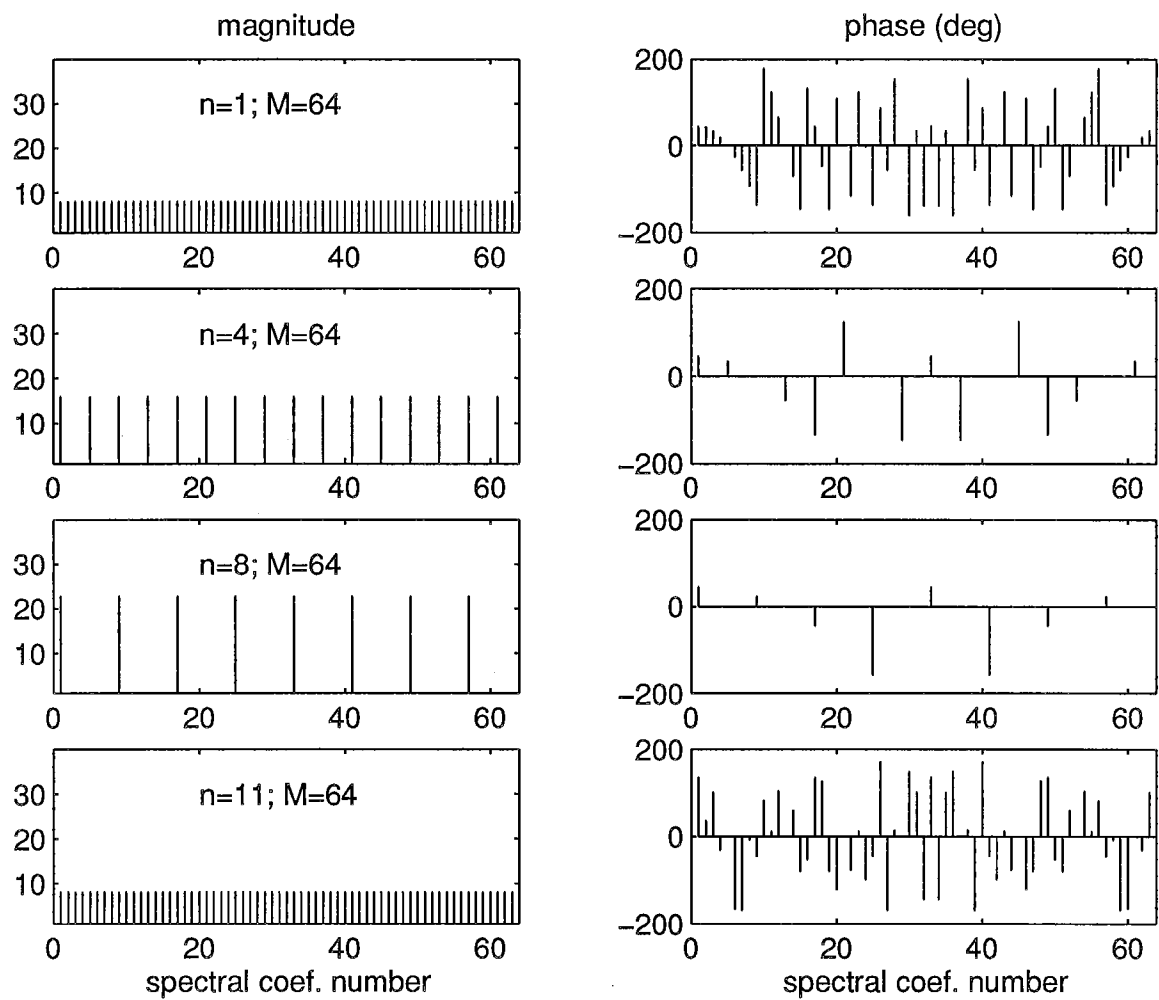


Fig. 5.12. Amplitude and phase of the spectral coefficients of the code  $C_k = \exp(jn\pi k^2/M)$ , with  $M=64$ . Four cases,  $n = 1, 4, 8, \& 11$ , are plotted.

cohering, the weaker signal the spectrum consists of the original signal and a few symmetrically distributed side bands with lower powers. This increases the spectrum width of the signal but does not bias the velocity. For a given notch width, the self SNR is significantly better than that for the random phase coding, thus, we can use a notch filter width larger than  $M/2$  (for  $M=64$ ) and still recover  $v_2$  with a tolerable standard error. This will effectively increase the region of  $v_2$  recovery in the  $\{p_1/p_2, w_1\}$  space.

For a given notch filter width and the signal time series length,  $M$ ,  $n=1$  would yield the best self SNR. The whitening of the residual of the stronger signal also the best for this value. However, as noted earlier in section 4, there is an upper limit to the whitening that can be achieved. As we increase the code parameter,  $n$ , the whitening property changes to matching property (perfect matching occurs at  $n=16$  for  $n_w=0.75$ ), which can suppress the contribution of the residual of the stronger signal to the autocorrelation more effectively. However, for  $n_w=0.75$ , maximum value of  $n$  is 8. Thus, if we select  $n_w = 0.75$ ,  $n=8$  would result in the best matching property in the residual of the stronger signal (for  $n=8$ ,  $\max(n_w)=0.75$ ), but would produce a lower self SNR.

To determine the best value of  $n$  for  $n_w=0.75$ , a simulation study was performed with  $n$  as a variable. The spectrum width of both signals is maintained at  $4 \text{ m s}^{-1}$ . The overlaid power ratio,  $p_1/p_2$ , and velocities,  $v_1$  and  $v_2$ , are varied over 0 to 70 dB and  $\pm 28 \text{ m s}^{-1}$ , respectively. The standard error in recovered  $v_2$  is shown in Fig. 5.13. It is clear from this figure that  $n=8$  is the optimum value for the code. The standard error in  $v_2$  progressively decreases and reaches a lowest value at  $n=8$ , and then again starts to increase. There is a symmetry about  $n=32$ . This is because the phase code is the same for  $n=x$  and  $n=M-x$ , when reduced to  $(0-2\pi)$ . Note that the selected  $n_w$  is more than the maximum usable value for  $9 \leq n \leq 56$ . However, for  $9 \leq n \leq 14$  (and also for  $50 \leq n \leq 56$ ), partial cohering takes place, thus, we are able to recover  $v_2$ , but with a progressively increasing standard error. For codes with  $n$  between 16 and 48, the recohering entirely fails because of the larger than maximum allowed notch filter width, although the code spectrum is flat!

The code  $C_k = \exp(jn\pi k^2/M)$ , with  $n/M=8/64$ , is a sequence of complex numbers with which we have multiplied the 2nd trip signal to change its spectrum, or  $\phi_k = (n\pi k^2/M)$  is the sequence of phase shifts required to be applied to the 2nd trip signal samples when the 1st trip signal is coherent. Note that this is not the phase shift sequence for the transmitted pulses. To obtain the phase switching sequence, proceed as follows: Let  $\psi_k$ ,  $k=0,1,2,\dots$ , be the phase switching sequence for the transmitter pulses. The return samples for the 1st trip will have the same phase shifts, and the 2nd trip signal samples will have phase shifts  $\psi_{k-1}$  (the same sequence shifted by one pulse). Therefore, when the 1st trip signal is made coherent by multiplying the raw time series by complex numbers  $C_k^*$  (or phase shifted by  $-\psi_k$ ), the resulting phase shifts in the 2nd trip time series is the sequence  $(\psi_{k-1} - \psi_k) = \phi_k$ . Given the sequence of phases,  $\phi_k$ , we can compute  $\psi_k$  as

$$\psi_k = - \sum_{m=0}^k \phi_m = - \sum_{m=0}^k (n\pi m^2/M) ; \quad k=0,1,2, \dots \quad (5.12)$$

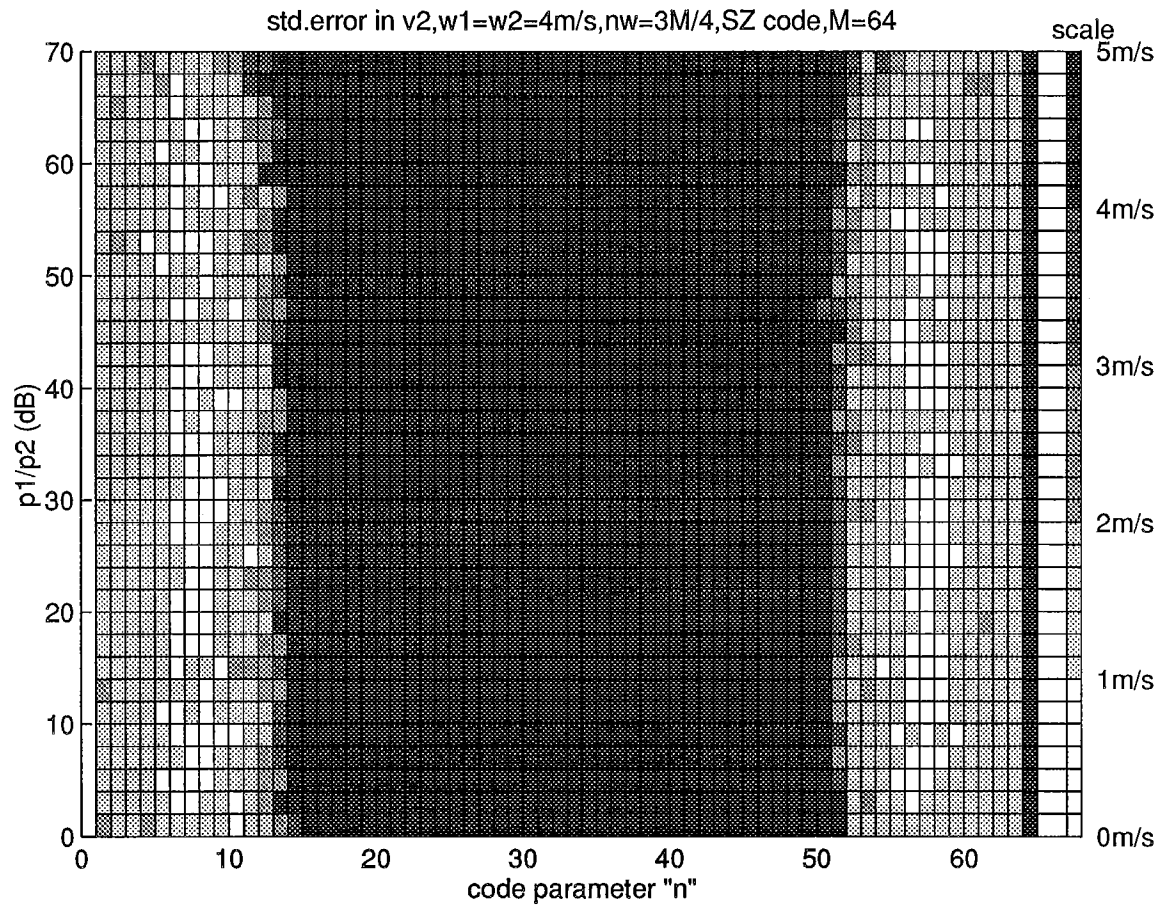


Fig. 5.13. Standard deviation of the error in velocity,  $v_2$ , of the weaker signal as a function of code parameter,  $n$ . Phase code,  $C_k = \exp(jn\pi k^2/M)$  with  $M=64$ . Each rectangle represents standard deviation obtained using 20 simulations with the indicated parameters. Gray scale on the right depicts the quantization levels.

With  $M=64$  and  $n=8$ , this sequence has a periodicity of 32, although  $\phi_k$  has a periodicity of 8. All the phase values are multiples of  $\pi/8$ , and hence are easy to realize using a digital phase shifter (a 4-bit phase shifter is sufficient). We refer to the code given by equation (5.12) as the **switching code** or the **SZ code** in general, and specifically the **SZ(8/64) code** for  $n=8$  and  $M=64$ . The phase sequence,  $\phi_k$ , will be referred to as the **modulation code**.

For a sample sequence length other than 64, optimum  $n$  lies somewhere between  $M/8$  and  $M/10$ , and it is not necessary that  $n$  be an integer. The only difficulty in practice would be that the switching code may have a periodicity much longer than the number of samples,  $M$ , and the phase shifts needed may not be exactly realizable with a commercial  $m$ -bit digital phase shifter which generally has the smallest phase increment of  $2\pi/2^m$  radians.

A more detailed discussion on the SZ code is included in the part-2 of this report.

### 5.5.2. The decoding algorithm for optimum systematic code.

The decoding algorithm is similar to the random phase algorithm except that the phase code is SZ(8/64), and the notch width is different. The random phase algorithm is repeated here with these changes for convenience of the reader. *This algorithm does not use long PRT data.*

<<<-----START of algorithm

1. Input time series  $E1_k$ ;  $k=0,1,2, \dots M-1$ .
  - ▶ 1st trip is coherent; 2nd trip is phase coded by a sequence  $\phi_k = n\pi k^2/M$ ;  $k=0,1,2,\dots M-1$ .
2. Cohere the 2nd trip.
  - ▶  $E2 = E1 \exp \{-j \phi_k\}$
3. Autocovariance process  $E1$  and  $E2$  to get  $p1, v1, w1$  and  $p2, v2, w2$ .  
(the outputs are estimates; the symbol  $\wedge$  is omitted for convenience.)
4. Compute  $w1/w2$  ratio.
  - ▶ if  $w1/w2 > 1$ , trip=2, 2nd trip is stronger - process  $E2$ .
  - ▶ if  $w1/w2 < 1$ , trip=1, 1st trip is stronger - process  $E1$ .
5. If  $w1/w2 > 1$ , interchange  $E1$  and  $E2$ , and all the parameters on line number 3.
  - ▶ with this interchange,  $E1$  is the time series with stronger signal coherent.
  - ▶ we need to recover  $p2, v2$  and  $w2$  of the weaker signal.

[ Note: The processing steps 6 to 17 are same for the two cases in step 4, with  $E1$  replaced by  $E2$ . This is accomplished by the step 5 and the trip numbers are restored in the step 18.]
6. Compute spectrum of  $E1$ .
  - ▶  $SI' = \text{DFT} [ E1 ]$

7. Notch  $3M/4$  coefficients centered on  $v1$  to get  $SI$  from  $SI'$ .
  8. Compute mean power  $p$  from the remaining coefficients.  
Multiply  $p$  by 4 to get mean power  $p2$ .
  9. Compute power ratio  $pr = 10 \log_{10}(p1/p2)$  (dB.)
  10. If  $pr < 20$  dB, correct error in  $p1$  estimate.
    - ▶  $p1' = p1 - p2$
    - ▶ compute corrected power ratio  $pr = 10 \log(p1'/p2)$  (dB)
  11. If  $pr < 20$  dB correct the error in spectrum width  $w1$ .
    - ▶  $err(w1) = 8.75374 - 1.02952 pr + 0.0415391 pr^2 - 0.000566432 pr^3$   
This is polynomial fit to the error curve for  $v_a = 32 \text{ m s}^{-1}$ .  
[For other values of  $v_a$  multiply all constants by  $(v_a/32)^{1.5}$  ]
    - ▶ corrected  $w1 = w1 - err(w1)$
  12. Cohere the weaker signal in  $SI$ .
    - ▶  $e1 = \text{IDFT} [ SI ]$
    - ▶ if trip = 1,  $e2 = e1 \exp\{-j \phi_k\}$
    - ▶ if trip = 2,  $e2 = e1 \exp\{j \phi_k\}$
    - ▶ compute magnitude spectrum,  $q = | \text{DFT} [ e2 ] |$
  13. Apply smoothing filter to  $q$ .
    - ▶  $q = \text{SF}( q; m)$ ; (choose filter length  $m=9$  for  $M=64$ ).
  14. Subtract the residual stronger signal.
    - ▶  $a_k = \min \{ q_k, q_{(k+M/2)} \}$ ;  $k=1,2, \dots M/2$ .
    - ▶ subtract  $a_k$  from both  $q_k$  and  $q_{(k+M/2)}$ ;  $k=1,2, \dots M/2$ .
  15. Compute autocorrelation for 1 pulse lag,  $R(1)$  for  $q$ , and compute approximate mean velocity  $v2'$ .
  16. Delete coefficients outside  $M/3$  interval centered on  $v2'$ .
  17. Recompute  $R(1)$  and  $v2, w2$ .
  18. If trip = 2, interchange parameters  $(p1,v1,w1)$  and  $(p2,v2,w2)$ .
  19. Output 1st and 2nd trip parameters and go to next data set.
- <<<-----END of algorithm

### 5.5.3. Simulation results and discussion.

To evaluate the performance of the algorithm, a simulation study was performed along the same lines as that for random phase coding in section 4. A test program inputs a set of parameters for the 1st and the 2nd trip signals into the simulation program to generate an overlaid time series, and this time series is processed by the algorithm to recover the parameters. These recovered parameters are compared to the actual parameters of the two signals computed individually by the autocovariance processor before addition.

In the simulations, the power ratio,  $p1/p2$ , and the velocity difference  $(v1-v2)$  were varied over 0 to 70 dB, and  $\pm 28 \text{ m s}^{-1}$  respectively. A scatter plot of the error in recovered  $v2$  is in Fig. 5.14. The unambiguous velocity,  $v_a$ , is again  $32 \text{ m s}^{-1}$  with a PRT = 0.7812 ms. The spectrum widths are set to  $4 \text{ m s}^{-1}$  for both the signals. Each point on the plots corresponds to one simulation with  $M = 64$  samples. The mean and standard deviation of the error are also shown in the figure. The standard error is approximately  $1 \text{ m s}^{-1}$  over a large dynamic range of the  $p1/p2$  ratio. Compare this with Fig.4.12 for the random phase case, and note a significant improvement in the velocity recovery.

A large number of simulations were run with  $p1/p2$ ,  $w1$ , and  $(v1-v2)$  as parameters. The spectrum width of weaker signal, and the number of samples, are kept constant ( $w2=4 \text{ m s}^{-1}$ ;  $M=64$ ). The standard error in the estimated velocity,  $v2$ , summarizes the performance of the optimized systematic code (Fig. 5.15). Compare this with the corresponding Fig.4.19 for the random phase coding. Even with a  $3M/4$  notch width, we are able to achieve a standard error of  $1 \text{ m s}^{-1}$  in the region of recovery in  $\{p1/p2;w\}$  space, and the region of recovery is also much larger.

This section presents a study of the optimized systematic phase code and its performance. A comparison of performance of this scheme with the random phase method discussed earlier clearly shows that the optimized systematic code (SZ code) is better.

There is scope for further improvement in the algorithm because we have used a fixed notch width of  $3M/4$  coefficients. As discussed in the case of random phase coding in Section 4, this notch width is an overall optimum in the sense of maximizing the region of recovery in the  $\{p1/p2;w\}$  space with an upper bound on the standard error in  $v2$ . This choice of notch width results in roughly the same SNR over all the recoverable  $\{p1/p2;w\}$  space, but this SNR is the maximum achievable SNR only along the  $p1/p2=R_p$  curve (i.e., at the limit of recovery). There may be some room for improving the standard error in the region of recovery by adaptive notch filter width which maximizes the SNR. These aspects are discussed in the second part of this report.

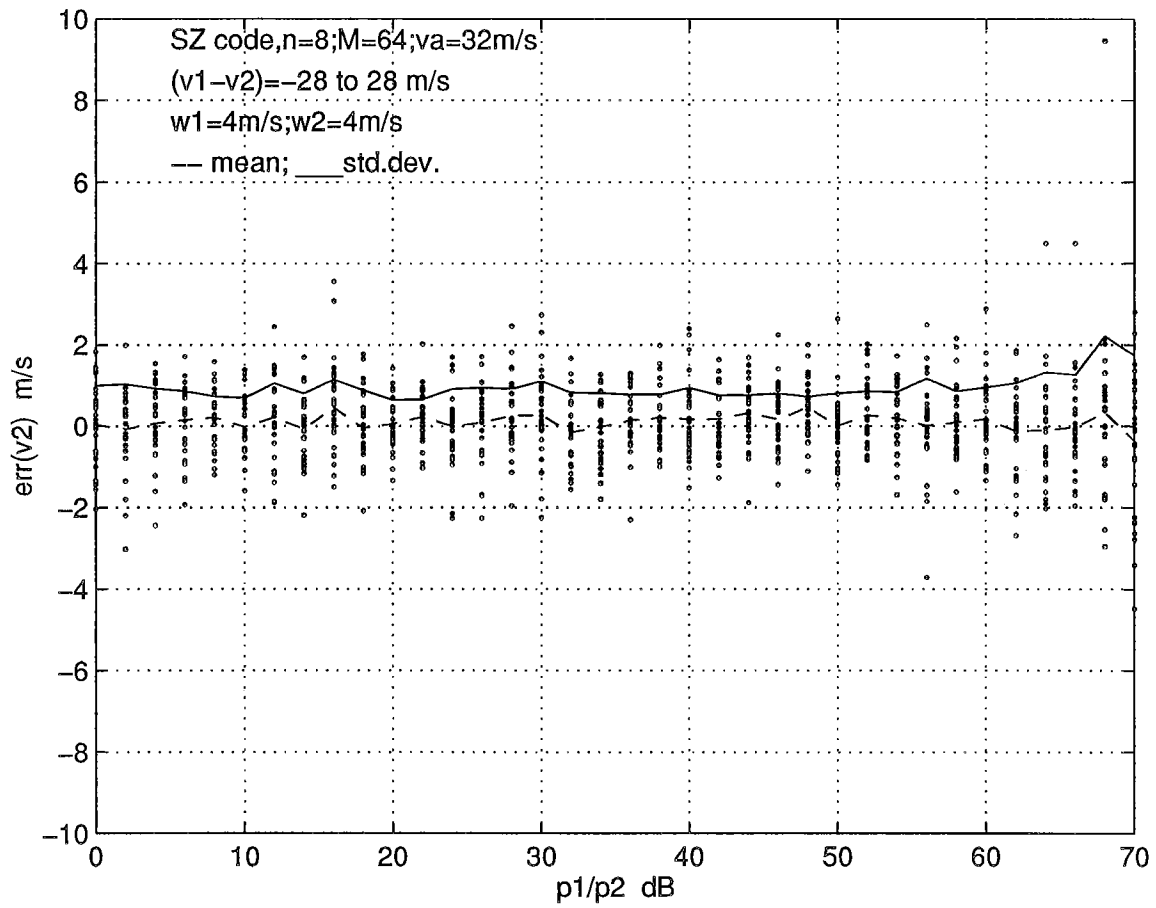


Fig. 5.14. Error in recovered  $v_2$  as a function of  $p_1/p_2$ . Dots are simulation results with indicated parameters. SZ phase code with  $n/M=8/64$  and notch width of  $3M/4$  are used.